A Study of Complex Phase Behaviour Arising In Heavy Oil / Bitumen Mixtures Using X-ray Imaging

by

Leisl Dukhedin-Lalla

A thesis submitted in conformity with the requirements
for the degree of Doctor of Philosophy
Graduate Department of Chemical Engineering and Applied Chemistry
University of Toronto

ISBN 0-612-11708-1

Canada

Name LEISL DUKHEDIN-LALLA

Dissertation Abstracts International is arranged by broad, general subject categories. Please select the one subject which most nearly describes the content of your dissertation. Enter the corresponding four-digit code in the spaces provided.

CHEMICAL ENGINEERING
SUBJECT TERM

0542
SUBJECT CODE

UMI

Subject Categories

THE HUMANITIES AND SOCIAL SCIENCES

COMMUNICATIONS AND THE ARTS
Architecture 0729
Art History 0377
Cinema 0900
Dance 0378
Fine Arts 0357
Information Science 0723
Journalism 0391
Library Science 0399
Mass Communications 0708
Music 0413
Speech Communication 0459
Theater 0465

EDUCATION
General 0515
Administration 0514
Adult and Continuing 0516
Agricultural 0517
Art 0273
Bilingual and Multicultural 0282
Business 0688
Community College 0275
Curriculum and Instruction 0727
Early Childhood 0518
Elementary 0524
Finance 0277
Guidance and Counseling 0519
Health 0680
Higher 0745
History of 0520
Home Economics 0278
Industrial 0521
Language and Literature 0279
Mathematics 0280
Music 0522
Philosophy of 0998
Physical 0523
Psychology 0525
Reading 0535
Religious 0527
Sciences 0714
Secondary 0533
Social Sciences 0534
Sociology of 0340
Special 0529
Teacher Training 0530
Technology 0710
Tests and Measurements 0288
Vocational 0747

LANGUAGE, LITERATURE AND LINGUISTICS
Language
- General 0679
- Ancient 0289
- Linguistics 0290
- Modern 0291

Literature
- General 0401
- Classical 0294
- Comparative 0295
- Medieval 0297
- Modern 0298
- African 0316
- American 0591
- Asian 0305
- Canadian (English) 0352
- Canadian (French) 0355
- English 0593
- Germanic 0311
- Latin American 0312
- Middle Eastern 0315
- Romance 0313
- Slavic and East European 0314

PHILOSOPHY, RELIGION AND THEOLOGY
Philosophy 0422
Religion
- General 0318
- Biblical Studies 0321
- Clergy 0319
- History of 0320
- Philosophy of 0322

Theology 0469

SOCIAL SCIENCES
American Studies 0323
Anthropology
- Archaeology 0324
- Cultural 0326
- Physical 0327

Business Administration
- General 0310
- Accounting 0272
- Banking 0770
- Management 0454
- Marketing 0338

Canadian Studies 0385
Economics
- General 0501
- Agricultural 0503
- Commerce-Business 0505
- Finance 0508
- History 0509
- Labor 0510
- Theory 0511

Folklore 0358
Geography 0366
Gerontology 0351
History
- General 0578
- Ancient 0579
- Medieval 0581
- Modern 0582
- Black 0328
- African 0331
- Asia, Australia and Oceania 0332
- Canadian 0334
- European 0335
- Latin American 0336
- Middle Eastern 0333
- United States 0337

History of Science 0585
Law 0398
Political Science
- General 0615
- International Law and Relations 0616
- Public Administration 0617

Recreation 0814
Social Work 0452
Sociology
- General 0626
- Criminology and Penology 0627
- Demography 0938
- Ethnic and Racial Studies 0631
- Individual and Family Studies 0628
- Industrial and Labor Relations 0629
- Public and Social Welfare 0630
- Social Structure and Development 0700
- Theory and Methods 0344

Transportation 0709
Urban and Regional Planning 0999
Women's Studies 0453

THE SCIENCES AND ENGINEERING

BIOLOGICAL SCIENCES
Agriculture
- General 0473
- Agronomy 0285
- Animal Culture and Nutrition 0475
- Animal Pathology 0476
- Food Science and Technology 0359
- Forestry and Wildlife 0478
- Plant Culture 0479
- Plant Pathology 0480
- Plant Physiology 0817
- Range Management 0777
- Wood Technology 0746

Biology
- General 0306
- Anatomy 0287
- Biostatistics 0308
- Botany 0309
- Cell 0379
- Ecology 0329
- Entomology 0353
- Genetics 0369
- Limnology 0793
- Microbiology 0410
- Molecular 0307
- Neuroscience 0317
- Oceanography 0416
- Physiology 0433
- Radiation 0821
- Veterinary Science 0778
- Zoology 0472

Biophysics
- General 0786
- Medical 0760

EARTH SCIENCES
Biogeochemistry 0425
Geochemistry 0996
Geodesy 0370
Geology 0372
Geophysics 0373
Hydrology 0388
Mineralogy 0411
Paleobotany 0345
Paleoecology 0426
Paleontology 0418
Paleozoology 0985
Palynology 0427
Physical Geography 0368
Physical Oceanography 0415

HEALTH AND ENVIRONMENTAL SCIENCES
Environmental Sciences 0768
Health Sciences
- General 0566
- Audiology 0300
- Chemotherapy 0992
- Dentistry 0567
- Education 0350
- Hospital Management 0769
- Human Development 0758
- Immunology 0982
- Medicine and Surgery 0564
- Mental Health 0347
- Nursing 0569
- Nutrition 0570
- Obstetrics and Gynecology 0380
- Occupational Health and Therapy 0354
- Ophthalmology 0381
- Pathology 0571
- Pharmacology 0419
- Pharmacy 0572
- Physical Therapy 0382
- Public Health 0573
- Radiology 0574
- Recreation 0575
- Speech Pathology 0460
- Toxicology 0383

Home Economics 0386

PHYSICAL SCIENCES
Pure Sciences
Chemistry
- General 0485
- Agricultural 0749
- Analytical 0486
- Biochemistry 0487
- Inorganic 0488
- Nuclear 0738
- Organic 0490
- Pharmaceutical 0491
- Physical 0494
- Polymer 0495
- Radiation 0754

Mathematics 0405
Physics
- General 0605
- Acoustics 0986
- Astronomy and Astrophysics 0606
- Atmospheric Science 0608
- Atomic 0748
- Electronics and Electricity 0607
- Elementary Particles and High Energy 0798
- Fluid and Plasma 0759
- Molecular 0609
- Nuclear 0610
- Optics 0752
- Radiation 0756
- Solid State 0611

Statistics 0463

Applied Sciences
Applied Mechanics 0346
Computer Science 0984
Engineering
- General 0537
- Aerospace 0538
- Agricultural 0539
- Automotive 0540
- Biomedical 0541
- Chemical 0542
- Civil 0543
- Electronics and Electrical 0544
- Heat and Thermodynamics 0348
- Hydraulic 0545
- Industrial 0546
- Marine 0547
- Materials Science 0794
- Mechanical 0548
- Metallurgy 0743
- Mining 0551
- Nuclear 0552
- Packaging 0549
- Petroleum 0765
- Sanitary and Municipal 0554
- System Science 0790

Geotechnology 0428
Operations Research 0796
Plastics Technology 0795
Textile Technology 0994

PSYCHOLOGY
General 0621
Behavioral 0384
Clinical 0622
Developmental 0620
Experimental 0623
Industrial 0624
Personality 0625
Physiological 0989
Psychobiology 0349
Psychometrics 0632
Social 0451

The UNIVERSITY of TORONTO LIBRARY MANUSCRIPT THESIS DOCTORAL AUTHORITY to DISTRIBUTE

NOTE: The AUTHOR will sign in one of the two places indicated. It is the intention of the University that there be **NO RESTRICTION** on the distribution of the publication of theses save in exceptional cases.

(a) Immediate publication in microform by the National Library is authorized.

Author's signature Leisl Dubreuil Fillo Date March 1, 1996

- OR -

(b) Publication by the National Library is to be postponed until _____ 19_____ (normal maximum delay is two years). Meanwhile this thesis may not be consulted in the University Library except with written permission on each occasion from me.

Author's signature_____ Date_____

This restriction is authorized for reasons which seem to me, as Chair of the Graduate Department of _____, to be sufficient.

Signature of Graduate Department Chair _____

Date _____

BORROWERS undertake to give proper credit for any use made of the thesis, and to obtain the consent of the author if it is proposed to make extensive quotations, or to reproduce the thesis in whole or in part.

Signature of Borrower	Address	Date

Acknowledgments

This project would not have been a success without the assistance and support of many people. I would like to thank Professor John Shaw for his insight, encouragement and support throughout this entire project. Without the camaraderie and help of my colleagues in our research group this undertaking would not of have been as much fun. Thanks are due to Jalal, Habib, Soheil, Hadi and Clive. I would like to thank all the support staff of the Department of Chemical Engineering especially those in the machine shop. Finally, I would like to thank my family and friends, I am very lucky and grateful to be surrounded by some very caring and supportive people - thanks to Feels, Neil, Jr. and Mel, and Mom and Dad.

I would like to acknowledge financial assistance from CANMET -ERL, AOSTRA, Ontario Graduate Scholarship Program and equipment support from Amoco Research Center, Naperville, USA.

Table of Contents

List of Figures

List of Tables

Title : A Study of Complex Phase Behaviour Arising In Heavy Oil / Bitumen Mixtures Using X-ray Imaging

Degree : Doctor of Philosophy, 1996

Name : Leisl Dukhedin-Lalla

University : Department of Chemical Engineering, University of Toronto

ABSTRACT

A new approach for performing phase equilibrium studies with opaque hydrocarbon mixtures at elevated temperatures and pressures has been developed and tested. Using x-ray radiographic imaging, density differences as small as 40 kg/m^3 were distinguishable between two liquid phases in a hydrocarbon mixture. The phase behaviour of a series of Athabasca bitumen vacuum bottoms (ABVB) + n-dodecane + hydrogen mixtures were investigated. Complex phase behaviour and phase transitions were observed with some of the mixtures. Preliminary pressure - temperature phase diagrams for four mixtures of ABVB + n-dodecane + hydrogen were constructed along with a pressure - composition phase diagram at 674 K. Complex phase behaviour arose with mixtures of the ABVB + n-dodecane + hydrogen and processed crude systems that had asphaltene contents greater than 12 wt.% and 797 K+ fractions greater than 30 wt.%.

Samples of the "solid" phase which existed at low temperatures and which appeared at temperatures >650 K for one of the ABVB + n-dodecane + hydrogen mixtures were analyzed and

it was found that the "solids" had H/C ratios of 1.3 and 0.85, aromatic contents of 57 and 47 with solubilities in toluene of 100 wt.% and 95 wt.%, respectively. Enthalpies of fusion, determined from the slopes of the pressure - temperature trajectories and a fugacity model, for the "solids" present at low temperatures were approximately 8 J/g based on a molecular weight of 5000 g/mol.

With the view cell apparatus it was also possible to make absolute fluid density measurements by calibrating the relationship between fluid density and intensity. Using these relationships, densities of the heavy oil-bitumen mixtures were determined at elevated temperatures.

These new findings of complex phase behaviour with heavy oil-bitumen mixtures were compared with current industrial heavy oil upgrading processes. These phase diagrams explain common operating practices and problems arising with these processes. For example, zones exhibiting complex phase behaviour are largely being avoided by many of the operating, low conversions and plugging of transfer lines in pressure let-down systems can be explained by the presence of complex phase behaviour.

1.0 Introduction

1.1 World Energy Picture

A recent survey in *The Economist*[1] reported on world energy consumption and predicted that the world's energy situation is heading for another drastic shift nearly 30 years after the major oil crisis of the early 1970's. This upset would see a huge increase in energy demand which would be dictated not by the rich countries but by the fast-growing developing countries of Latin America and Asia. The beginning of the 21st century will see the rich countries' share of the total energy consumption dipping below 50% for the first time during the industrial era while the developing countries share will have increased from 27% to 40% (see Figure 1.1.1).

The World Energy Council[1] suggests that by the year 2020, with a "high-growth" prediction, the world's energy demand could be as high as double the current demand. This translates to an oil consumption of more than 90 million barrels a day of oil, an increase of 27 million barrels a day over OPEC's entire present output (see Figure 1.1.2).

During the 1980's there has been an increase in the oil demand in Asia of more than 80%; however, this impact has been moderate since it only represents about 20% of the world's consumption. Similar trends have also been seen in Latin America. As long as the rich countries account for the major share of the energy consumption small changes in their economies overshadow the increase of the demand of the developing countries. Improved

energy efficiency and two recessions have buffered the effect of the current growth in the developing countries and kept the oil market slack. If the predictions are to be believed, small increases in the demand for energy by developing countries in the future will affect the oil markets tremendously since they will represent close to 50% of world energy demand. While these predictions may seem alarming, the sheer shift in the demography of the world's population will mean that one could actually view these predictions as being too conservative. The world's population will increase by 2.7 billion, to over 8 billion by 2020 and 60% of this increase will be directly attributable to population increases in Asia and Latin America. Currently, 40% of the world's population live in two Asian countries, China and India, which have seen energy consumption increase 22 times since 1952 and 3 times since 1970 respectively. China, the sixth largest oil producer had become a net oil importer by 1993 [2,3].

Figure 1.1 : Energy Demand[1]

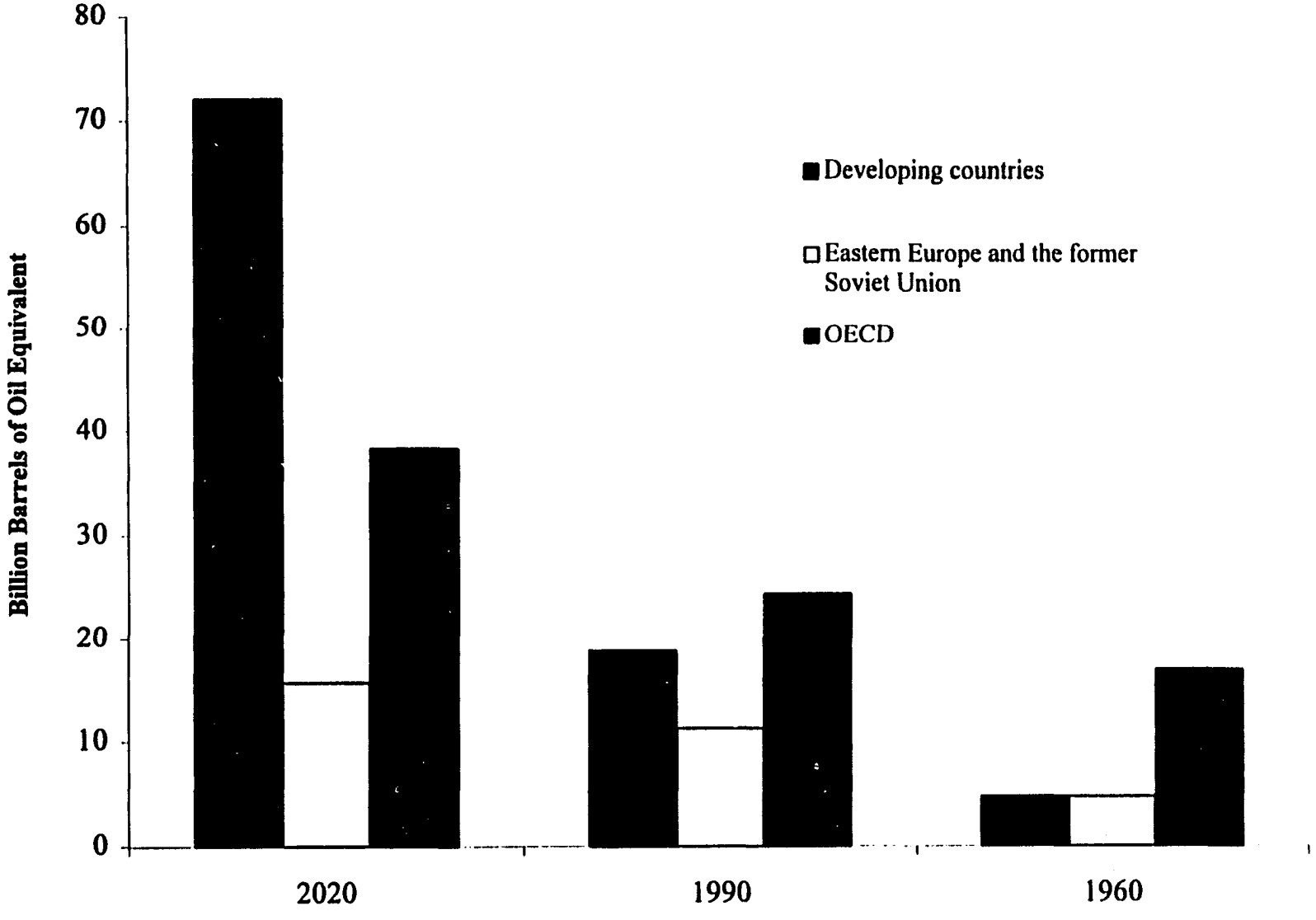

Figure 1.2 : Energy Supply by Type[1]

The increase in world energy demand and consumption cannot be met by the current world oil reserves. While research and investment into renewable energy sources continue, their prospects for implementation are debatable. Renewable sources such as wind, solar and biomass energy are viable but their widespread implementation and commercialization remain doubtful. Also on shaky ground is the prospect of nuclear power; most developed countries, including Canada, have seen a sharp decrease in investment in nuclear power as a result of pressure from environmental groups and the general public.

The growth in population and consequent increased energy consumption by countries like China and India translate into two major energy demands : the need for electricity and the need for gasoline. During the economic prosperity that existed in North America during the early 1950's and in Japan during early 1960's, the price of cars and electronic equipment was substantially higher than today and these items were considered to be luxuries whereas today these products are considered to be necessities. This huge need for electricity and gasoline will create a massive demand for oil.

The World Energy Council estimates that there is enough oil to last for 60 years at the current rate of consumption (this time estimate would be a lot less if the predictions are to be believed) and another 170 years supply of the more expensive "unconventional" oil which includes heavy crudes and bitumen (Figure 1.3). Hence the major concern for future energy demands is not the lack of fossil fuel reserves but the cost necessary to

develop these reserves. While it is agreed that the opening up of the former Soviet Union and more relaxed foreign investment policies in China will allow for exploitation of the vast reserves of oil in these countries, this scenario seems unlikely. These countries do not have the necessary infrastructure for harvesting these reserves. Huge investments would be needed for upgrading and refitting of the oil producing facilities in these countries.

Currently Canada and Venezuela are the only two countries that have invested considerable effort and research into the processing of the "unconventional" oil reserves [7]. Canada's early interest in the efficient and profitable upgrading of heavy oils and bitumens is understandable due to the very large reserves in Alberta and Saskatchewan. More than 90% of Canada's oil reserves [4] exist in Alberta and Saskatchewan and 60% of these reserves exist as bitumen in the oil sands (Figure 1.4). Canadian upgraders have shown the ability to produce high quality, light oil products, which are more valuable than diesel fuel and road asphalt, called " Synthetic Crude Oil". The efficiency of processing heavy oils and bitumens however has yet to be optimized. Questions such as where the "bottom of the barrel" is do not yet have clear answers. Today's refineries are demanding increased flexibility with respect to varying feedstocks and have very little latitude with respect to capital and operating costs [5,6]. A detailed understanding of these heavier crudes, their phase behaviour and the variety of problems that arises during processing such, as asphaltene precipitation and excessive coking is required to ensure flexibility and profitability.

Figure 1.3 : Alberta bitumen reserves[4, 7]

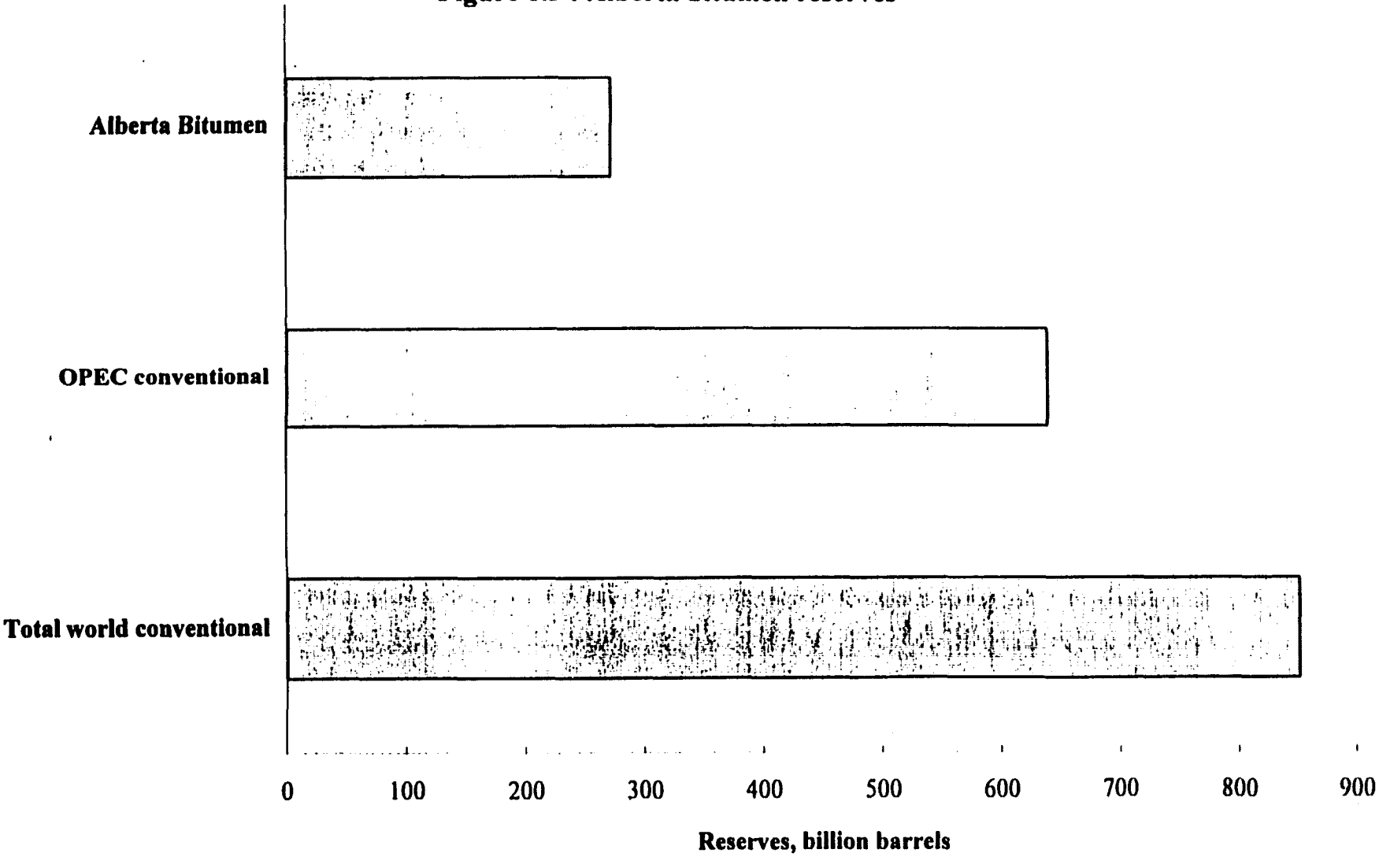

Figure 1.4 : Remaining Alberta Reserves[4, 7]

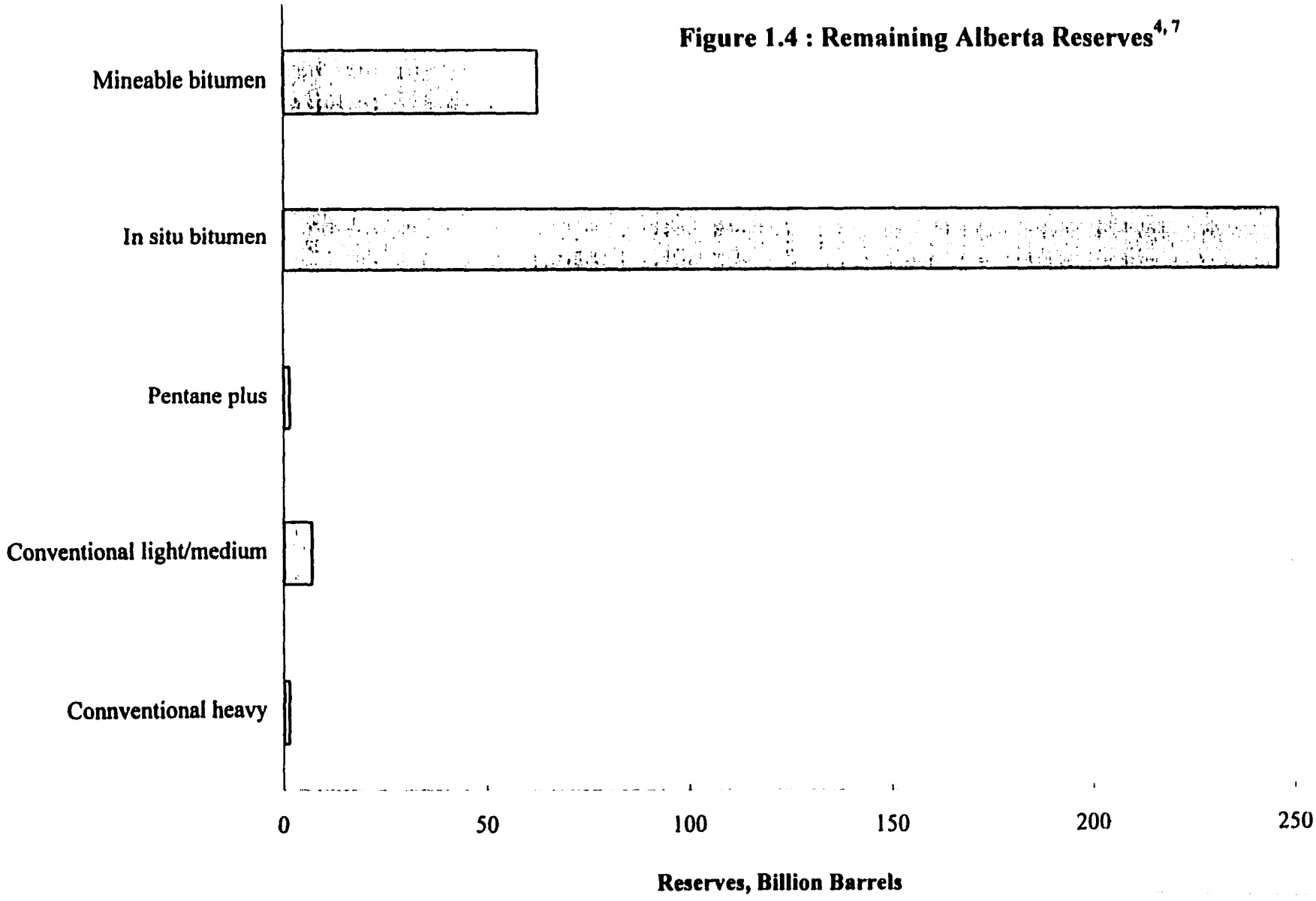

1.2 Objectives

Objective No. 1

The primary objective of this research project is to investigate the phase behaviour of a typical heavy oil/bitumen from Canada's reserve. Preliminary investigations [8,9] carried out during a M.A.Sc. research program have shown that model coal liquids and model heavy oil systems exhibit surprisingly complex phase behaviour under typical processing conditions. To date, these findings have been qualitative and further investigation is needed. However, specific examples which demonstrate complex phase behaviour, at or above room temperature and at elevated pressures, include: asymmetric reservoir fluids [10] and heavy oil + gas mixtures [11]; these systems have been shown to exhibit vapor- liquid - liquid -solid and vapor-liquid-liquid phase behaviour, respectively, and verify the existence of such behaviour for these systems. Phase equilibria diagrams will provide an important tool for determining processing conditions, reactor design and provide data for thermodynamic modelling. To date, phase diagrams for heavy oil mixtures have not been found in the open literature and it is almost certain that such diagrams do not exist. Along with providing phase diagrams for a heavy oil system this thesis will also explore some of the factors that may affect phase behaviour, e.g., asphaltene content, aromatic carbon content and hydrogen to carbon ratio.

Objective No. 2

The second objective of this thesis is to develop a new x-ray based technique for studying phase equilibria of opaque hydrocarbon systems. Performing phase equilibria studies with

heavy oil systems at elevated temperatures and pressures, typical of processing conditions, poses a significant challenge. Typical experimental apparatus for phase equilibria studies like the Cailletet apparatus and related equipment which rely on visual observation cannot be used for phase equilibria studies with opaque fluids. Direct sample techniques have been proven unreliable. Techniques based on conductivity probes [12] have been used to detect asphaltene precipitation since the appearance of solid is accompanied by an abrupt change in electrical conductivity. These techniques have yet to be proven operational at elevated temperatures and pressures and while the onset of solid precipitation can be detected, more complex behaviour like vapor-liquid-liquid-solid cannot be resolved. Results with conductivity probes would also become less reliable if the phase behaviour arises as a discrete phase dispersed in a continuous one since the technique is a point measurement. Gamma densiometry is also another technique that can be use to discern different phases in opaque systems. Gamma densiometry[13,14] has been used extensively in the study of two phase flow and provides density differences along a line a vessel. The initial capital cost of gamma cells is relatively high and was not investigated further.

In communication with Amoco Research Center in Naperville, Illinois, this laboratory learnt of an x-ray imaging system that was being used to conduct settling studies for coal de-ashing experiments[15]. The apparatus was being used to determine the rate of sedimentation of high mineral content ash in a coal liquefaction stream[16]. X-ray radiographs of solid and liquid phases are easily discernible since x-ray absorbance is a

function of atomic density, e.g., medical radiologists can distinguish easily the difference between bone and organs. This laboratory was offered the x-ray imaging equipment by Amoco. Consequently, the second objective of this research project is to determine whether x-ray radiography can be used to distinguish opaque hydrocarbon liquid phases with very small density differences and to upgrade the apparatus to be able to conduct phase equilibria studies of systems at elevated temperatures and pressures.

Objective No. 3

The third objective is to link observed phase behaviour with operating conditions of existing processes and associated problems. Mixtures of partly processed crudes and model unprocessed crudes were used to investigate the phase behaviour of typical heavy oil / bitumen mixtures.

These objectives have been met and key results have been presented at several conferences [110, 111, 112] and published in the literature[108, 109].

1.3 Layout of the Thesis

An overview of the heavy oil upgrading technologies which is needed to link operating conditions and processing problems to phase behaviour is provided in Chapter 2. This detailed study of the heavy oil upgrading schemes and operating conditions was accomplished over a one year period. All the processes reviewed are summarized in

Tables 2.1.1 and 2.1.2 and a plot of pressure versus temperature showing the operating conditions was constructed and is presented in Figure 2.2.1. The importance of this review becomes clear in Chapter 5 where operating conditions are related to phase behaviour of a model bitumen mixture. A brief overview of complex phase behaviour including the interference of a solid on complex fluid phase behaviour is also provided in Chapter 2. Phase diagram theory is utilized to construct preliminary phase diagrams for the model bitumen mixtures investigated in this research project as the data are sparse.

The x-ray imaging apparatus is described in Chapter 3. Details of the general layout, individual components, experimental setup, operation and challenges are also provided. This x-ray imaging facility was assembled over a two year period. The x-ray imaging technique was tested with model systems and these results are the first set of results presented in Chapter 4. The results of phase equilibria studies, performed over a one year period, with a series of partly processed crudes and a series of model crude mixtures are also reported in Chapter 4. Direct observation and concrete evidence of complex phase behaviour in heavy oil mixtures are provided. Using the thermodynamic approach described in Chapter 2, preliminary phase diagrams, not available presently in the literature, were constructed and are also presented in Chapter 4. The major findings from this Ph.D. thesis project are discussed in Chapter 5 and the link between complex phase behaviour of bitumen mixtures and operating practices in the heavy oil upgrading industry is made. Conclusions are drawn in Chapter 6.

2.0 Literature Review

This literature review serves two purposes. One purpose is to provide an overview of the heavy oil upgrading processes, their operating conditions, processing strategies and processing problems (section 2.1). Since many of the current heavy oil upgrading processes are proprietary an extensive review of the open literature including patents was undertaken. This review has been found to valuable by many practitioners. Those familiar with processing technologies may choose to skip section 2.2. The second purpose is to provide the theoretical framework for the construction of phase diagrams presented in this thesis. This ultimately provides the basis for the construction of phase diagrams presented in this thesis. Since the data obtained in this research project is fragmentary in nature, the most sophisticated theoretical tools are used to extract the maximum amount of information from the data to construct preliminary phase diagrams consistent with physical laws.

2.1 A Review of Heavy Oil Upgrading Process Technologies

As the world's supply of high quality, low sulphur crudes is depleted crude oil quality is predicted to decline. This prediction has led refineries to consider increased processing flexibility for heavier feedstocks like heavy oils and bitumens. Today, heavy oil reserves are greater than conventional crude reserves and since the early 1980's considerable effort

has been directed towards upgrading and processing of heavy oils and bitumens in Canada.

A fairly broad and encompassing classification[17] of a heavy oil is characterized by a viscosity at 293 K equal to or greater than 20 cSt, a distillable fraction below 623K of less than 25 wt. %, ^{0}API gravity less than 17 (density greater than 0.950 g/cm^3), a hydrogen to carbon ratio (H/C) typically around 1.5 and a Conradson Carbon (C.C.) wt. % greater than 10 wt. %. Asphaltene content of heavy oils are usually greater than 5 wt. % and can be as high as 18 wt. %.

The processing of heavy oils can be divided into two main categories (see Fig. 2.1.1 and 2.1.2), the first category being upgrading by coking or by carbon rejection and the second category being upgrading with a minimization of coking (or without carbon rejection). Each process cited is reviewed briefly for completeness and all the processes are summarized in Tables 2.1.1 and 2.1.2. Heavy oil upgrading technology by coking can be further divided into two types of processes. The first type of processing is based on deasphalting whereby asphaltic material is extracted by precipitation with a light hydrocarbon solvent and the deasphalted oil is then further processed to desirable products. The solvent can be either a light paraffin or an alcohol. The second classification of processing by carbon rejection involves thermal cracking whereby coking occurs with the formation of a solid phase, that removes impurities, metals, nitrogen and high asphaltic material, and a lighter phase which can be further processed under less severe conditions.

Figure 2.1.1

Heavy Oil Upgrading

Processing with Carbon (Coke) Rejection
Non-Catalytic without Hydrogen

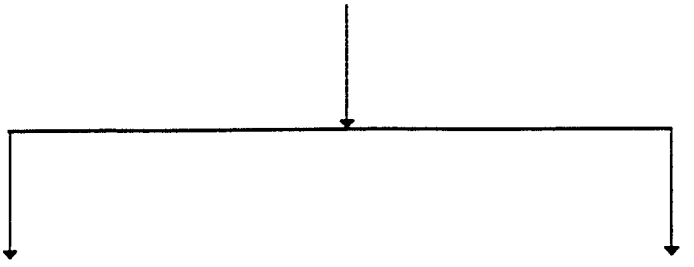

SOLVENT DEASHPHALTING

- Solvent Deashphalting
- ROSE - (Residum Oil Supercritical Extraction)

COKING

Coke Drums

- Delayed Coking
- Eureka

Fluidized Beds

- Flexicoking - fluid coking
- ART - (Ashphalt Residual Treating)
- Coke Fluidized Bed Cracking
- HOT - (Heavy Oil Treating)
- Dynacracking Process

Fluidized Beds with a Riser

- RCC - (Reduced Crude Oil Conversion)
- HOC - (Heavy Oil Cracking)

Figure 2.1.2

Heavy Oil Upgrading

Processing without Carbon (Coke) Rejection

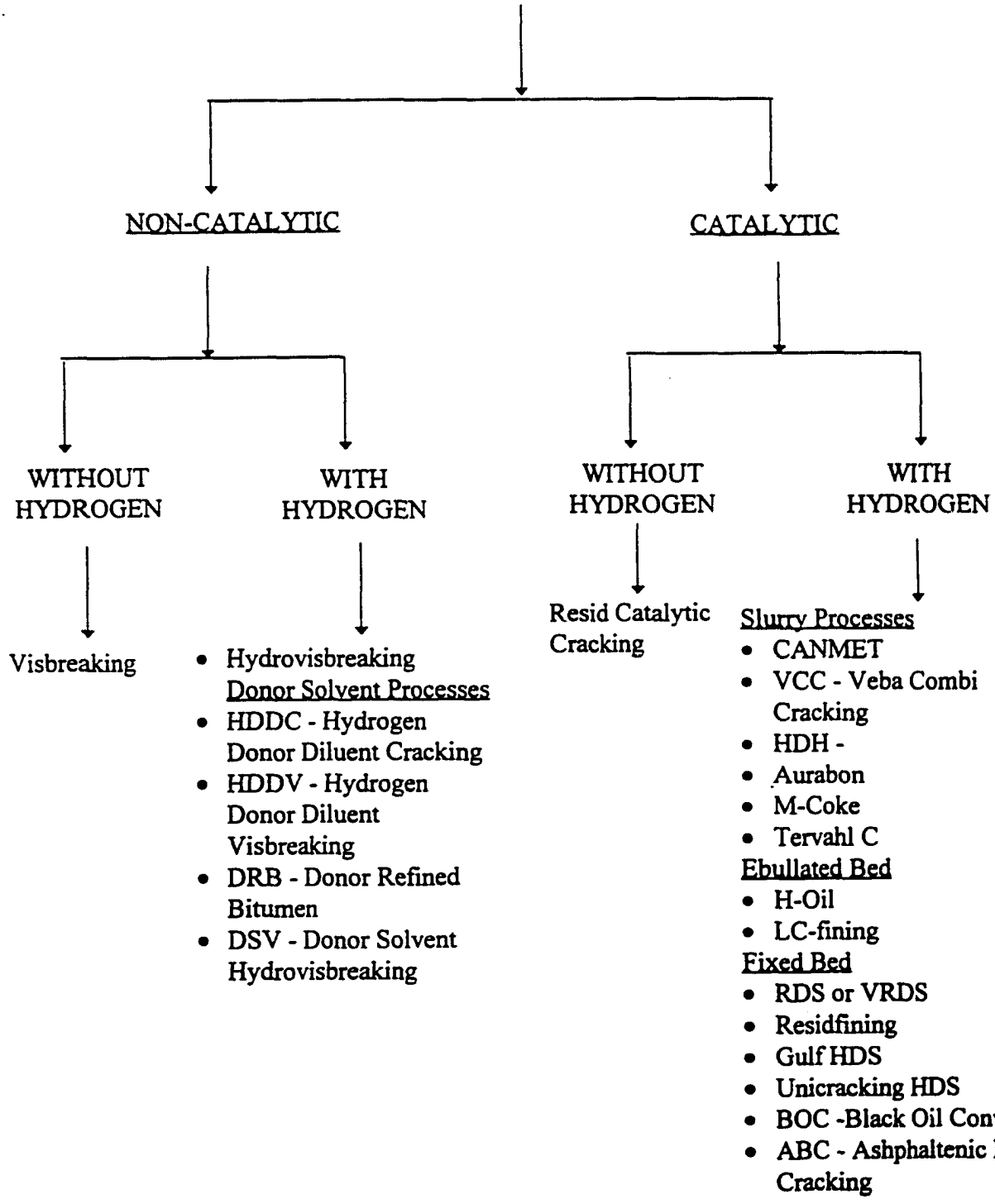

Table 2.1.1 - Heavy Oil Upgrading - Processing with Coke Rejection

Process	Licensor	T (K)	P(MPa)	Reactor Type	Feedstock Type	Feed °API	Feed C.C.wt.%	Yields Gas wt.%.	Yields Oil wt.	Yields Coke.wt. %
Solvent De-asphalting	Institut Francais du Petrole	423 - 453	4	Solvent extractor	Arabian Heavy Resid	3.5	23	Dry gas	DAO 66	Asphalt 34
ROSE	Kerr-McGee	470	3.5	Solvent-extractor	Arabian Light Vacuum Resid	6.9	11.4		DAO 80	Asphalt 20
Delayed Coking	M.W. Kellogg	760 - 783	0.2 - 0.4	Coking Drums	Maya Resid	2.6	25.5	Dry gas	Oil 48.5	Coke 38.3
Eureka	Kurecha &Chiyoda	693 - 703	0.1	Coking Drums	Middle Vacuum Resid	7.4	20	Gas 4.8	Oil 65.6	Coke 29.6
Flexicoking	Exxon	783 - 810	0.1	Fluidized Bed	Athabasca Bitumen	8.87	12.7	Gas 8.7	Oil 76.6	Coke 14.7
ART	M.W. Kellogg	773 - 813	0.1	Fluidized Bed with Riser	Maya Crude	22.1	12.5	Gas 11.7	Oil 78.1	Coke 10.2
KK	AIST Japan	973 - 1073	0.1	Fluidized Bed with Steam Stripping	Vacuum Resid	17.9	23.6	Gas 38.9	Oil 47.2	Coke 13.9
Dynacraking	HRI.	773 - 813	2.7 - 4.1	Fluidized Bed with 3 zones		5.6	16.1	N/A	Oil 67	N/A
RCC	UOP	810 - 895	0.07 - 0.25	Vented Riser		19.2	6.9	Dry gas 13.2	Oil 48.5	Coke 38.3
HOC	M.W. Kellogg	797 - 802	0.1	Fluidized Catalytic Cracker	Arabian Light Mix	20.36	3.8	Dry gas 4.1	Oil 85.1	Coke 10.8

Table 2.1.2 - Heavy Oil Upgrading - Processing with Coke Minimization

Process	Licensor	T (K)	P(MPa)	Reactor Type	Feed Type	Feed °API	Feed C.C.wt. %	Yields Gas wt.%.	Yields Oil wt.%	Yields Coke.wt. %
Visbreaking	many	750 - 773	5.17	Coil Cracker	Mid - East Resid	8	17.5	Gas 3.5	Gas oil 18.6	Residue 77.9
Visbreaking	many	700 - 716	5.17	Soaker Drum	Mid. - East Resid	10.28	16.5	Gas 2	Gas oil 34	Residue 64
Hydro-vsbreaking	many	650 - 700	8 - 9	Soaker Drums	Arab Light Vacuum Resid	10.2	14.5	Gas 14.7	Oil 58	Residue 27
HDDC	Exxon Res. & Eng.	720 - 740	2.6 - 3.1		Kuwait Asphalt	1.2	25.3	Gas 2.2	Oil 41.8	Residue 56
HDDV	Exxon Res. & Eng.	715 - 730	2.4 - 2.8		Hawkins Residuum	3.87	22.4	Gas 2.3	Oil 31.6	Residue 66.4
DRB	Gulf Canada	683 - 733	3.5 - 5.5	Donor Solvent	Athabasca Vacuum Resid			Gas 5.2	Oil 61.7	Coke 33.1
CANMET Hyrdo-cracking	Lavalin & Petro Canada	708 - 728	13.6	Upflow reactor	Arabiran Light Vacuum Resid	7.36	22.3	Gas 8.66	Oil 76.6	Coke 14.74
VCC	Veba Oel Germany.	728 - 737	15 - 26	Vertical Slurry	Deasphalted Bottom	0	29.3	Gas 5.5	Oil 89.5	Coke 5
HDH	Intevep Venezuela	724	13 - 14	Vertical Slurry	Morichal Vacuum Residuum	5.2	19.6	Gas 9.82	Oil 81.2	Coke 9.2
LC-fining	Lummus Crest & Amoco Res.	705	15.5	Ebullated Bed	Heavy Vacuum Bottoms	4.4	22.15	Gas 6.4	Oil 85.9	Coke 7.7
H-oil	HRI	727	15.5	Ebullated Bed	Kuwait Vacuum Bottoms			Gas 9.5	Oil 69.2	Resid 21.3
Tervahlc	Inst.Franc. du Petrol	683	15	Slurry Reactor	Aramco Vacuum Resi	10.6	16.2	Gas N/A	Oil N/A	Coke 36
Unibon-RCD-BOC	UOP Process Div.	653 - 693	18	Fixed bed	San Ardo Crude	13.8	8.52	Gas 0.6	Oil 80.3	Coke 17.9
ABC	Chiyoda Cem.Co	683	13.8	Fixed Bed	Khafji Vacuum Resid	5.08	23.6	Gas 2.4	Oil 75.8	Coke 21.8

Heavy oil processing by minimization of coking can be classified by the following criteria: the processes that are catalytic or non-catalytic and the processes which operate with or without hydrogen. Catalytic processes which operate with hydrogen addition are classified as hydroconversion processes which are further categorized by reactor type. Catalytic processes that operate without hydrogen are classified as resid catalytic cracking. Non-catalytic processes with hydrogen addition are classified as hydrovisbreaking, donor solvents and hydropyrolysis, and non-catalytic processes without hydrogen addition are called visbreaking processes.

Currently many of the heavy oil upgrading schemes are combinations of several of these processing technologies. The various processing technologies are discussed with a review of the operating temperatures and pressures, feedstocks and yields. This review is limited to processing technologies used for the initial treatment of heavy oils and bitumen. While this review discusses a wide spectrum of processing technologies, it is limited to processes that are employed widely in North America and for which details are available in the open literature. Such an overview provides a picture of current operating philosophies in industry and reflects where processing problems arise.

2.1.1 Processing with Carbon (Coke) Rejection

Heavy oil upgrading with carbon rejection can be divided into two classes : deasphalting processes and thermal processes. These processing strategies are discussed below.

2.1.1.1 SOLVENT DEASPHALTING

Deasphalting [18,19]

Solvent deasphalting, using propane as the solvent, has been in use since the early 1930's to produce a light deasphalted oil for feedstocks such as a lube oil. Today a similar process is used to deasphalt heavy oils using heavier solvents. Solvent deasphalting is licensed by Institut Francais du Petrole on behalf of Ashvahl. The objective is to produce a deasphalted oil (DAO) with a minimum amount of asphaltenes and metals as a possible feedstock for further processing. Typical solvents being utilized are pentane cuts and light gasoline since they are able to extract a greater portion of the heavy oil while concentrating the asphalt phase. The deasphalting process is made up of three main steps: the flocculation and precipitation of the asphalt, separation of the DAO and the asphalt and the washing of the asphalt to recover the solvent and DAO. In a typical deasphalting scheme, feedstock is extracted with a solvent at operating conditions close to the critical point of the solvent. If pentane is being used as the solvent then typical operating conditions are between 423K to 453 K and around 4 MPa with a solvent to feedstock ratio between 3-5 . These operating conditions provide the maximum

extraction yields with a minimum of asphaltenes (C_7 insolubles) in the DAO. The DAO and solvent mixture then enters a flashing unit to recover the solvent while the asphalt is further stripped to remove any solvent and DAO. Typical yields with a heavy Arabian resid with an ^{0}API of 3.5 and C.C. wt. % of 23 wt. % was deasphalted with a pentane fraction as a solvent. A deasphalted oil yield of 66 wt. % was obtained with an ^{0}API of 12.0 and a C.C of 11 wt. %.

Residuum Oil Supercritical Extraction (ROSE) [18,20,21]

Typically solvent recovery in a conventional solvent deasphalting process depends on distillation of the solvent in a series of flashing and steam stripping units. The Residuum Oil Supercritical Extraction (ROSE) licensed by the Kerr-McGee refining company uses a supercritical solvent recovery scheme which provides a more energy efficient process for solvent recovery. Yields of DAO from solvent extraction can be improved with an increase in the solvent to feed ratio however as this ratio increases the cost associated with solvent recovery also increases. The ROSE process achieves this in a cost effective manner even with a solvent to feed ratio as high as 10:1. In the ROSE process three basic products are recovered form the petroleum resid: asphaltene, resins and DAO. Resins are an intermediate fraction lighter than asphaltenes but heavier than DAO. Feedstock is mixed with several volumes of solvent (light hydrocarbon) at temperatures and pressures close to the critical point of the solvent. The heavy asphaltene fraction is extracted, separated and then further stripped to remove any solvent. The solvent-resin oil phase is

then further heated until a second phase separation occurs, as the retrograde condensation phase is entered, and an intermediate resin fraction is removed from the mixture. The remaining solvent-oil solution is then heated to a temperature above the critical temperature of the solvent, whereby the oil becomes insoluble in the supercritical solvent and the DAO and solvent are separated. Energy efficiency is achieved by using the supercritical solvent in a series of heat exchangers to heat the resin oil-solvent and the DAO-solvent solutions prior to separation. The ROSE process claims solvent recovery between 85% to 93%. With an Arabian light vacuum residuum with an ^{0}API of 6.9 and C.C content of 11.4 wt. % the ROSE process yielded a 80 wt. % DAO using pentane as the solvent and 67.2 wt. % DAO with butane as the solvent.

2.1.1.2 COKING

While deasphalting processes are designed to isolate and separate the heavy asphaltene phase without significantly altering their molecular structure, thermal treatments and coking processes are design to do the exact opposite. Coking can be considered as a severe thermal cracking process in which one of the end products is, to all intents and purposes, carbon (the coke formed also contains very high boiling hydrocarbons). The processes can be grouped into three classes depending on reactor type, i.e., coke drums, fluidized beds and fluidized beds with risers.

2.1.1.2.1 Coke Drums

Delayed Coking [18,22]

The Delayed Coking process has been licensed by several companies such as Foster Wheeler, Lummus Crest Inc., and M.W. Kellogg. The process was developed to minimize refinery yield of residual oil by severe thermal cracking of heavy feedstocks such as vacuum resids and tars. Initially severe thermal cracking led to coking of heaters. The technology was further developed to allow feedstocks temperatures to be raised above the point of coking without significant coke formation in the heaters. By operating the pre-heaters to the coking reactors at minimum retention times (i.e., maximum velocities) coking deposition is minimized. Feedstocks enter a fractionator for distillation from which the heavy fraction is fed to preheaters for further processing. Mild cracking and vapourization in the preheaters produce a vapour-liquid mixture which enters the coke drums. The vapours are further cracked as it flows up through the drums, these overhead vapours are then returned to the fractionator and are separated into distillable fractions. The typical processing scheme has two drums, one in service while the other is being de-coked with high pressure water jets. Operating temperatures in the coking drums are typically around 760 K to 783 K and operating pressures are approximately 0.2 MPa to 0.4 MPa. Yields from a Maya resid with an ^{0}API of 2.6 and C.C. content of 38.2 wt % produced 27 wt.% coke, 13.2 wt. % light gas, 19.3 wt.% naphtha and 27.2 wt.% gas oil.

Eureka [23,24]

The Eureka process was developed jointly by the Kurecha Chemical Co. and the Chiyoda Chemical Engineering Constr. Co. Ltd . Its main process feature is similar to the delayed coking and heavy residue cracking processes in that the thermal cracking of heavy residues is performed simultaneously with steam stripping under atmospheric pressure so that both the reactant and the product pitch are handled in the liquid state. This step removes the need for solids handling operation of the coking drums and the process claims feedstock flexibility

Heavy oil is fed to the preheater where it is heated to about 613 K; it then enters the bottom of a fractionator where it is mixed with a recycled oil. This mixed feed is then further heated and sent to a reactor operating at around 773 K. There are three reactors which are operated in a batchwise mode but with continuous flow by means of switching valves between the reactors. Both cracking and coking reactions occur in the reactor with heat being supplied by the addition of superheated steam and the incoming feed. The superheated steam also acts as a stripping agent to remove the cracked products, gas and oil. The products are then returned to the fractionator along with the steam for further refining. The remaining material in the reactor gradually increases in viscosity as the polycondensation reactions continue. At a predetermined point which produces the desirable pitch, the reactor is quenched with water and the product is drawn off as a highly viscous fluid into a stabilizer where further cooling produces pitch flakes. Clearly

this process requires an optimum operating level since cracking and coking reactions are occurring simultaneously. Typical reactor temperatures are around 693 K to 703 K under atmospheric pressure. Yields from a Middle Eastern Vacuum residue, with an ^{0}API of 7.4, C.C. content of 20 wt. % and asphaltene content (C_7 insolubles) of 5.7 wt. %. were 4.84 wt.% gases, 14.88 wt.% naphtha, 50.73 wt.% gas oil, 65.61 wt.% cracked oil and 29.55 wt.% pitch.

2.1.1.2.2 Fluidized Beds

Flexicoking [18,25,26,27]

Flexicoking technology is licensed by Exxon Research & Engineering Co. Flexicoking is a combination of fluid coking and coke gasification. The process was first commercialized in 1976. The residuum feed is preheated to about 588 K to 643 K and then sprayed into the reactor where it is contacted with a hot fluidized bed of coke. This coke is recycled from a coke heater at a sufficient rate to keep the reactor at temperatures between 783 K to 810 K. The cracked vapour passes through to cyclones at the top of the reactor where most of the entrained coke particles are separated, the vapour products are also quenched and sent to a vessel located at the top of the reactor. These vapours are then sent to a fractionator for further processing. The coke produced from the cracking reaction exists as a thin film on the coke particles. This coke is then removed by a steam stripping section at the bottom of the reactor. The system is designed and operated so that about 60 to 90 % of the coke produced in the reactor can be gasified. This gas can be

further processed to produce syngas or to recover hydrogen in the dual gasification option. Athabasca bitumen with an ^{0}API of 8.9 and C.C content of 12.7 wt.% was processed by Flexicoking and gave yields of 13.8 wt.% naphtha, 21.3 wt.% distillate ,41.4 wt.% gas oil, approximately 14.7 wt.% of the feed was converted to light gases and coke.

Asphalt Residual Treatment (ART) [18,28]

The Asphalt Residual Treatment (ART) technology is licensed by the M.W.Kellogg Co. The primary objective of the process is to remove the high C.C. and metal content components from heavy residua. The basic principle of the fluid decarbonization / demetallizationn process is to contact the feed at high temperature and short hydrocarbon residence time with a hot solid material which has an affinity for asphaltene and metals. Feedstock along with solid contacting agent and steam are fed to the bottom of the bed. The fluidized bed is designed to provide very short contact time between feed and solid agent. At the top of the reactor vaporized hydrocarbons are rapidly separated from the particulate solids in a large disengaging zone. The deasphalted/demetallized resid is then quenched, further treated to remove any water and light gases, and sent for subsequent downstream processing in a heavy oil or fluid catalytic cracker. The separated solids are sent to a regeneration system. Typically the contacting agent is microspheres of calcined clay which are regenerated at temperatures between 922 K to 1088 K. Operating temperatures in the fluidized beds are usually between 773 K to 813 K while the solids

are supplied to the reactor at temperatures around 838 K to 950 K. Yields from a feedstock with an ^{0}API of 23 and C.C content of 12.5 wt. % processed at a reactor temperature of 773K and contacting agent temperature of 923 K were 85.5 wt. % demetallized -deasphalted oil, 7.6 wt. % light gases and 6.9 wt. % solid deposit.

Coke Fluidized Bed Cracking (KK) [29]

The primary investigator of the Coke Fluidized Bed Cracking (KK) process is the Agency of Industrial Science of Technology, Research and Development Association of Petrochemicals from Heavy Oil, Japan. The basic objective of the process is to produce olefins from heavy oils by thermal cracking and coking at high temperatures. The thermal cracking units are made up of a heater and a reactor which contain a densely fluidized bed of coke particles. Coke particles are transported upwards in to the fluidized bed by steam injected at the bottom of the unit. Feed oil is injected with steam into the fluidized bed, and is contacted with hot coke particles and thermally cracked. Typical residence times are around 3-4 seconds and cracking temperatures are between 973 K and 1073 K. Product distribution can be varied by adjusting the reactor temperature. Coke produced by the cracking reactions is deposited on the surface of the particles and regenerated in subsequent heater units. The product stream is quenched and separated. This process has reported coking problems in the line from the reactor to the quenching unit. Typical yields from a vacuum resid with an ^{0}API of 17.9 and residual carbon content of 23.6 wt.

% processed at 1024 K with a residence time of 3.9 seconds were 38.9 wt.% gases, 47.2 wt. % cracked oil and 13.9 wt. % coke.

Dynacracking [30]

In the 1950's Hydrocarbon Research Inc. (HRI) developed the Dynacracking process, a non-catalytic process for upgrading of crude oils and residua. The program was not developed further after 1955. Renewed interest in the technology, due to changing feedstocks came in the early 1980's[11]. The Dynacracking reactor is unique in design in that it has three zones; a hydrocracking zone (top) , a stripping zone (middle) and a gasification zone (bottom) in a fluidized bed of inert alumina particles. Feed, recycled distillate and hydrogen enter the top section of the reactor into the hydrocracking zone which is maintained at temperatures between 773 K and 823 K. The feed is then cracked into gaseous hydrocarbons, naphtha, distillate and coke. The coke, with some of the heavy distillate, deposits onto the inert particles and then moves downward into the stripping zone which is filled with packing material. This allows the heavy liquid to be stripped from the coke and the inert particles. In the bottom gasification section the coke deposited on the inert particles is contacted with stream and air at temperatures around 1200 K to 1255 K to produce a hydrogen rich synthesis gas mixture. The synthesis gas is used in the stripping section of the reactor and as a fluidization gas for all three zones. Operating temperatures, total pressures and hydrogen pressures in the hydrocracking zones are between 773 K to 823 K, 2.7 MPa to 4.1 MPa and 0.5 MPa to 1.2 MPa

respectively The process has two modes of operation, a liquid mode with low and high severity and a gas mode. The high and low severity liquid modes produce a larger fraction of distillate and naphtha respectively. Yields from a feedstock with ^{0}API of 5.6 and carbon residue content of 16.1 wt. % were 35 wt.% naphtha, 15 wt.% distillate, 17 wt.% heavy oil and 33 wt. % of light gas and coke. This process is comparable to the Flexicoking process but is unique in that the particles used are alumina, and the reactor and regeneration are combined into one unit. Regeneration is conducted with steam containing oxygen and cracking takes place under a partial hydrogen atmosphere.

2.1.1.2.3 Fluidized Beds with a Riser

Reduced Crude Conversion (RCC) [18, 31, 32]

The Reduced Crude Conversion (RCC) technology is licensed by UOP Inc. The process is designed to handle heavy oils with a high content of coke precursors and heavy metal poisons that would not be acceptable for Fluid Catalytic Cracking (FCC) processing as well as crudes with substantial amounts of sulphur and nitrogen. Virgin atmospheric distillate feed is introduced into the reaction zone of a riser where it is contacted with hot, active and selectively conditioned catalysts, that are less susceptible to heavy metal poisoning. After a controlled residence time of about 3 to 4 seconds at temperatures ranging between 810 K and 895 K and pressures between 0.07 MPa and 0.25 MPa, vapour products are instantaneously separated, using a patented ballistic separator, from the catalyst and sent to a cyclone separator. The quick separation of catalyst from the

product stream ensures that undesirable secondary reactions are minimized. Spent catalyst is then regenerated at relatively low temperatures between 990 K and 1020 K. Yields from a feedstock with an ^{0}API of 19.2, a nickel and vanadium content of 65 ppm and a Ramsbottom carbon content of 6.9 wt.% were 4.1 wt. % gas, 55.6 vol. % gasoline, 15 vol. % distillate, 10 vol. % heavy oil and 10.8 wt. % coke which represented an overall conversion of 76.7 vol.%.

Heavy Oil Cracking (HOC)[33, 34, 35]

The Heavy Oil Cracking (HOC) process is licensed by M.W. Kellogg Co. and is a special version of the typical FCC process in which reduced crudes are cracked in a riser at optimal conditions. Typically in a FCC unit the riser outlet temperature is used to determine operating conditions, reaction kinetics and yields but riser inlet temperatures can be at least 40 K higher. With gas oil cracking, catalyst regenerator temperatures are rarely higher than 975 K and catalyst deactivation is not significant. However, with heavy oil cracking, catalyst regenerator bed temperatures must be higher to burn-off the greater quantity of coke and regenerator bed temperatures can get as high as 1035 K to 1255 K. These higher regenerator bed temperatures affect the riser inlet temperatures, since regenerated catalyst is introduced at the riser inlet. More importantly, high regenerator bed temperatures also cause hydrothermal deactivation of the catalyst. In order to control regenerator bed temperatures HOC units are equipped with internal bed coils and catalyst coolers. Heat removed is used to produce high pressure steam. The HOC unit also has

complete carbon combustion and a single step regenerator design. Typical riser operating temperatures and pressures are between 797 K and 802 K and around 0.1 MPa respectively. Yields from a mixed crude with an ^{0}API of 20.36 and with 4 wt.% C.C content were 4.1 wt.% dry gas, 85.1 wt.% oil and 10.8 wt.% coke.

Another approach to catalyst regeneration in Fluidized Catalytic Cracking (FCC) units is to undertake the process in a two step method. The design by Total Petroleum Inc. of these FCC units for heavy resid upgrading adopts this approach [36, 37]. The first step to catalyst regeneration is conducted at temperatures around 970 K to prevent hydrothermal deactivation and approximately 60 % of the carbon and most of the hydrogen is burned-off. In the second regeneration step the catalyst can be treated at a higher temperature around 1070 K since the occurrence of hydrothermal deactivation has been reduced by the removal of most of the hydrogen in the first step and the combustion becomes purely a graphite burn. Typical riser operating temperatures are between 773 K and 833 K at 0.1 MPa.

2.1.2 Processing with Coke Minimization

2.1.2.1. NON - CATALYTIC

2.1.2.1.1 Without Hydrogen

Visbreaking [38,39]

Visbreaking technology, first used in the early 1930's and 1940's for mild pyrolysis of crudes to produce an incremental gasoline and to reduce fuel oil viscosity, is being re-

considered for heavy oil upgrading. Visbreaking requires a low-cost conversion of standard equipment and can be implemented quickly. The visbreaking technology is based on the straight thermal conversion of the crude and can be divided into two types of processing schemes: coil cracker and soaker drum. In the coil cracker scheme, feed is first preheated then introduced into a coil cracking unit which operates at temperatures and pressures around 723 K and 0.5 MPa respectively and residence times of about one minute. The entire thermal conversion takes place in the coil crackers. The effluent is then quenched and sent to a fractionator. Visbreaking with a soaker drum scheme is very similar; feed is preheated and fed to a visbreaking furnace and on to a soaker drum which operates at slightly lower temperatures and longer residence times than the coil cracker unit. Operating temperatures are between 700 - 716 K and residence times are between 10 -20 minutes. Each process has its own advantage and disadvantage from compactness of design to ease of servicing and product yields. With the coil cracking unit, yields from a Mid-East Vacuum Resid with an ^{0}API gravity of 8 and C.C. content of 15.5 wt. % were gas - 3.5 wt.% , oil - 18.6 wt.% and residue - 77.9 wt.%. With the soaker drum unit, yields from a Mid-East with an ^{0}API gravity of 10.3 and C.C. content of 16.5 wt.% were gas - 2 wt.%, oil - 34 wt.% and residue - 64 wt.%.

2.1.2.1.2. With Hydrogen

Hydrovisbreaking [40]

Hydrovisbreaking processes differ from visbreaking processes in one significant aspect, the use of hydrogen. Hydrovisbreaking like visbreaking is often used to make heavy oils

more transportable. In a typical visbreaking process scheme, feed is preheated either through heat exchange with a product stream or directly then introduced into a visbreaker, soaker type, where it is reacted under a hydrogen blanket. The product stream is then sent to a separation unit. Operating conditions for hydrovisbreaking are temperatures between 650 K and 700 K and pressures between 8 MPa and 9 MPa. Typical yields for a feedstock with an ^{0}API gravity of 10.2 and C.C content of 14.5 wt.% were gas - 15 wt. %, gas oil - 58 wt.% and residue 27 wt.%

Donor Solvent

Donor solvents were first used in coal liquefaction processes in the early 1930's, however it was not until the late 1950's that the process was considered for petroleum processing. These processes are important since they are the starting point for many technologies used currently in industry and can be found in combination with other processes.

HDDC[41] & HDDV[42, 43]

The HDDC (hydrogen donor diluent cracking) and HDDV (hydrogen donor diluent visbreaking) processes were investigated by Exxon Research and Engineering in the 1950's. The HDDC process was developed to thermally crack crude residua to more valuable products by using a reaction diluent. The process is based on the idea that the hydrogen donor solvent will provide readily available hydrogen to aromatic and

asphaltenic radicals. This hydrogenation prevents further dehydrogenation, condensation and polymerization reactions which can lead to coke formation. The diluent is typically a donor solvent like tetralin (tetrahydronaphthalene) which is dehydrogenated giving up four molecules of hydrogen and can be catalytically (easily) hydrogenated to naphthalene and then recycled. Other diluents like partially hydrogenated refinery process streams were found to be efficient and practical hydrogen donors. The HDDC process operates at temperatures between 720 K to 740 K and pressures between 2.6 MPa and 3.1 MPa with a ratio of diluent to feed between 1 and 5. Yields from an asphaltic crude with an ^{0}API of 1.2 and C.C. content of 25.3 wt.% were coke - 1.0 wt.%, $< C_5$ - 4.9 wt.%, C_5 - 727 K - 44.1 wt.% and > 727 K 45 wt.% which translated to a conversion of approximately 55 wt.%.

The HDDV process is very similar to the HDDC process except that hydrogenation takes place in the visbreaker units, i.e., in the coil reactor or combination coil and soaker unit. Operating temperatures are between 715 K and 730 K and pressures between 2.4 MPa and 2.8 MPa. Yields with the HDDV are slightly lower than with the HDDC process, e.g. with a feed of ^{0}API 3.8, C.C. content of 24.6 wt. % conversion was approximately 36 wt.%, $< C_5$ 2 wt.%, C_5 - 727 K - 33.6 wt.% and > 727 K 64.4 wt.% .

Donor Refined Bitumen (DRB) [44, 45, 46]

The Donor Refined Bitumen (DRB) process is licensed by Gulf Canada. This process

uses a petroleum derived hydrogen donor solvent stream to convert heavy oils and bitumens to lighter products. The raw bitumen or heavy oil is first separated by a series of flashing units to produce overhead distillates which are sent directly to a crude blending facility. The remaining vacuum residue (777 K + fraction) is blended with the donor stream and raised to the desired reaction temperatures in a tubular furnace. Similar to other donor solvent processes, hydrogen is transferred from the donor solvent stream to thermally generated free radicals from the residuum. The donor stream is then recovered by distillation and rehydrogenated in a fixed bed hydrotreater. The DRB operating temperatures are between 683 K and 733 K and operating pressures are around 5.5 MPa. The conversion is typically around 70 wt.% of the 777 K + fraction with coke yields between 5 - 10 wt.%. For example, the processing of Athabasca residuum (777 K +) fraction yields 5.2 wt. % light gases, 23.7 wt.% naphtha, 7.7 wt.% middle distillate, 30 wt.% gas oil and 33.1 wt.% residuum.

2.1.2.2 CATALYTIC

2.1.2.2.1 With Hydrogen

Slurry Processes

CANMET Hydrocracking [18, 47, 48, 49, 50, 51]

The CANMET hydrocracking process was developed by the Energy Research Laboratories of Energy Mines and Resources Canada with Petro-Canada in the early

1980's. The process is now licensed by Petro-Canada and Lavalin. The process was designed to upgrade heavy crude oil or refinery vacuum bottoms. The process is described as a high conversion, high demetallization, residuum hydrocracking process which uses an additive to suppress coke formation and achieve high conversion of heavier fractions. The feed is mixed with a small amount of processing additive (a proprietary iron-coal compound) that is prepared easily and at a low cost. The mixed-feed additive stream is heated and contacted with hydrogen, and then sent to an upflow reactor. Product is removed from the overhead and separated into a hydrogen rich recycle gas stream, process gas, distillate and a residual pitch fraction. This technology boasts being able to handle a wide feed stock variability , very high metals , high asphaltene and CCR content. Typical operating conditions are temperatures between 708 K to 728 K and pressures around 13.6 MPa. Yields from a Light Arabian (827 K +) residuum with a 87 wt. % pitch conversion were C_4 - 478 K - 28.4 vol. %, 478 K - 616 K- 34.8 vol. %, 616K - 797 K - 32.8 vol. % and 797 K + 9.2 vol. %, asphaltene conversion 51 wt.%.

Veba Combi Cracking (VCC) [52, 53]

The technology of the VCC process is based on the former Bergius-Pier technology for the conversion of heavy residual oils and coal into light distillate. The Berguis-Pier technology utilized high pressure hydrogenation technology in direct coal liquefaction processing during the 1930's. A brief description of the process is as follows : the heavy oil is contacted with hydrogen and an additive (activated coke, lignite carbon black, red

mud or iron II oxide) and preheated before entering a liquid phase hydrogenation reactor which is operated in the upflow mode. Usually there are three serially connected vertical slurry phase reactors. Unconverted feed and additive are separated from the gaseous products and recycle gas in a hot separator operated at the same temperature as the reactor. The bottoms product from the hot separator is then cooled in a vacuum distillation unit to recover additional distillate. The gaseous distillate products enter a gas phase hydrogenation fixed bed catalytic reactor which operates at the same pressure as the liquid phase reactors but at lower temperatures and under trickle bed flow conditions. This second reactor system provides hydrotreating and mild hydrocracking. After cooling and condensation the gas and liquid products are separated in a high pressure cold separator. The liquid product is the synthetic crude.

The VCC technology has claimed that one of its main advantages is its feedstock flexibility and its lack of dependence on feedstock quality at high conversion mode of processing. Conversion of 773 K + fraction ranges between 85 wt. % to 95 wt.% and 35 wt. % to 45 wt.% for several feedstocks at the higher and lower operating temperatures of the liquid phase hydrogenation reactors respectively.

HDH [54, 55]

The HDH process is licensed by Intevep, Venezuela and development of the process began in the early 1970's. The basic premise of the HDH technology is a high

conversion, hydrocracking process for increasing liquid yields and decreasing fouling in the reactor by the removal of polynuclear hydrocarbons from the unconverted residuals and recycling the upgraded, polynuclear hydrocarbon free residual to the hydrocracker reactor. Polynuclear hydrocarbon is defined as xylene soluble material which is known to contain coke precursors in the hydrocracking reactions. Heavy crude or residuum feedstock is preheated and mixed with a typical hydrocracking catalyst such a Co-Mo on alumina, red mud and iron ores. The preheated feed and catalysts are mixed with hot hydrogen and fed to the hydrocracker. Typically the reactor is an upflow slurry reactor although investigations have been carried out with ebullated bed type reactors (premixing is not required with this type of reactor). The effluent from the hydrocraker is then separated into a light hyrocarbon stream and a residual hydrocarbon stream. The residual stream is then further separated in a vacuum flash unit and the vacuum residual is treated with a solvent which separates the polynuclear hydrocarbons. The raffinate from the solvent washing step is recycled to the reactor.

It was found that the amount of polynuclear hydrocarbon removed is dependent on the solubility or alternatively the incompatibility of the light hydrocarbon solvent with the residual. For example, when kerosene (463 K to 603 K) with a 12 wt.% of aromatics is used as the solvent fewer polynuclear hydrocarbons are separated in comparison with naphtha (323 K to 463 K) or alkanes (hexane to octane). Typical operating conditions for the HDH process are temperatures between 693 K and 724 K and pressures around 13 to 14 MPa. A 472 K resid of heavy Cerro Negro Venezuelan crude was processed in an

ebulatted bed at 693 K and 13.8 MPa. A conversion of 55 wt. % of 783 K + fraction was obtained with kerosene as the solvent in the separation step. Conversions in the upflow reactor were significantly higher at 93 wt. % conversion of the 783 K fraction with a Zuata Venezuelan heavy crude ($API^0 = 3$). Operating temperature and pressure in the reactor were 724 K and 13.1 MPa respectively with kerosene employed as the solvent.

Hyvahl C [56, 57]

The Hyvahl C process is licensed by the Institut Francis du Petrole (IFP). The process utilizes soluble salts of metals belonging to the Vb, VIb, VIIb and VIII groups, e.g., molybdenum, tungsten, cobalt and nickel compounds. The catalyst is introduced into the reactor as a solution in an organic solvent or as an aqueous solution. In the typical process stream the catalyst solution is injected into the fresh hydrocarbon feed to a concentration between 20 and 100 ppm by weight. The mixed stream is heated in a furnace operating at temperatures between 693 K to 743 K and then passed into the reactor with hydrogen. The reactor contains a bed of rings made of solid refractory material ,i.e., not porous and without internal surfaces. Typical operating conditions in the reactor are temperatures between 653 K and 703 K and pressures between 9 MPa and 15 MPa. The reactor effluent is then sent to a high pressure separator which separates the stream into a hydrogen and light hydrocarbon gas phase and a liquid phase which contains the suspended catalyst. The gas phase is further treated to remove any hydrogen sulphide and then recycled to the reactor. The liquid phase is further separated at low pressure into two

fractions : < 623 K and a residue . The residue contains the > 623 K boiling hydrocarbons and the divided catalyst (as sulphides.) The liquid stream is cooled to 473 K and washed with a light aromatic hydrocarbon. The mixture is then decanted and separated into catalyst and hydrocarbon. The hydrocarbon raffinate which is a mixture of light aromatic solvent and residue is sent to the fractionator.

Ebullated Bed

LC Fining [58-64]

The high conversion LC-fining process is licensed by Lummus Crest Inc. The process was developed in the early 1980's and is an extension of the LC process designed for the hydrogenation of high boiling hydrocarbons. The high conversion LC fining process proposes the control/removal of coke precursors in three ways: a) extremely high hydrogen partial pressures or very active catalyst, b) coke precursors can be maintained in solution by adding diluents or by recycle of a suitable product fraction, c) coke precursors can be removed by filtration or centrifugation. The process utilizes an ebullated bed catalytic reactor. In a typical process scheme, feed and hydrogen are heated separately and then sent to the ebullated reactor in upflow, through an expanded bed of catalyst. A portion of the liquid is trapped at the top of the reactor and recycled to the bottom. This provides the velocity for bed fluidization and also helps in temperature control so that the reactor operates isothermally. Typical reactor operating conditions are temperatures between 672 K and 727 K and pressures around 15.5 MPa. Catalyst is replaced

replaced continuously and hence reactor shutdowns are minimized. The reactor effluent is sent to a high pressure - high temperature separator. The vapour stream from the separator is let down in pressure, heat exchanged and sent for condensate removal. The previous step is a major difference from most conventional high pressure recycle gas configurations and boasts considerable savings. The liquid stream from the separator is let down in pressure and passed onto a recycle stripper. The liquid recycle is cooled to temperatures in the range between 477 K and 588 K

The recycle stripper step separates coke precursors, heptane and toluene insolubles, from the liquid recycle prior to introduction into the reactor. This coke precursor removal step allows for higher rates of conversion and reduces plugging of the catalytic bed. The recycle is provided to minimize the ratio of mid-distillates to residue in the liquid phase in the lower hydrogenation zone. Typical yields from a heavy vacuum bottoms with an API° of 4.4 and C.C content of 22.15 wt.% were gas - 6.4 wt.%, oil - 85.9 wt.% and coke - 7.7 wt.%.

H-Oil [65-69]

The H-Oil catalytic hydroconversion process is licensed by the Hydrocarbon Research Inc. and Texaco. The heart of the H-Oil process is its ebullated bed reactor. The reactor is a backmixed, isothermal reactor designed to overcome typical problems encountered with fixed-bed catalytic reactors during processing of heavier residual feedstocks. In a typical

reaction scheme, feed and hydrogen enter the reactor at the bottom while catalyst is fed from the top. Feed and hydrogen are then pumped upward through the catalyst bed which helps to maintain bed fluidization. The reactor is also equipped with an internal recycle conduit which further ensures that the catalyst, feed and gas are evenly distributed and that the catalyst is kept in random motion. This constant backmixing prevents plugging of the catalyst bed with solid entrained in the feed or deposited on the catalyst.

Vapour product removed from a vapour space at the top of the reactor - is cooled, and condensed partially. The gaseous portion which is mostly hydrogen is purified, reheated and recycled to the reactor. A portion of catalyst - free heavy effluent from the reaction zone is also recovered and fractionated. A sample of liquid in the boiling range of either 633 to 783 K or 783+ K is recycled to the reactor along with the feed. In the case of 783+ K recycle a higher fresh feed space velocity is required to obtain the same residuum conversion and the product distribution would be yield a higher concentration of heavy gas oil. If the 633 to 783 K recycle is used a lower fresh feed space velocity is employed and a higher product yield of naphtha can be obtained. Conversions from a Kuwait vacuum bottoms without and with recycle of the 783 + K fraction were 89.3 wt. % and 92.8 wt.% of the 783 + K fraction respectively. Operating conditions were temperature around 727 K and hydrogen pressure around 15.5 MPa. Yields from Athabasca bitumen with an API of 8.3 and 783 + K fraction of 51.4 wt.% and recycle of the 783 + K were gases - 8.3 wt.%, C_4 - 466 K - 15.9 wt.%, 466 - 550 K - 15.3 wt.%, 550 - 793 K - 56.6 wt. & and 783 + K - 5.2 wt. %.

Fixed Bed

Asphaltenic Bottom Cracking (ABC) [18, 70-73]

The ABC (asphaltenic bottom cracking) process is licensed by the Chiyoda Chemical Engineering & Construction Co. Ltd. The process is a catalytic hydrotreating process for heavy oils and residua. The process boasts a proprietary catalyst which is capable of hydrocracking asphaltenes into heptane soluble materials while decreasing the vanadium content of heavy crudes at a lower hydrogen consumption than existing desulphurization catalysts. The process units consists of a fixed-bed high pressure catalytic reactor and a solvent deasphalting unit. Feed is mixed with asphalt from the solvent deasphalting unit and fed to the reactor with hydrogen The reactor effluent is then sent to a series of high and low pressure separators which separates the hydrogen, dry gas and hydrogen sulphide. The effluent is then treated in a solvent deasphalting unit whereby the deasphalted oil and asphalt are separated. Since the unreacted asphalt is recycled, very high conversions can be obtained. Typical operating conditions are temperatures between 633 K and 703 K (usually around 683 K) and pressures between 8.9 MPa and 17.7 MPa (usually around 13.8 MPa) Yields from a Khafji vacuum resid with an API^0 of 5.08 and C.C. content of 23.6 wt.% were gas -2.4 wt. %, deasphalted oil - 75.8 wt.% and asphalt - 21.8 wt.% in the once through process.

RCD-BOC [74, 75]

The RCD -reduced crude desulphurization and BOC - black oil conversion processes are licensed by UOP Inc. Process Division. The RCD process removes contaminants such as nitrogen, sulphur and heavy metals from reduced crudes. The process employs a fixed bed catalytic reactor operating at moderately high hydrogen pressures. The BOC process is an extension of the RCD process and combines hydrocracking and resid desulphurization of vacuum bottoms. The process, which also utilizes a fixed bed catalytic reactor, achieves a 70% - 80% desulphurization and 60 % - 70 % conversion of vacuum bottoms. The process can be combined with an FCC or hydrocracker unit so that products from the BOC process can be further treated to produce kerosene. In a typical BOC process scheme, hydrogen and vacuum bottoms are fed separately to a heater and then mixed at the entrance of the fixed bed catalytic reactor. To prevent thermal degradation and premature coking of the catalyst, temperatures are controlled carefully and catalytic conversion of the non-distallables is limited to approximately 70 % of the total projected conversion. Typical operating conditions are temperatures between 653 K and 693 K and pressures around 18 MPa. In this step along with hydroconversion, sulphur, asphaltenes and metals are also removed. The effluent from the reactor is sent to a hot separator and the liquid product from this unit is further processed in a thermal conversion heater. The overhead vapours from the reactor are cooled, separated and the hydrogen is recycled to the reactor. The effluent from the conversion heater is then sent to a series of flash drums and vacuum columns where the distillable gas oils are recovered and residuals are sent to be blended with the FCC slurry oils. Typical yields from a San

Ardo crude with an API^0 of 13.8 and C.C. content of 8.52 wt.% were gas - 0.6 wt. %, C_5 - 616 K -24.2 wt.%, 616 K - 839 K - 56.1 wt.% and coke - 21.8 wt.%.

2.2 Overview of Heavy Oil Upgrading

It is hoped that the reader will appreciate the complexity and variety of heavy oil / bitumen upgrading processes, as outlined in the above section, which in many cases reflect an art and not a science. The goal of all the processing technologies however is the same - operate at optimum conditions to produce the highest quality product in the most cost effective manner possible. The process of petroleum refining is viewed by many as technology based, for the most part, "on rules of thumb", heuristic knowledge, instinct and experience. This approach has been successful in the past but, as our need to obtain a greater quantity of superior product from inferior resources and more importantly - from more difficult to handle and process feedstocks - increase, this approach must be reviewed. One of the greatest challenges in fine tuning heavy oil upgrading technologies lies in the enormous complexity and variability of petroleum molecules. Petroleum molecules are a by-product of organic matter and thus rightly reflect the diversity of life. But just as we have common characteristics in all life forms we must seek such characteristics in petroleum molecules.

A plot of pressure versus temperature showing operating conditions for the heavy oil upgrading processes is presented in Figure 2.2.1. Clearly, there are regions of similar operating strategies. The high temperature and pressure processes such as the H-Oil,

VCC, HDH and CANMET hydrocracking all operate in the range between 650 - 750 K and 12 - 15 MPa while the donor solvent processes such as the DRB, HDDC and HDDV operate over a broader range but at lower severities between 650 - 850 K and 2.5 - 6 MPa with the final region occupied by the carbon rejection processes operating at higher temperatures from 750 - 1000 K but at atmospheric pressure. Not surprisingly the over all yields of "coke" or in most cases the least desired product is a function of operating temperature and pressures. Coke is defined as a solid by-product with a density greater than 1 g/cm^3, H/C ratio of less than 1 and as being insoluble in toluene or benzene. The high temperature and pressure processes predict yields with the lowest amount of coke while the carbon rejection processes produce the highest yields of coke. It is hoped that this investigation of phase behaviour will elucidate why operating conditions appear to be compartmentalized into specific regions of temperature and pressure.

The wide variety of processing schemes has arisen for many reasons: variability in feedstocks, different types of catalyst, specific product value, and simply different operating philosophies. For example in the case of varying feedstocks, feeds with very high sulphur content (sour crudes) must be processed in a slightly different manner. Similarly feeds with very high heavy metals contents and high aromatic content poses different challenges. Often differences in feedstocks are a function of origin (feeds from the Middle East have a lower sulphur content than feeds from Venezuela.) One of the main reasons for the diversity of operating schemes is the large number of companies devoted to petroleum refining, each of which has developed in - house technologies and

individual operating strategies. Consequently, as the number of processing schemes has increased over the years, the number and variety of catalysts have increased exponentially. Since attention has been refocused on the upgrading of heavy oils and bitumens many well established petroleum refining schemes have been modified. And as a result many of the processes reviewed are based on much older operating strategies, e.g., the H-Oil process is a modification of the H-Coal process developed early in this century. Finally, operating strategies are obviously a function of economics. Higher severities (higher temperatures and pressures) translate to higher operating costs and, as a result, different methods to reduce costs have been explored. For example, the donor solvent process are one attempt to improve conversions and yields of valuable products while maintaining lower severities.

Approaches to heavy oil / bitumen upgrading by and large reflect "coping" within existing technological frameworks. However operators are good at exploiting local optima and over time relatively high yields and conversions are realized even with difficult to process feedstocks. The pattern which has emerged is a grouping of high pressure and low pressure processes, all successful, with a large pressure gap in between (area A on Figure 2.2.1). This gap arises even though the feeds are kinetically active under these conditions. Such a pattern is consistent with the occurrence of multiphase behaviour, an intermediate pressure phenomenon, as the appearance of three or more organic phases would play havoc with processes designed to handle liquid and vapors.

Figure 2.2.1 Heavy Oil Upgrading Processes

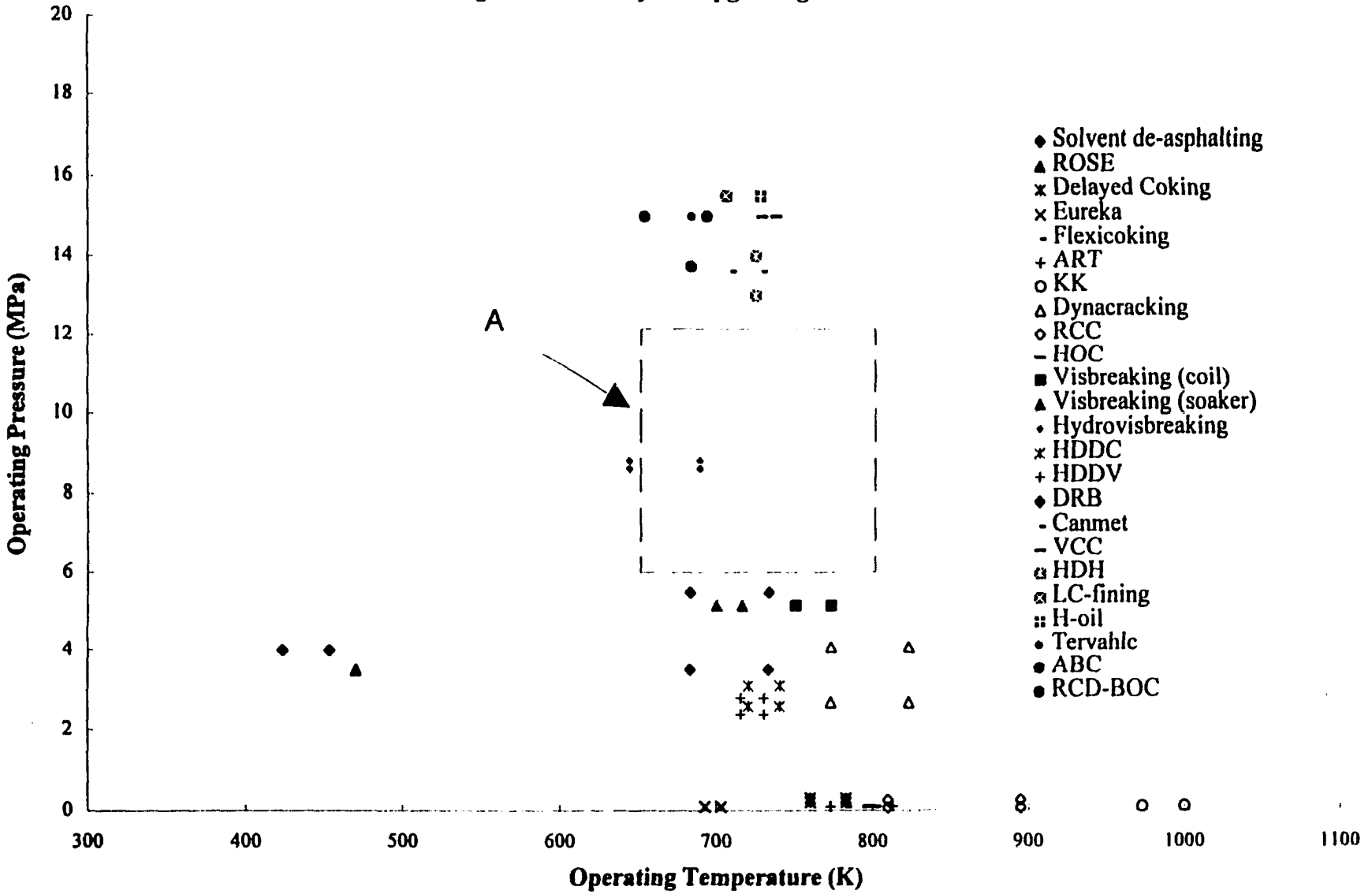

2.3 Complex Phase Behaviour

2.3.1 The Phase Rule

Consider a system composed of C components existing in equilibrium in P phases, and assume that all C components exist in all of the phases. In addition to temperature and pressure, the intensive state of each phase is defined by (C - 1) composition variables such as mole fractions or concentrations. The total number of variables including temperature and pressure that may vary independently is, therefore, (C + 1) for each phase. For P phases there are P (C + 1) variables. Now consider the number of equations available to solve for the P (C + 1) unknowns. These equations express the equilibrium between phases. Thus (P - 1) equations are obtained by equating the temperature of the phases. An equal number of equations is also obtained by equating the pressure of the different phases. Finally, a set of (P -1) equations may be written for the chemical potential of each component in the P phases. Adding these equations gives a total number of (P - 1)(C + 2) equations. When this number of equations is subtracted from the number of unknowns, the number of independent intensive properties that may be varied to define the intensive properties of the phases of the system is obtained and the result is referred to as the Gibbs phase rule:

$$F = C - P + 2$$

Applying the Gibbs phase rule to a single-phase single-component system, the number of intensive properties required to define the state of the system is equal to 2. Thus intensive properties such as temperature and pressure can be varied independently. Similarly, for a

single component system existing in two phases one variable is independent with three phases and the state of the system is defined by a point i.e. a triple point.

The Gibbs phase rule also gives the dimensions of the space needed to represent the complete phase behaviour of a *C* component system e.g. with a minimum number of phases, P =1, for the single-component system , F =2, and thus the phase behaviour can be represented in a two dimensional pressure - temperature plane. For a two component system , F =3 and thus a three dimensional space, pressure-temperature-composition space, is needed to represent the system.

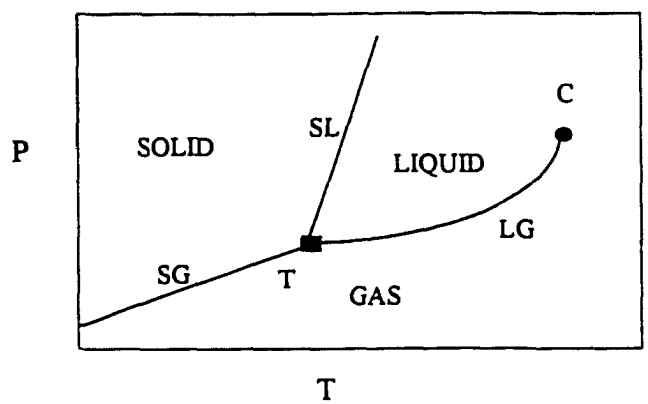

Figure 2.3.1 - Typical phase behaviour for a single component system

For a single component system a typical phase diagram is shown in figure 2.3.1. The point where three single phase regions meet is called a triple point (T) and, similarly, the point where two phases (liquid and gas) become identical is designated as the critical point (C). Liquidous, sublimation, vapour pressure curves separate solid and liquid, solid and gas and liquid and vapour regions.

2.3.2 Binary Mixtures

For a binary system the phase rule tells us that the maximum number of phases that can coexist is equal to four ($F = 2 + 2 - P$) and a three dimensional space is need to describe the phase behaviour where solid, liquid and gas phases can coexist in diverse combinations.

Now let us consider two liquids L_1 and L_2 that are not completely miscible at all conditions. If the mutual solubility of the two liquids increases with temperature at a constant pressure to complete miscibility in all proportions, that region of liquid-liquid immiscibility is bordered by a liquid-liquid critical point (L_2=L_1). Other critical phenomena that can also arise are so - called L and K points. The L point is the low temperature point where a light liquid becomes critically identical to a heavy liquid in the presence of gas (L_2=L_1G) and the K point is defined as the high temperature point where the light liquid becomes critically identical to the gas in the presence of a heavy liquid (L_2L_1=G). The L and K points are also referred to as the lower critical end point (LCEP) and the upper critical end point (UCEP) respectively. When a LCEP - L_2=L_1G and a UCEP - L_2L_1=G coincide three phases become identical, i.e., $L_2 = L_1 = G$ and this point is called a tricritical point.

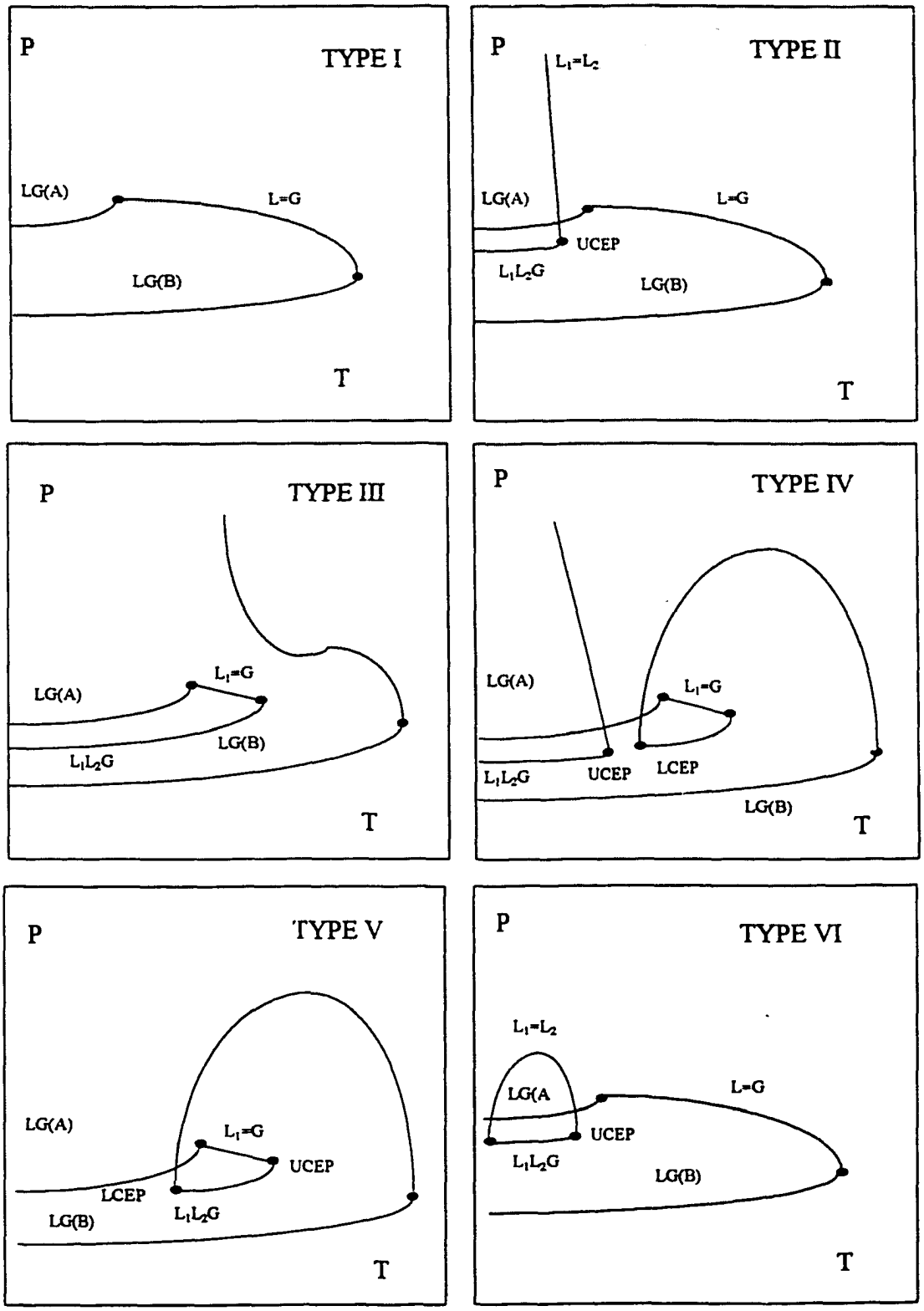

Figure 2.3.2.1 Van Konyenberg and Scott classification of fluid phase behaviour[88]

In 1980, Van Konyenberg and Scott [88] categorized the phase behaviour of binary fluids into six main types. These classifications reflect all possible combinations of critical and other phenomena for binary organic fluids. This classification scheme is shown in Figure 2.3.2.1.

In Type I phase behaviour the liquids are miscible in all proportions and only one critical curve is found, the liquid-vapor critical curve L=G which runs continuously from the critical point of component A to the critical point of component B. Type II phase behaviour shows a similar continuous liquid-vapor curve but the liquids are not miscible in all proportions and a liquid-liquid critical curve L_2=L_1 and a three phase line L_2L_1G are also present. The L_2=L_1 curve and the L_2L_1G curve meet at a UCEP where L_1 becomes critically identical to the gas phase in the presence of L_2 denoted by - L_2L_1=G. Notice that the liquid-liquid critical curve can run to infinite pressures. Type V phase behaviour is characterized by three phase equilibrium L_2L_1G with a LCEP, where L_1 and L_2 become critically identical in the presence of the gas denoted by - L_2=L_1G, a UCEP and a discontinuous critical curve. The first branch of the critical curve connects the critical point of the more volatile component with the UCEP and the second branch runs from the LCEP to the critical point of the less volatile component. In Type IV phase behaviour the three phase L_2L_1G has two branches. The low temperature branch shows a UCEP L_2=L_1G and is comparable with L_2L_1G equilibrium found in Type II systems. The high temperature branch shows a LCEP L_2=L_1G and a UCEP L_2L_1=G and is comparable with L_2L_1G equilibrium found in type V phase behaviour. In Type III phase behaviour, the two

branches of L_2L_1G found in type IV phase behaviour are combined, as are also, two of the three branches of the critical curve found for type IV. Type VI phase behaviour demonstrates three phase equilibrium - L_2L_1G with a LCEP $L_2=L_1G$ and a UCEP $L_2=L_1G$. The LCEP and UCEP are connected to a $L_2=L_1$ critical curve, which shows a pressure maximum. Another possibility is the existence of a second $L_2=L_1$ critical curve at high pressure with a pressure minimum - high pressure immiscibility. A more detailed explanation can be found in the literature [91].

2.3.3 Ternary mixtures

The classification scheme of phase behaviour for binary fluids as proposed by Van Koynenburg and Scott [88] provides a sound basis for understanding the phase behaviour of more complex mixtures. The interpolation of these six basic types of fluid behaviour has been utilized widely to predict and explain complex phase behaviour in systems with more than two components. One such example is the modelling of reservoir fluids [89, 90], as found in the oil recovery processes, where retrograde phenomena have been addressed.

Retrograde condensation of a heavy liquid in the presence of a light liquid phase and a gas phase is an important phenomena in reservoir engineering. In this situation, on decreasing the pressure at a constant temperature, the appearance and subsequent disappearance of a heavier liquid is observed in the three phase region (L_1L_2G). In order to explain this phenomenon a better understanding of the three phase region was needed.

Asymmetric binary mixtures of alkanes, which are models for oil recovery systems, with a heavy component (B) and a light component (A), have been shown to exhibit Type V phase behaviour (see Figure 2.3.3.1)[89] . In type V phase behaviour a three phase region

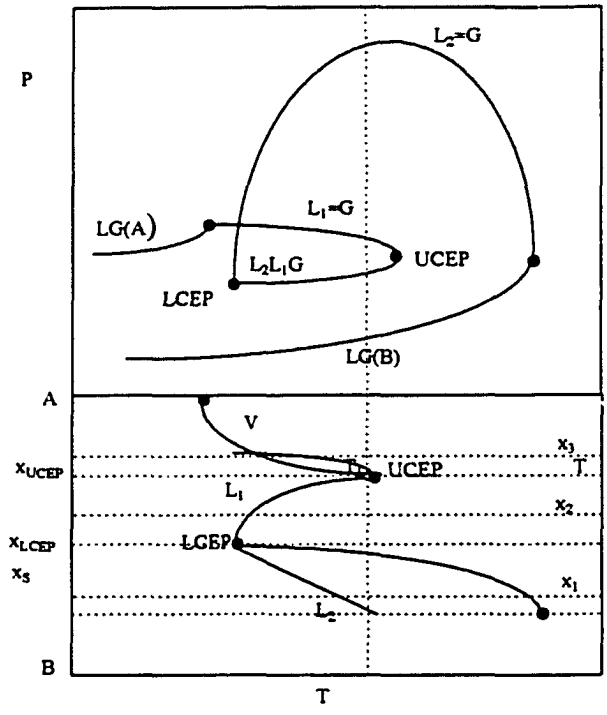

Figure 2.3.3.1 - Phase behaviour of asymmetric binary mixture showing Type V behaviour [89]

begins near the critical point of the light component A. It starts at a LCEP where component B rich heavy liquid phase (L_2) and component A rich light liquid phase (L_1) are critical in the presence of the gas and ends at the UCEP where the L_1 and the gas are critical in the presence of L_2. The critical curve is made up of two branches; one branch - L_1 = G which connects the critical point of component A to the UCEP and a second

branch - $L_1 = L_2$ which connects the critical point of component B to the LCEP. Now as we increase the number of components in this system from two to three the available degrees of freedom increase and, consequently, the L_1L_2G line becomes a region in the P-T space. Figure 2.3.3.1 shows the phase behaviour of an asymmetric binary mixture and Figure 2.3.3.2 a,b,c show the behaviour at mole fractions x_1, x_2 and x_3 where x is the mole fraction of the heavy component and $x_1 > x_2 > x_3$. For the highest concentration of the heavy component, x_1, the three-phase region starts at the point where the line x_1 = constant intersects the L_2 branch of the L_1L_2G curve and ends at the UCEP. In this case only part of the L_1L_2G curve can be observed. For the mole fraction x_2 the whole L_1L_2G curve can be seen and for the mole fraction x_3 a part of the L_1L_2G curve can be seen. Figures 2.3.3.2 a',b'and c' show the expansion of this system to a ternary mixture where the third new component is miscible in both of the other two components. Notice that the L_1L_2G curve becomes a region. The addition of a miscible third component to a binary system has been shown to shift the three phase region to higher temperatures and pressures [89] . Furthermore as the amount of the third component in the mixture increases the L_2L_1G region shrinks. Eventually, the LCEP and the UCEP coincide at the tricritical point. In Figures 2.3.3.1 a' and b' phase diagrams the retrograde condensation of the heavier liquid L_2 is possible and appears in the vicinity of the LCEP.

If a third component which is immiscible in both constituents of the binary mixture is added then the three phase region is shifted to lower temperatures but higher pressures and the L_1L_2G region is expanded [5] . Figure 2.3.3.3 shows P-T diagrams of the binary

mixture of n-decylbenzene + ethane with the addition of carbon dioxide (phase diagram I having the highest concentration of carbon dioxide and phase diagram IV showing just the binary). If the LCEP is present in the phase diagram with this particular mixture then retrograde condensation of the heavy liquid phase is possible. These findings were very significant and demonstrated that complex phase behaviour can be shifted in the pressure-temperature space by the addition of the appropriate component. For the present study hydrogen acts in much the same manner as carbon dioxide in the present case except the three phase region would be shifted to higher pressures i.e., the pressure effect would be greater. The effect of adding light gases can be anticipated by looking at the critical temperature of the light gas. The critical temperature of the following light gases are such that carbon dioxide > methane > nitrogen > hydrogen. Hence with the n-decylbenzene + ethane + carbon dioxide the three phase region is shifted to higher pressures and lower temperatures and the pressure "effect" and temperature "effect" are observed. As the critical temperature of the light gas decreases the temperature "effect" is less dominant and the pressure "effect" becomes more dominant. If hydrogen replaces carbon dioxide as the light gas then the three phase region would be shifted almost vertically up in pressure with very little shift in temperature.

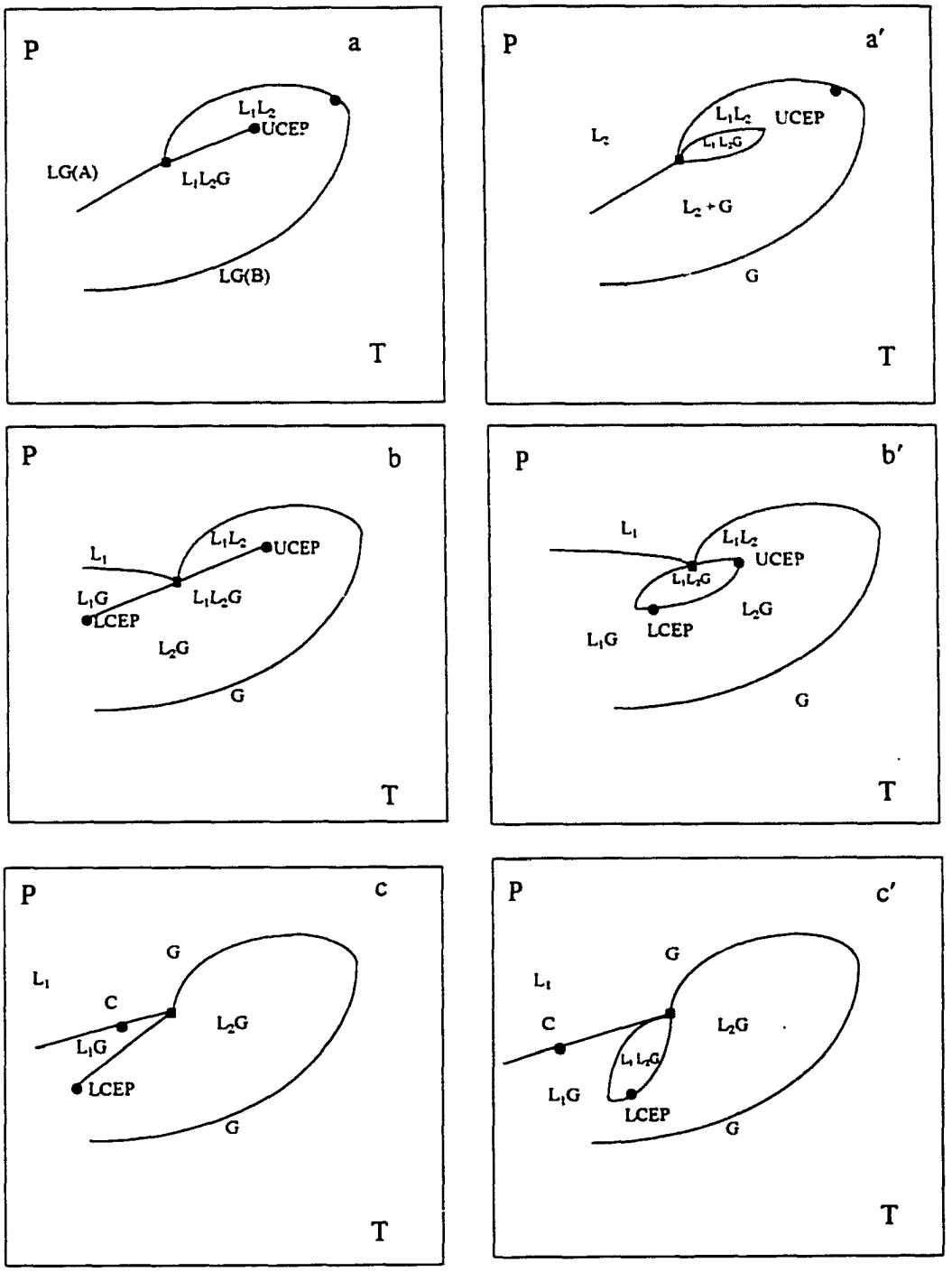

Figure 2.3.3.2 Expansion of P-T diagrams of Type V phase behaviour from binary mixtures to ternary mixtures [89]

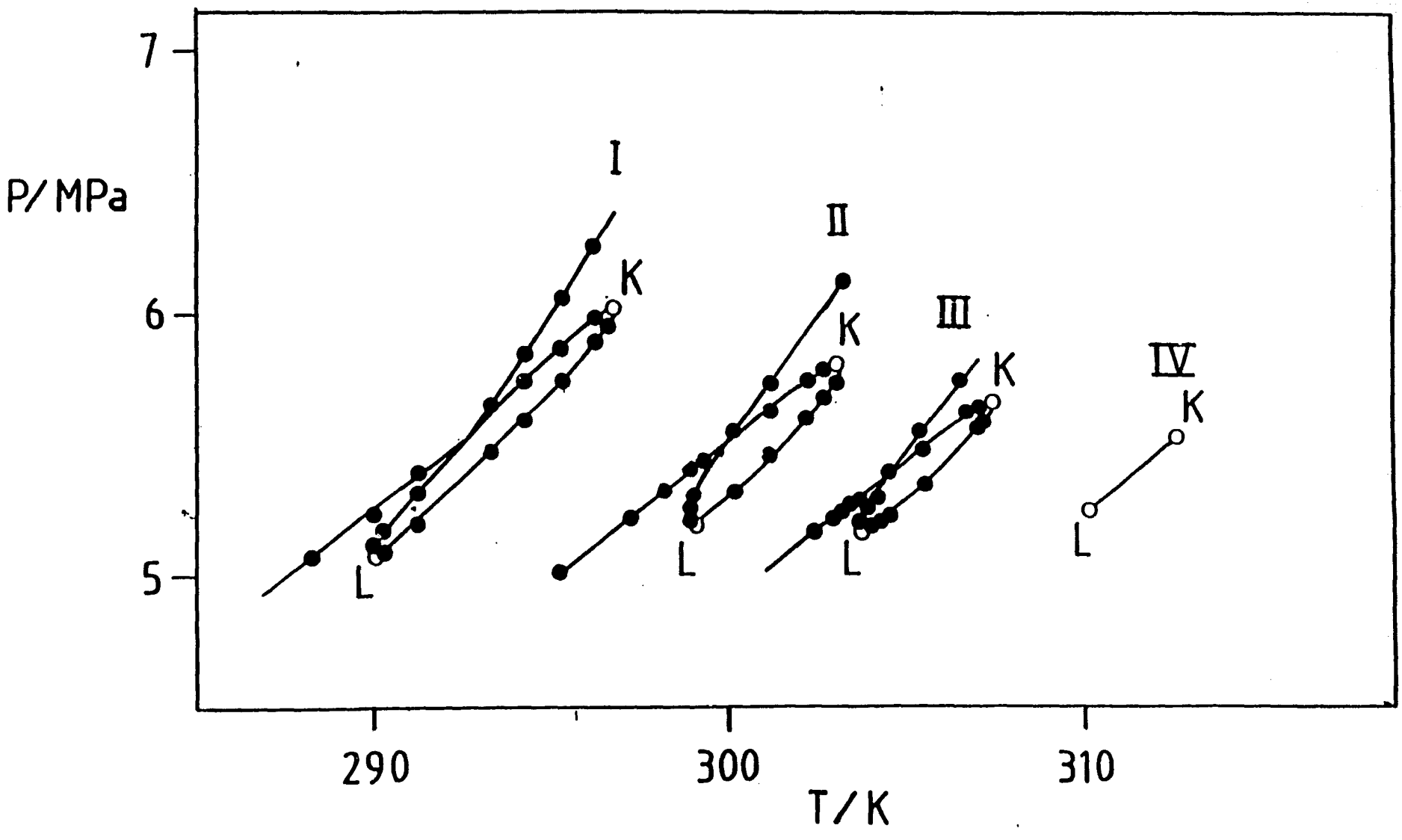

Figure 2.3.3.3 P-T diagrams of n-decylbenzene + ethane + carbon dioxide [90]

I) 40 mole % carbon dioxide, II) 20 mole % carbon dioxide, III) 10 mole carbon dioxide and IV) n-decylbenzene + ethane binary

2.3.4 Appearance of Solid in Binary Fluid Phase Diagrams

As can be expected the appearance of a solid phase can further complicate the phase behaviour and, conversely, it can also simplify the phase behaviour by masking the appearance of some types of phase behaviour. The phase behaviour characteristics of asymmetric binary mixtures of n-alkanes have been investigated previously and are characterized by type V phase behaviour [92]. Typically as the carbon number of the less volatile component increases, the triple point moves to higher temperatures and lower pressures. As a result the onset L_2L_1G shifts to lower temperatures and hence the LCEP is also shifted. This effect is more pronounced on the LCEP than on UCEP and consequently the L_2L_1G line lengthens. Figure 2.3.4.1 shows the possible effect on type V phase behaviour of a solid of the less volatile component (B) with increasing carbon numbers. If the triple point of component B is high enough, solid formation interferes with the three phase L_2L_1G line. As the carbon number of component B increase the SLG region shifts to higher temperatures and will ultimately intersect with L_2L_1G. This intersection point is called the quadruple point (Q) i.e., the point at which four phases are in equilibrium - solid, liquid $_1$ (more volatile component), liquid$_2$ (less volatile component) and gas.

Figure 2.3.4.1 shows the increasing complexity of the phase behaviour with increasing carbon number of the less volatile component B, with carbon number increasing from Figure 2.3.4.1 A to F. As the carbon number increases the appearance of a solid begins to suppress the three phase region and, in fact, leads to $L_2 = L_1$ becoming metastable as

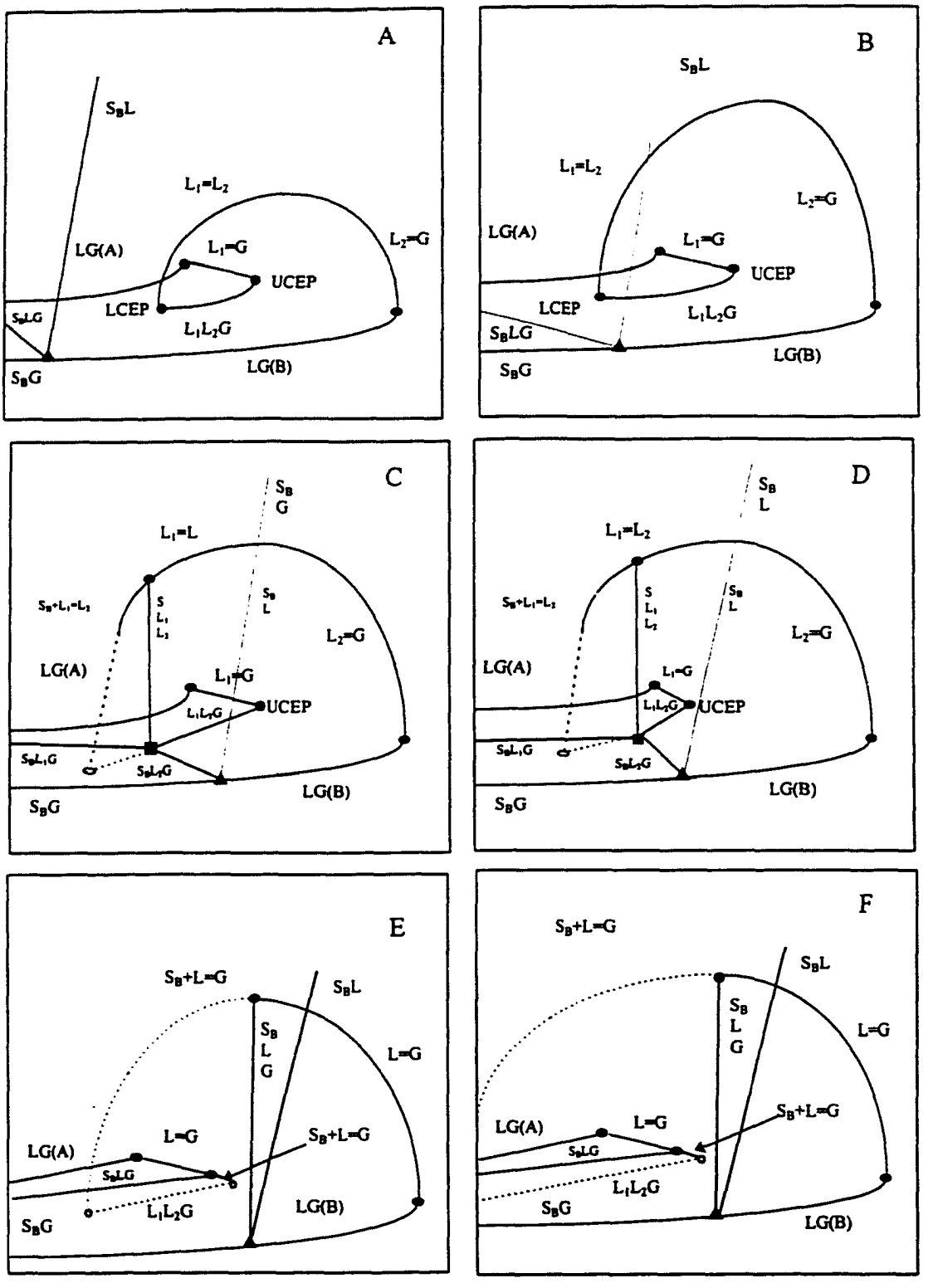

Figure 2.3.4.1 Effect of appearance of solid on Type V phase behaviour [92]

shown by the dashed line. Eventually the interference of the solid (with increasing carbon number) leads to total suppression of the L_2L_1G region.

2.3.5 Appearance of a Solid Phase in Ternary Mixtures

As with the extension of Type V phase behaviour for binary fluids to ternary fluids, the appearance of a solid in ternary mixtures can also be approached as an extension of the phase behaviour for binary fluids with the interference of a solid. Studies with reservoir fluid models [94] have shown that this approach is successful in describing the phase behaviour.

2.3.6 Appearance of a Solid Phase in More Complex Mixtures

The extension of binary fluid phase behaviour to more complicated mixtures provides a good theoretical approach for constructing phase diagrams. As the number of components increases the number of available degrees of freedom also increases and in the pressure - temperature space, points become lines and lines become regions etc. for every degree of freedom that becomes available. This extension leads to a very important consideration in the construction of phase diagrams and that is the sequencing of phase behaviour surrounding what would be points in space in binary fluids. Consider the expansion around a Q-point (SL_1L_2G point for a binary fluid). As it expands to a region in a multicomponent case the surrounding phases are of a specific sequence, i.e. the SL_1L_2G would be surrounded by the SL_1L_2, L_2L_1G, SL_2G and SL_1G, hence it would not be

possible to have direct phase transitions from say SL_1L_2G to SL. This constraint must be considered when constructing phase diagrams since it is often impossible to observe all phase transitions.

This theoretical approach to understanding the effect of a solid on complex phase behaviour has been applied to several systems and in particular to reservoir fluids. The system of propane + butane + ethane + phenanthrene [94], which is a model reservoir fluid, exhibited SL_2L_1G phase behaviour which was shown to be predicted by expanding the four phase behaviour associated with binary mixtures to more components. Figure 2.3.4.2 shows P-T projections for the propane + butane + ethane + phenanthrene system with a constant ratio of butane + ethane + phenanthrene and varying amounts of propane. This approach provided a sound theoretical basis for explaining the retrograde condensation that arises with reservoir fluids during recovery processes. It is this approach which will be used to develop phase diagrams and characterize the phase behaviour which may arise with heavy oil / bitumen mixtures.

While this cursory overview of phase behaviour and phase diagram theory provides a brief background to very complex phenomena it is not exhaustive and a more detailed explanation and general review can be found in the literature [93].

3.0 Experimental

3.1 Experimental Set-up

The arrangement of the experimental set-up is shown in Figure 3.1.1. Many pieces of the apparatus were obtained as a gift from Amoco Research Center, Naperville, USA. The building, assembly and testing of the entire experimental set-up took approximately two years to accomplish. The first main piece of equipment in the general layout is the Phillips MN-167 X-ray tube gun followed by the view cell. X-rays are emitted from the gun and are directed to the window of the view cell. The emerging x-rays are then directed to the Siemen Sirecon image intensifier located directly behind the view cell. The image intensifier enhances the x-rays and converts them to produce an optical image. This optical image is then picked by a KP 113 Hitachi CCD video camera fitted with a 35 mm imaging lens. This entire set-up of x-ray gun (view cell, image intensifier and video camera) is housed in a lead lined box which is equipped with a series of fail-safe switches. This safety set-up ensures that the x-ray gun deactivates once any of the doors of the lead-lined housing are opened. Since the video camera is also housed in the lead lined box any focusing of the lens requires the operator to remove a 90 kg lead covering. Since this procedure is tedious and time-consuming, a simple stepper motor operated focusing unit was assembled to allow the operator to adjust the camera from outside the lead lined housing.

Figure 3.1.1 Experimental Set-Up

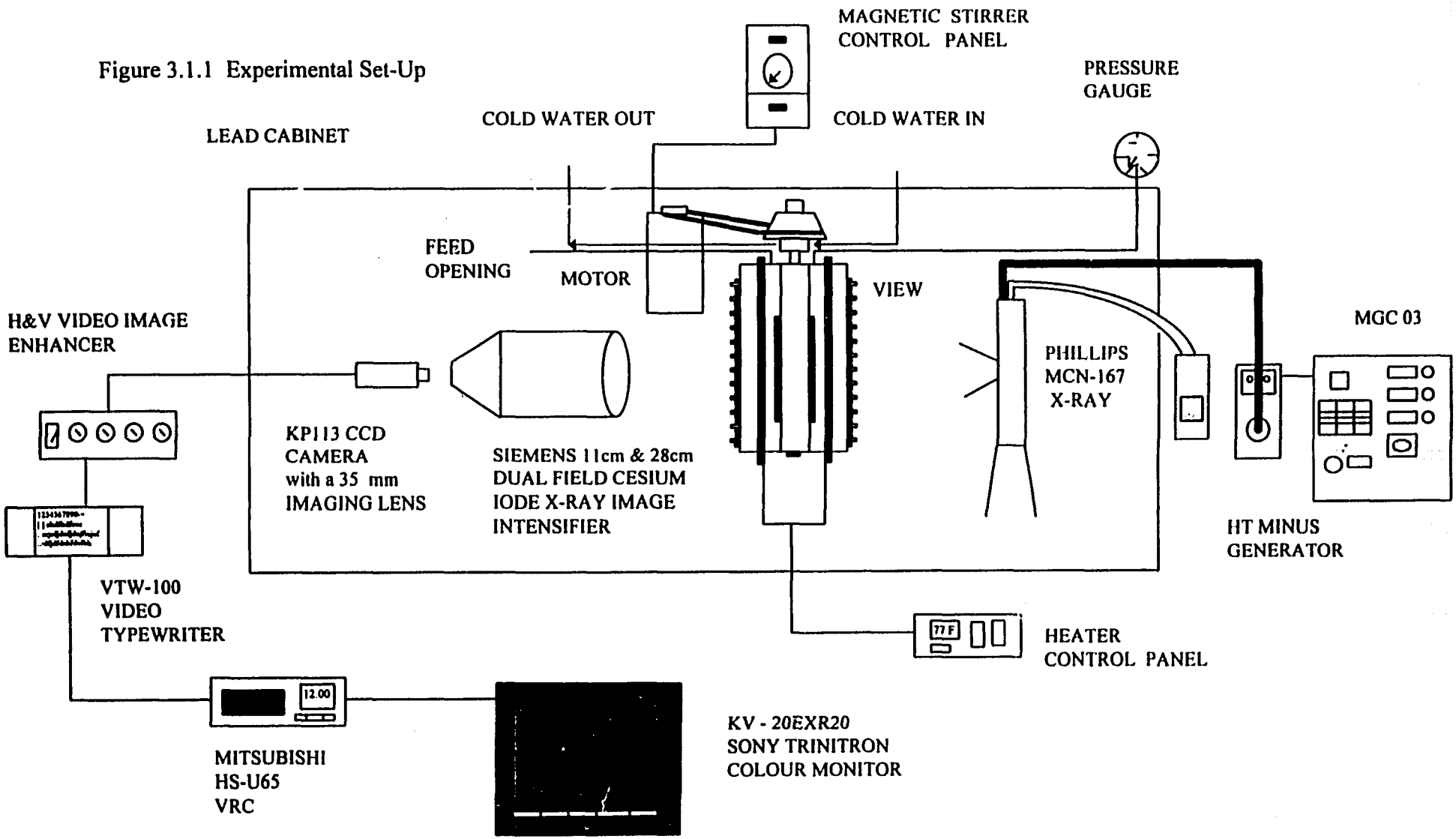

The camera sends a black and white video signal to a Vidicraft H&V image enhancer which is connected to a Mitsubishi Twin Digital/Swift Servo HS-U65 VHS video recorder and to a Sony Trinitron KV-20 EXR20 TV monitor. The video recorder is also connected to a VTW-100 video typewriter while allows the operator to record any pertinent information, like temperature and pressure, on the video tape during the experiment.

Once the image has been recorded on the video tape any frame can then be digitized using the Jandel Video Analysis Software. This processing package allows for pseudo coloring enhancement whereby a specific shade of gray is assigned a particular colour.

3.2 X-rays [76, 77, 78]

X-rays are a form of electromagnetic radiation and are identical in nature with visible and all other types of radiation that constitute the electromagnetic spectrum (ultraviolet, infrared, gamma - rays, microwaves and radio waves.). The wavelength of x-rays is between 1 A° and 1000 A°. X-ray photons are characterized by wavelength λ and energy E where λ(nm) $\cong$ 1.24/E(keV). When an electron accelerates through a potential difference it acquires kinetic energy; if the electron then collides with matter in its path, some or all of this energy will be dissipated. The dissipated energy is converted into heat, light and x-rays. More specifically x-ray photons are produced when a high energy electron beam decelerates as it approaches the electron cloud that surrounds the atomic

nucleus. Characteristic radiation is produced following the ejection of an inner orbital electron by high energy particles and subsequent transition of the atomic orbital electrons from states of high energy to those of low energy.

X-rays can be produced in an x-ray tube by acceleration of electrons to a high velocity in an electrostatic field and then suddenly stopping them by collision with a solid body placed in their path. The x-rays radiate in all directions from the spot on the target where the collisions take place. The x-rays are due to the interaction of fast-moving electrons with the electrons and positively charged nuclei which constitutes the atoms of the target. X-rays may be classified in two general groups according to the method in which they are generated i.e., in gas tubes or in high vacuum tubes.

Before the invention of vacuum tubes, x-rays were produced by gas tubes. A glass envelope filled with gas at a certain pressure is subjected to a high potential difference across the tube which will ionize the gas to form to positive ions. These positive ions can then bombard the cathode (cold) and liberate high energy electrons. The high energy electrons would then impinge on the anode and x-ray photons would be produced. Gas x-ray tubes are often plagued with operational difficulties and erratic behaviour inherent to the gas itself and the positive ion bombardment that takes place during operation. A high vacuum x-ray tube eliminates these problems by using a hot cathode to emit high energy electrons. The X-rays used for this project were generated by a hot cathode, high vacuum x-ray tube.

A typical configuration for a high vacuum, hot cathode, x-ray tube is shown in Figure 3.2.1. The x-ray tube is fundamentally a glass bulb which has been evacuated to attain a high vacuum equipped with a cathode - filament and an anode-target. The filament is of a high melting point metal usually tungsten. Electrons are emitted from the hot tungsten filament cathode and the quantity of electrons emitted is a function of the filament temperature and thus can be regulated by the amount of current passing through the filament.

When the tube is operated, the beam of electrons flowing from the cathode to the anode constitutes an actual flow of current which is directly measurable in mA. This value is taken as a measure of the intensity of the x-rays emitted by the tube. The filament is arranged in a cup shape to concentrate the flow of electrons on to a specific area of the anode, i.e., a focal spot. Some tubes are designed with two foci, a large focus used for radiography which utilizes the maximum current and a smaller focus that gives a reduced output and is used for fluoroscopy or image projection giving an enlarged image on the film.

The anode is a block of metal, which has a high thermal conductivity (usually copper), which carries a cathode disc or target. Again because of its thermal properties, tungsten is often used as the anode disc. The disc is positioned at 60^0 -70^0 with respect to the direction of the incident accelerated electrons. A small portion of the energy dissipated by the high energy electrons is in fact used to produce x-ray photons , the rest of the energy

is transformed into heat. The amount of heat liberated is significant and must be removed from the anode to prolong the life of the x-ray tube. The x-ray tube used in this project employed a water cooling system to remove the heat and is equipped with an automatic shut off to ensure that over heating of the x-ray tube is prevented.

When a monochromatic beam of x-ray photons falls onto an object three main phenomena may occur, absorption, scatter and fluorescence (Figure 3.2.2). These phenomena form the bases of three important x-ray analysis techniques; the absorption phenomenon is the basis of radiographic analysis; the scattering phenomenon is the basis of x-ray diffraction; and the fluorescence phenomenon is the basis of x-ray fluorescence spectrometry. As shown in Figure 3.2.2 when a monochromatic beam of x-ray photons with wavelength λ and intensity I_0 falls onto an object with density ρ and thickness x a certain fraction (I/ I_0) of the radiation passes through the absorber. The amount of radiation that is absorbed is a function of the object's density, thickness and mass absorption co-efficient μ (a function of atomic number).

In the X-ray imaging system used by this laboratory, the object thickness (i.e., the width of the view cell) is a constant and the mass absorption co-efficient is also fairly constant since the materials being investigated are hydrocarbons. Hence the only variable in determining the amount of x-rays that are absorbed would be the density of the material. It is due to this dependence on density that it is possible to distinguish several phases. What must be determined is the smallest density difference that can be distinguished. In

consultation with a urologist, it was learnt that the resolution obtainable from radiographs used in the medical profession are within the order of 40 Houndsfield. The Houndsfield scale is such that 0 is equal to the density of air and 1000 is the density of water. Consequently 40 Hounsfield translates to a distinguishable density difference of approximately 0.04 g/cm^3.

The X-ray source used in this research is a Phillips MG-161 X-ray generating system with a MCN-167 tube head. This system provides a constant potential source of x-rays. Two focal spots (x-ray emitting surfaces) of 3.0 mm^2 and 0.4 mm^2 provide a higher current flow (a brighter image) and finer detail respectively. The system has a maximum output with the larger focal spot of 19 mA at 160 kV. The system is fitted with a water cooling system and a high voltage generator (Figure 3.2.1).

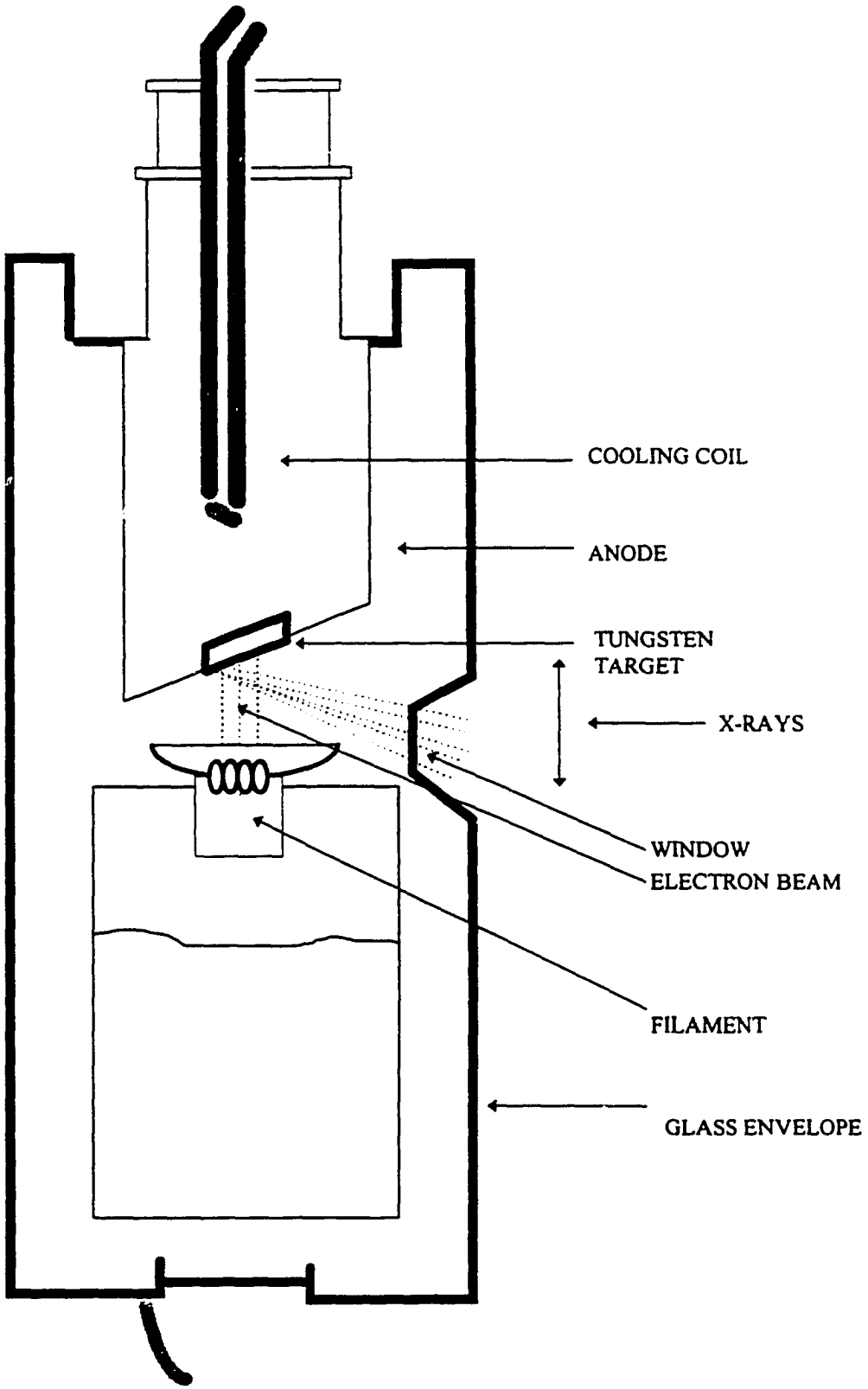

Figure 3.2.1 X-ray Gun

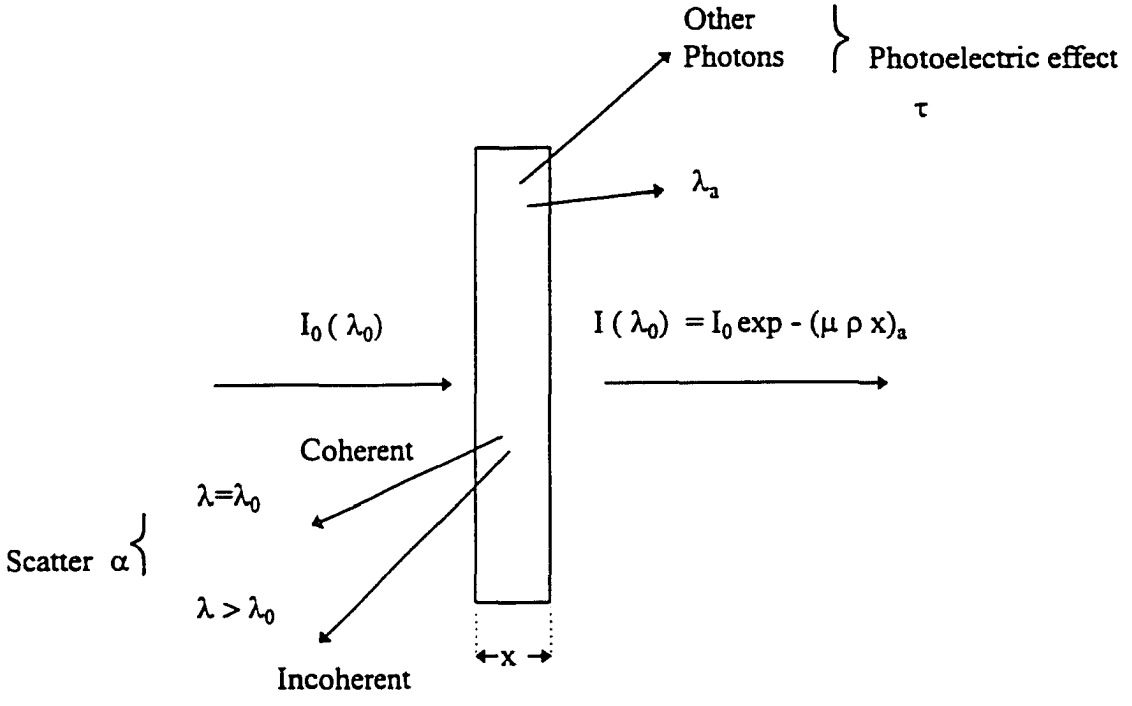

Figure 3.2.2 X-ray phenomena

3.3 Image Intensifiers [79, 80, 81]

The quality of fluoroscopic examination can be improved without an increase in the dose of radiation delivered by using an image intensifier to raise the amount of light and luminance of the image. X-ray image intensifiers can be categorized as follows : 1) x-ray or light image intensifier tubes, 2) systems for scanning x-ray images (television), 3) solid-state x-ray intensifier panels, 4) channel multiplier image intensifier devices.

The most widely used type of image intensification is the x-ray image intensifier tube. A typical image intensifier tube is made of an evacuated glass envelope containing the following major elements : 1) an input screen, 2) a photocathode usually with an input screen , 3) an electrostatically focused lens system, 4) a continuous ion or gettering pump, 5) an anode, 6) an output screen. (see Figure 3.2.1)

Once the x-ray beam has passed through the target object it enters the image intensifier tube. The input fluorescent screen absorbs the x-ray photons and converts their energy into light photons. The light photons then hit the photocathode causing it to emit photoelectrons. These electrons are accelerated from the photocathode by the large potential difference between the photocathode and the anode. As the electrons travel from the cathode to the anode they are focused by an electrostatic lens, which guides them to the output screen. The output screen emits light photons that carry the fluoroscopic image to the eye of the observer.

Until recently the phosphor input screens were usually composed of zinc cadmium sulfide crystals embedded in a resin matrix. The new generation of high resolution image intensifiers uses cesium iodide as an x-ray sensitive input screen. Two physical characteristics of the cesium iodide make it more effective : 1) cesium iodide has a greater packing density and 2) a more favorable effective atomic number. Since cesium iodide has a packing density three times greater than zinc cadmium sulphide crystals it means that more active material can be deposited in a given a space This also translates to a thinner phosphor screen which gives an improved resolution. For maximum photoelectric absorption the K-absorption edge of a phosphor should be as close as possible to the energy of the x-ray beam but clearly should not exceed the energy of the beam. Consequently the difficulty arises with an x-ray beam which is in fact a spectrum of energies while the K-edge energy is a point and with a phosphor screen is several points depending on the number of elements in the phosphor. Typical fluoroscopy is done at energies between 100 kV to 120 kV which corresponds to a mean energy between 33 keV and 40 keV. The K-absorption edges for cesium and iodide are 36.0 keV and 33.2 keV which are very close to the x-ray beam energies used in fluoroscopy. Cesium iodide also has a more appropriate atomic number since it absorbs 66% of the incident rays as oppose to less 33% with zinc cadmium sulfide.

The image intensifier used in this research project is a Siemens Sirecon 27/17 HN cesium iodide x-ray image intensifier.

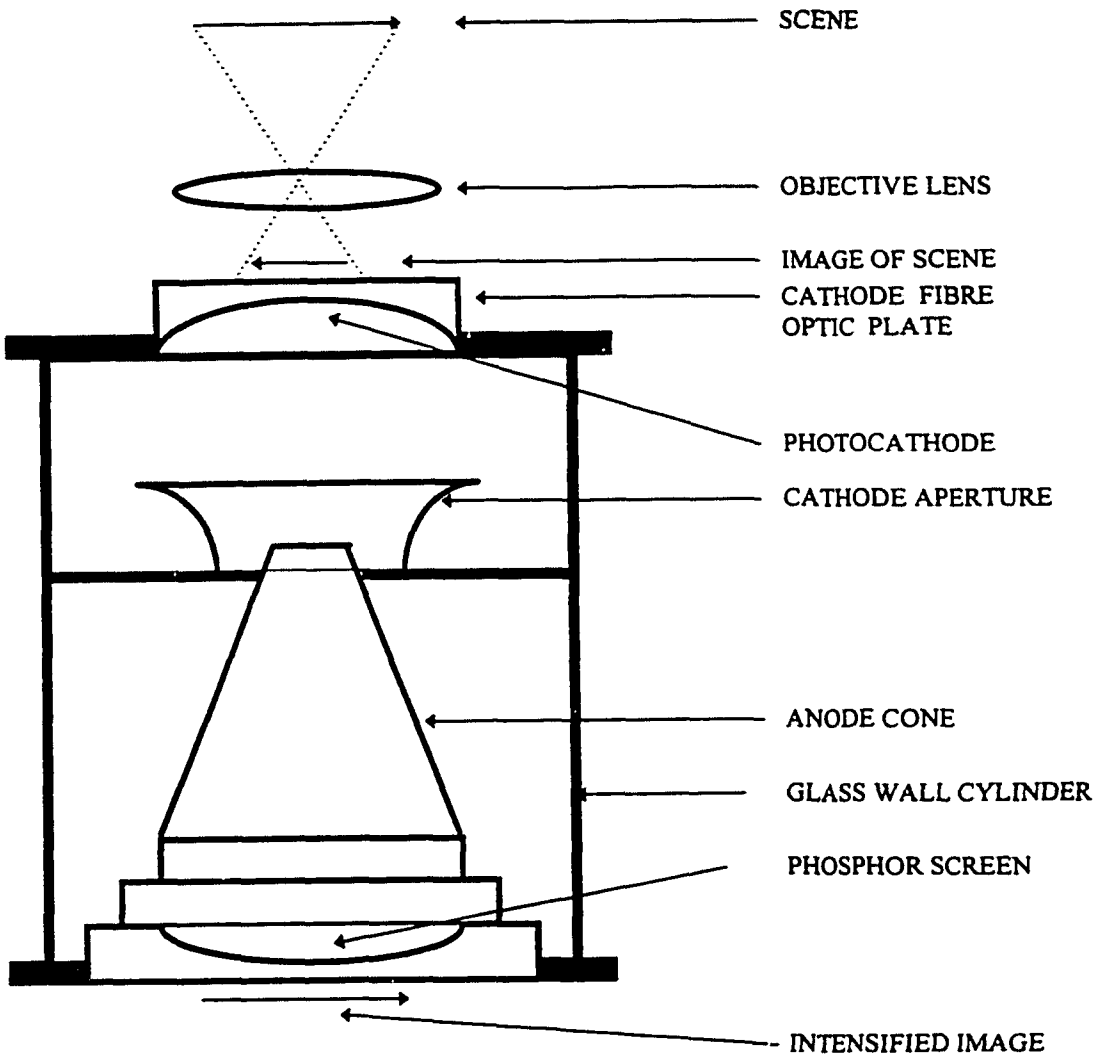

Figure 3.2.1 Image Intensifier

3.4 View cell

The view cell is a flat-sided "sandwich" style pressure vessel with a nominal volume of 1.5 L. The interior dimensions of the view cell are height - 30 cm, width - 10 cm and depth - 5 cm. The view cell is equipped with 0.635 cm thick beryllium plates that allow X-rays to pass through (i.e., the mass absorption coefficient of beryllium is very low). The plates are attached to the front and the back sides of the view cell and provide a window that is 30cm high and 2.5 cm wide. In order to ensure that bottom of the vessel is visible during operation the view cell was fitted with a stuffing block that has a flat bottom. Also the stuffing block has sides that are very steep and thus promote good mixing. With the stuffing block the view cell volume is reduced to 1.48 L. The vessel has a maximum allowable working pressure and temperature of 6.9 MPa and 700 K respectively.

As previously mentioned the view cell is a "sandwich" vessel and consequently requires seals between the two beryllium windows and the 316 stainless steel body. The search for an appropriate gasketing material was a challenge. Finally, after three different types of materials were explored a composite of graphite and stainless steel was chosen. The successful design was an inner compressible "cushion" of stainless steel overlayed with graphite. The stainless steel provides the necessary strength at high temperatures while the graphite which is very malleable provides a good seal at high pressures. Once a seal is acquired the lifetime of the gaskets is determined by experimental conditions e.g. if

the view cell must be dismantled for cleaning as a result of solids that cannot be removed with tetrahydrofuran, otherwise a seal is maintained with the same gasket for several experiments. The gaskets are custom made and require a lead time of approximately two months. Gaskets cannot be re-used once the view cell has been disassembled.

The three pieces of the "sandwich" style view cell and the beryllium windows are held together by twenty eight, 1.5875 cm fine threaded - 21 cm long studs. In order to achieve a seal these studs are torqued to approximately 135 Nm (100 ft-lbs) and in any case 316 stainless steel is not strong enough to handle this kind of service at elevated temperatures and pressures. There is also a fairly severe heating and cooling cycle that these studs must be able to withstand. To date, two types of materials for studs have been explored : 316 stainless steel and carbon steel grade B7. Both of these material did not stand up to the severe conditions and exhibited excessive scaling and pitting. Another metal that is being currently investigated is a high chromium content stainless steel alloy - ASTM 422 grade.

The view cell is equipped with an Autoclave Engineering Magna Drive II magnetic stirrer. The stirrer is fitted with two sets of propellers. This double propeller design provides excellent mixing. One set of propellers is located at the very bottom end of the shaft and the second set is approximately 10 cm from the bottom of the shaft. The bottom of the stirrer sits about 2.54 cm from the bottom of the view cell. The stirrer is located to the right of the view cell so that it does not block the view from the beryllium windows during operation. The stirrer is connected to cold water cooling lines.

A set of two ribbon heaters provides approximately 4.5 kW of power which is needed to heat up the 91 kg of stainless steel that is the view cell and its contents. These heaters require a three phase power supply. The heaters are placed symmetrically along the front and back of the vessel. The vessel is insulated with approximately 7.6 cm thick Kao ceramic wool. The X-ray window is not covered with insulation and is the location for the greatest amount of heat loss from the vessel. The heaters are controlled by a Eurotherm digital temperature controller model 919 and the temperature can be controlled to within ± 5 K of the set-point. The average heating rate with this arrangement is approximately 1.5 K / min. The temperature feedback thermocouple is located in a thermowell that is approximately 14.3 cm from the bottom and is about 7.62 cm from the center of the view cell. Four other thermocouples are placed along the outer skin of the view cell to and one thermocouple is placed on the wall closest to the image intensifier. The pressure is monitored by a standard Matheson pressure gauge and readings can be made within ± 30 kPa. The temperatures and pressures are recorded manually. The view cell is protected from overpressure by a rupture disc set for 6.9 MPa.

3.5 Experimental Start-up

In a typical experiment where Athabasca bitumen is being used as a component of the feed mixture, the set-up time is approximately three days. A sample of Athabasca bitumen is retrieved from its storage container by freezing the metal container and chiseling out the required amount. Freezing causes the bitumen to be brittle and therefore

easier to work with. The weighed sample is then heated, in a stainless steel pot, until the entire sample has melted. While the sample is being prepared, the view cell is heated to approximately to 623 K , this allows for the bitumen to be poured easily into the vessel. Since the inlet port of the vessel has only a 0.95 cm diameter and the bitumen is fairly viscous the sample must be introduced slowly into the view cell. Once all the bitumen has been poured into the vessel the heater is shut-off and the view cell is allowed to cool to room temperature.

The next step involves adding the other components of the feed into the view cell e.g. dodecane. Once the system has been charged with all the liquid and solid feed components, the view cell is sealed and pressurized with nitrogen to 6.9 MPa. Typically the vessel is left overnight to ensure that the system is completely free of leaks. The system is then depressurized and evacuated using an aspirator. The system is then flushed twice with whatever gas is being used in the experiment, e.g., hydrogen, and pressurized to the required pressure.

3.6 Experimental Operation

It is important to ensure that the X-ray generating system has undergone the appropriate warm-up sequence before beginning the experiment. The warm-up sequence is dependent on the length of time that the x-ray gun has not been in use. Three warm-up sequences are programmed into the Phillips X-ray MG-161 control unit and are designed for short down

times. If the x-ray system has been inoperative for longer than twelve weeks then a warm-up sequence plot is provided in the operating manual. Once the appropriate sequence has been conducted then the next step would be to turn on the cooling water main for the magnetic stirrer and ensure that these lines are not leaking. The system must be properly insulated and the insulation must not block the beryllium window of the view cell. It is important that the face of the view cell closest to the image intensifier is insulated sufficiently since extreme temperatures will damage the image intensifier. A thermocouple is placed on the wall at the outer edge of the image intensifier so that the temperature can be monitored periodically during the experiment.

An empty video cassette is then placed into the video recorder and labelled using the typewriter. At this point the system is ready to commence heating and the heater is switched on. Once the temperature in the view cell reaches about 373 K the magnetic stirrer is switched on. Typically, the stirrer is switched off every twenty-five minutes during the course of the experiment and the system is allowed to equilibrate for approximately 5 minutes (depending on the experiment). It should be noted that this procedure poses a particular dilemma : while it is necessary to ensure constant mixing, one must check the appearance or disappearance of phases during the experiment, which cannot be accomplished while the stirrer is operating.

The system is then heated to the first temperature set point and maintained at this set-point for approximately thirty minutes without stirring. This step is repeated until the

final temperature set-point is achieved. The limiting factor which determines the final temperature set-point is usually the pressure in the view cell. The system is allowed to cool by natural convection. Usually, the system in the view cell is also monitored and recorded during the cooling down phase. The temperature and pressure are recorded and the stirring sequence is maintained until the system is cooled down to approximately 473 K. The approximate run time for a typical experiment is about ten hours.

Once the view cell has reached room temperature, the pressure and temperature are recorded along with the image. The view cell is then depressurized and the liquid phase is siphoned out and collected. If there is a solid phase, a sample is retrieved from the bottom drain port of the view cell. This latter process is very cumbersome and requires a great deal of patience. Using a sharp probe small quantities of solid are obtained. It is necessary to ensure that a solid sample is obtained from a position not too close to the drain port in order to reduce any end effects that may alter the solid phase. Ideally, a sample from the middle of the solid phase should be retrieved. Once a sufficient amount of sample has been collected the view cell is then cleaned with tetrahydrofuran until all traces of material have been removed. This flushing process can require several volumes of tetrahydrofuran and in a most severe case a few days of solvent treatment.

3.7 Materials

The physical properties of the heavy crudes, partially processed whole bitumen and other chemicals are shown in Table 3.7.1 to 3.7. 3. The Athabasca bitumen vacuum bottoms was obtained from CANMET - ERL and the Gudao vacuum resid was obtained from the Alberta Research Council. The partly processed crude samples described in the Table 3.7.2 were obtained from Dr. Murray Gray , University of Alberta. The partly processed crude samples labelled CHN001 , CHN002, CHN003 were liquid samples obtained from a whole crude that was processed under a continous operation mode with 13.7 MPa hydrogen at 703 K with residence times of 1τ, 2τ, and 3τ respectively. Sample labelled CHN00* was a liquid sample obtained from a whole crude which had been processed under a continous mode operation with 13.9 MPa hydrogen at 703 K with a Ni/Mo catalyst. Hydrocarbons listed in Table 3.7.3 were obtained from Anachemia and were of research grade purity. Gases listed in Table 3.7.3 were obtained from CANOX and were also of research grade purity.

Table 3.7.1 Physical Properties of Heavy oils

	Athabasca Bitumen Vacuum Bottoms (ABVB)	Gudao Vacuum Resid (GVR)
Specific gravity	1.046 (24 ° C)	0.999
Elemental analysis (wt. %)		
carbon	84.3	85.4
hydrogen	10.9	10.7
nitrogen	0.80	0.72
oxygen	0.3	n/a
sulphur	3.5	2.6
Pentane insolubles (wt. %)	38.4	15.2
H/C	1.54	1.49
Aromatic carbon	35.4	20.0
525 + Resid	99.3	92.4

Table 3.7.2 Physical properties of Processed Crudes.

	CHN001	CHN002	CHN003	CHN00*
Specific gravity	0.9732	0.9479	0.9257	0.883
Elemental analysis (wt. %)				
carbon	83.20	84.33	84.12	86.50
hydrogen	10.30	10.79	10.70	11.60
nitrogen	0.445	0..351	0.391	0.323
sulphur	3.91	2.90	2.61	1.06
H/C	1.49	1.54	1.53	1.60
525 + Resid	33.48	21.26	15.50	21.00

Table 3.7.3 Physical properties of miscellaneous chemicals .

	Cyclohexane	Heptane	Benzyl alcohol
Formula	C_6H_{12}	C_7H_{16}	$C_6H_5CH_2OH$
ρ (g/cm^3)	0.779	0.684	1.049
T_b (K)	353.8	371.6	478.3
T_m (K)	279.6	182.6	257.7
T_c (K)	553.6	540.3	
P_c (MPa)	4.07	2.74	
Molecular weight	84.162	100.205	108.15

	Nitrogen	Carbon dioxide	n-Hexadecane
Formula	N_2	CO_2	$C_{16}H_{34}$
ρ (g/cm^3)	------	------	0.733
T_b (K)	77.4	------	560.0
T_m (K)	63.3	216.6	291.0
T_c (K)	126.2	304.1	722.0
P_c (MPa)	3.39	7.38	1.41
Molecular weight	28.013	44.010	226.448

Table 3.7.3 cont'd

	Hydrogen	n-Dodecane	Pyrene
Formula	H_2	$C_{12}H_{14+2C}$	$C_{16}H_{10}$
ρ (g/cm^3)	------	0.749	1.271
T_b (K)	20.3	489.5	666.0
T_m (K)	14.0	263.4	429.0
T_c (K)	33.0	658.2	892
P_c (MPa)	1.29	1.82	2.6
Molecular weight	2.016	170.34	202.26

4.0 Results

4.1 Experimental Verification of X-ray Imaging Method

During the initial assembly of the x-ray imaging system a substantial amount of time was spent in installing the heater and ensuring the view cell was sealed properly. The greatest difficulty was in locating gasketing material that would form a seal between the beryllium plates and the stainless shell of the view cell. It is during this period that a simple experiment to determine whether the x-ray imaging system would be able to discern the differences between two liquid phases with relatively small density differences was conducted. A simple hydrocarbon system that demonstrated liquid - liquid phase behaviour at ambient conditions was sought. The system heptane - cyclohexane - benzyl alcohol exhibits liquid - liquid - vapour phase behaviour over a range of temperatures at atmospheric pressure. Since this system has been well characterized in the literature[82] it was easy to reproduce experimentally. Fig 4.1.1 shows the liquid - liquid phase diagram for the heptane - cyclohexane - benzyl alcohol as a function of temperature and benzyl alcohol (vol.%) with varying heptane compositions.

Liquid mixtures with various heptane : cyclohexane ratios but a constant composition of benzyl alcohol (40 vol. %) were prepared. These mixtures exhibited liquid - liquid phase behaviour and density differences between the two liquid phases varied. The density of each liquid phase in the various mixtures was measured. Table (4.1.1) outlines the series of samples that were used.

Figure 4.1.1 Heptane - Cyclohexane - Benzyl Alcohol

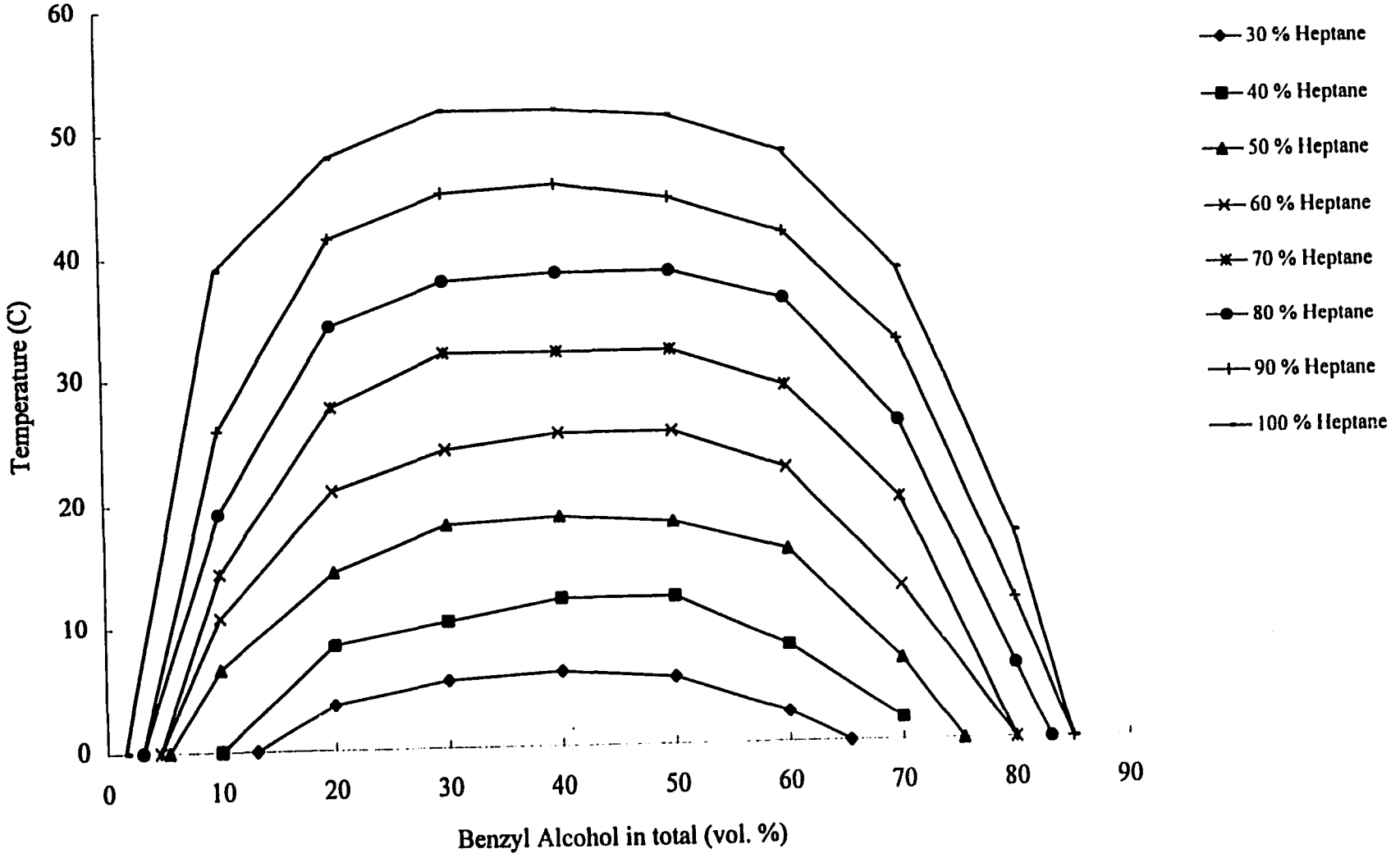

Table 4.1.1 Benzyl alcohol - Heptane- Cyclohexane system

Heptane (vol. %)	Cyclohexane (vol. %)	Liquid 1 (g/cm^3)	Liquid 2 (g/cm^3)	Density differences (g/cm^3)
60	0	0.701	0.936	0.235
54	6	0.720	0.960	0.240
48	12	0.740	0.950	0.209
42	18	0.762	0.935	0.173

Figure 4.1.2 is a representation of the types of images obtained from the x-ray imaging system and is provided to clarify the following digitized images. Liquid-liquid phase behaviour for the benzyl alcohol - cyclohexane - heptane system is shown in Figures (4.1.3.a) to (4.1.3.c) as photographs of the x-ray images of the system. Density differences as small as 0.173 g/cm^3 are easily discerned.

The second system investigated was a binary CO_2 - n-hexadecane system [83,84,85,86] that exhibits vapour-liquid-liquid behaviour at ambient temperatures. This system allowed further investigation into the limits of the x-ray imaging system without the need for heating the system. A binary system which demonstrates three phases exists as a line in the P-T-x plane. Reproducing these results is virtually impossible with a constant volume apparatus. Therefore to widen the zone of three phase behaviour from a line to a region, a small amount of nitrogen was added to the system. The effect of a small addition of nitrogen to a system has been shown [89,90] to simply shift the phase

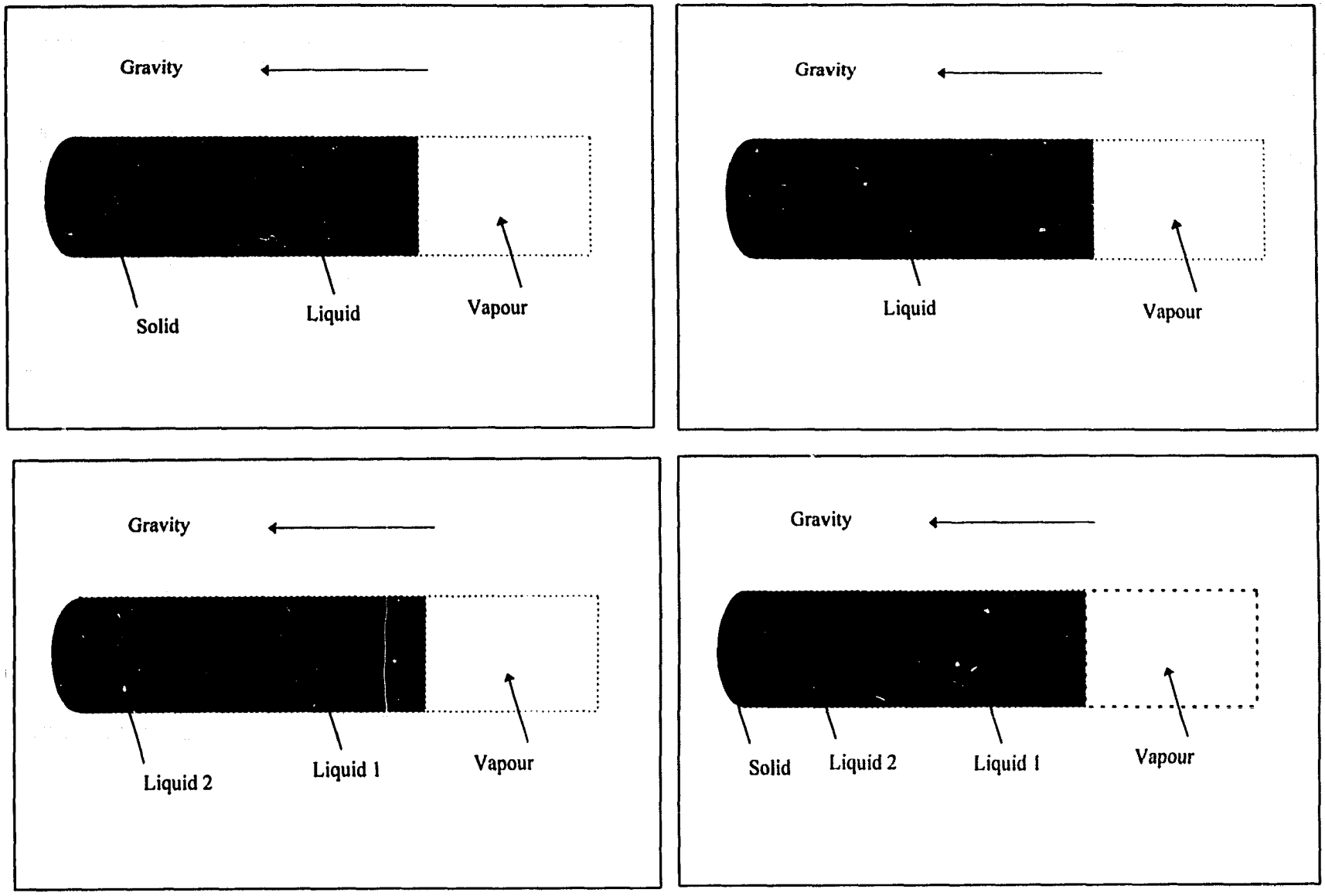

Figure 4.1.2 : Schematic of various types of phase behaviour as observed with the imaging system

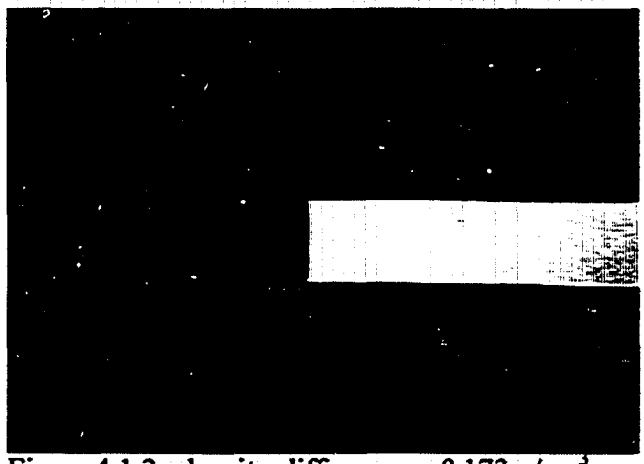

Figure 4.1.3a density difference = 0.173 g/cm^3

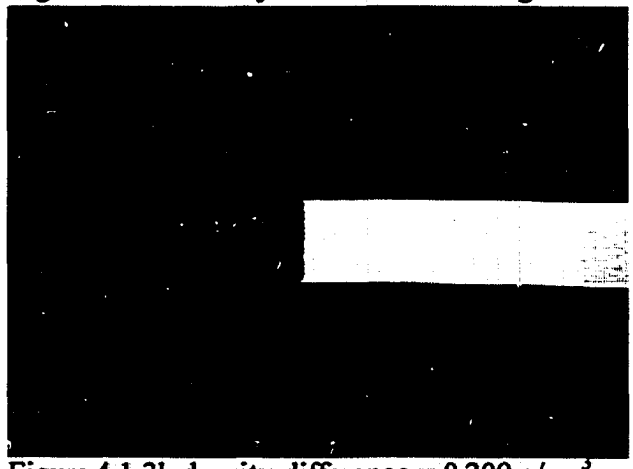

Figure 4.1.3b density difference = 0.209 g/cm^3

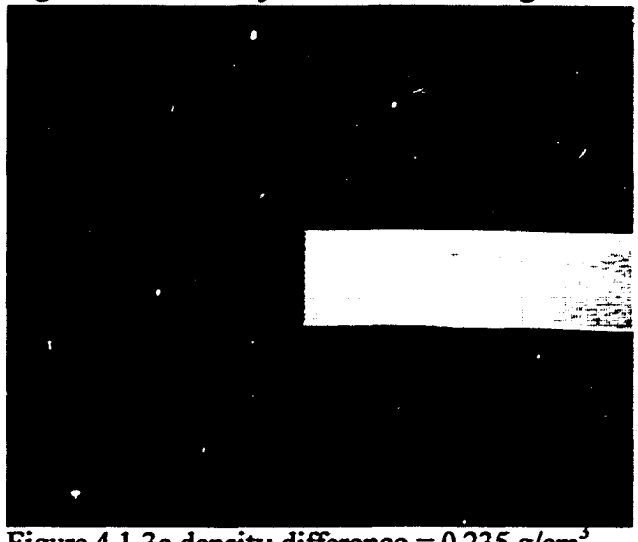

Figure 4.1.3c density difference = 0.235 g/cm^3

Figure 4.1.3 Digitized images of liquid-liquid-vapor phase behaviour with a heptane + cyclohexane + benzyl alcohol mixture

behaviour to slightly higher pressures and lower temperatures. With this system, vapour-liquid-liquid phase behaviour was observed at around 297 K and 6.2 MPa. Using the Peng-Robinson equation of state as employed in the *CMGProp* program[87] it was estimated that the density differences between the phases were in the order of magnitude of 40 kg/m^3 and approximate amounts of vapour, liquid 1 and liquid 2 were 58 vol. %, 40 vol. % and 2 vol. %. In order to ascertain whether this was indeed a second liquid phase the system was mixed and allowed to equilibrate over a two day period. The second liquid phase persisted. This result verified the ability of the x-ray imaging system to distinguish relatively small density differences (40 kg/m^3) and was comparable to x-ray radiograph discrimination obtained within the medical profession.

4.2 Phase Behaviour of Partly Processed Crudes

0.3 L samples of partly processed crudes labelled CHN001, CHN002, CHN003 were investigated under an initial hydrogen blanket of 2.07 MPa. The sample labelled CHN00* was investigated under a slightly lower initial hydrogen pressure of 1.4 MPa. This sample was studied at a lower initial hydrogen pressure since it was the lightest sample in the series and was expected to exceed the maximum allowable working pressure of the view cell since in the preceding experiment with the only slightly heavier CHN003 sample pressures very close to the maximum allowable working pressure of 6.9 MPa at 703 K were attained.

The results of these experiments are shown in Figure 4.2.1. as pressure versus temperature trajectories. Phase transitions observed during the heating-up curves are reliable because the mixtures are kinetically inactive until temperatures greater than 670 K. The samples labelled CHN002, CHN003 and CHN00* did not exhibit complex phase behaviour under the conditions employed. Simple vapour - liquid behaviour was observed in the temperature and pressure ranges of 298 K - 703 K and 2.07 MPa - 6.9 MPa.

The sample labelled CHN001 did exhibit complex phase behaviour. Phase transitions from vapour - liquid to vapour - liquid - liquid were first observed at around 623 K and 3.9 MPa. This three phase behaviour persisted up to a temperature and pressure of approximately 698 K and 6.37 MPa where a second phase transition to vapour - liquid - "solid" was observed. A direct phase transition from vapour - liquid - liquid to vapour - liquid - "solid" is highly improbable since this would require passing through a single point in the pressure - temperature space (see section 2.3.4 and Figures 4.2.2 and 4.2.3). It is most likely that phase transitions from vapour - liquid - liquid to vapour - liquid then to vapour - liquid - "solid" or vapour - liquid - liquid to vapour - liquid - liquid - "solid" then to vapour - liquid - "solid" had occurred but were not observed. Such an oversight is likely if the trajectory is very close to the single point where phase transitions from vapour - liquid - liquid to vapour - liquid - "solid" occurs since the size of the vapour - liquid - liquid - "solid" would be small, or if the system was being stirred during the intermediate phase transition.

Figure 4.2.1 : Pressure - temperature trajectories - Partly processed crudes

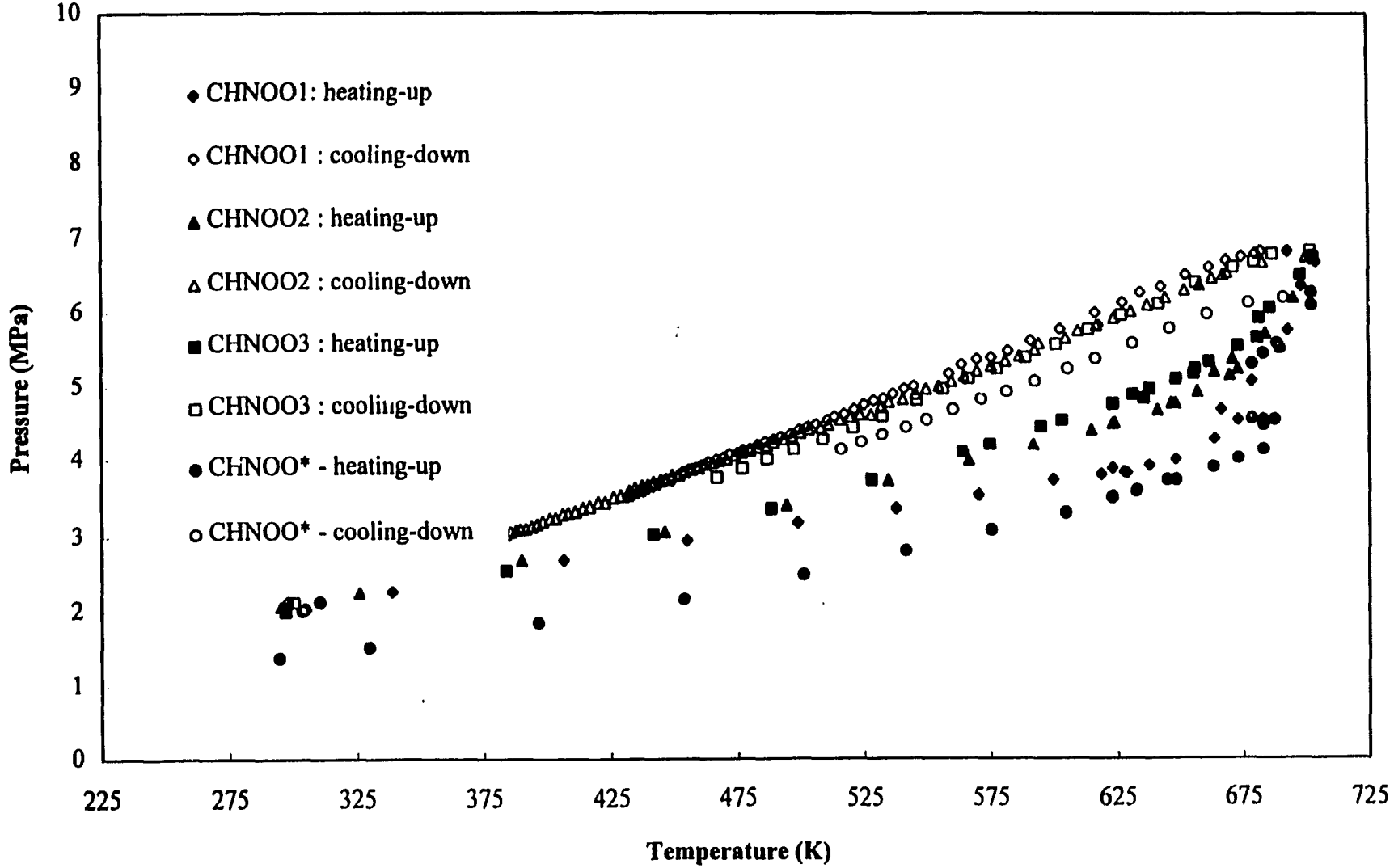

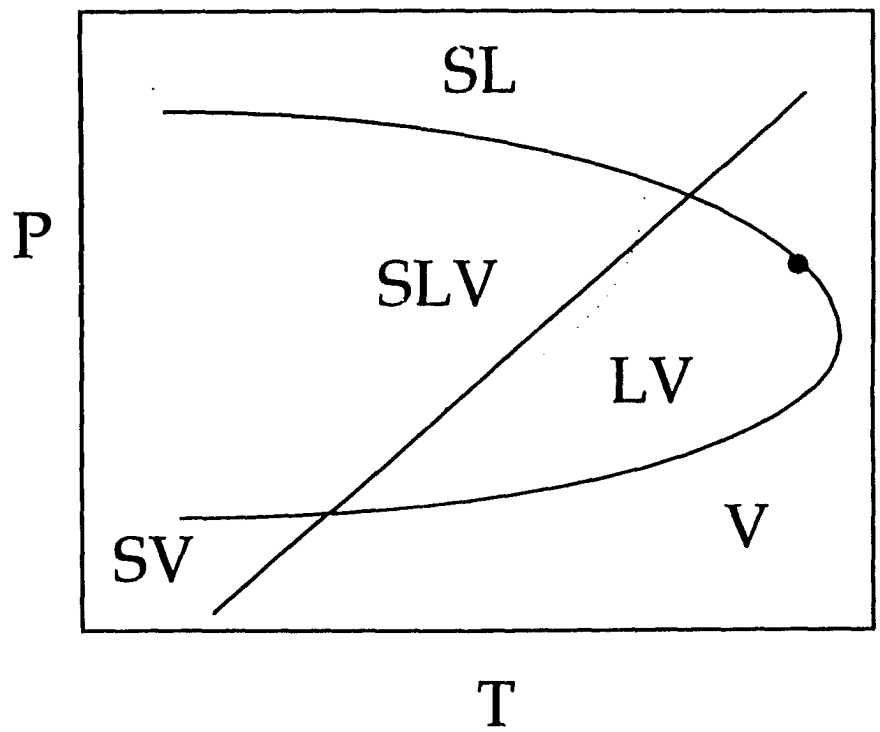

Figure 4.2.2. Representational phase diagram showing the effect of solid on vapour - liquid phase behaviour
Dashed curve represents a possible pressure-temperature trajectory

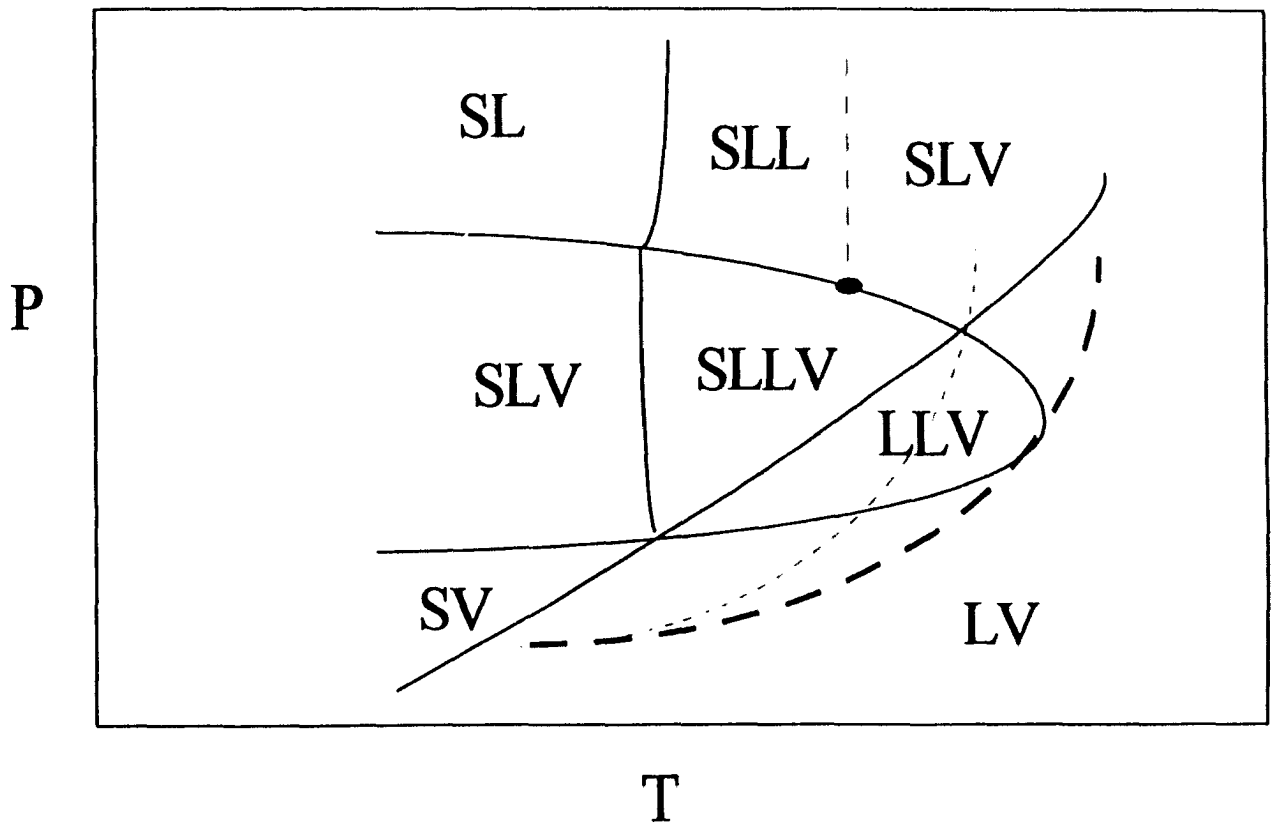

Figure 4.2.3. Representational phase diagram showing the impact of solid on vapour - liquid - liquid phase behaviour Dashed curves represent possible pressure-temperature trajectories

4.3 Phase Behaviour of Model Unprocessed Crude

A series of experiments was designed to investigate the phase behaviour of an Athabasca bitumen vacuum bottoms (ABVB) + n-dodecane + hydrogen mixture. This mixture was chosen for two reasons : one was that the mixture was a good model of a whole bitumen and two was that the critical temperature of n-dodecane was within the temperature range of operating conditions used in heavy oil upgrading processes. Complex phase behaviour is known to arise at temperatures close to the critical point of a component in a mixture. The total volume ABVB + n-dodecane was chosen to ensure that the system would be totally visible by the image intensifier even if the density of the mixture was to decrease to about half its initial density during processing. The initial hydrogen pressure was calculated to ensure that : 1) the pressure at 698 K would not exceed the maximum allowable pressure of 6.9 MPa , 2) the number of moles of hydrogen in each experiment was constant, and 3) the ratio of hydrogen to n-dodecane was constant (except for one experiment where only ABVB + hydrogen were employed).

A list of the experiments performed is given in Table 4.3.1. and the key results of these experiments can be found in Table 4.3.2. Runs # 1 - 4 and 7 were investigated to final temperatures of approximately 703 K. Runs # 5 and 6 were investigated to final temperatures of 648 K since the higher initial hydrogen pressure led to final pressures around 6.9 MPa at lower temperatures. Run # 6 was designed to be a replication of

experiment # 5 except with 1.25 times the amount of material as in run # 5. Pressure temperature trajectories for runs # 1-7 are shown in Figures 4.3.3 to 4.3.8.

As mentioned in section 4.2, phase transitions observed during the heating up curve of the pressure-temperature trajectories are more reliable than ones on the cooling down curve since these mixtures are not substantially kinetically active until temperatures greater than 670 K Run # 1 did not exhibit complex phase transitions in the temperature and pressure range of 293 - 698 K and 1.9 - 6.3 MPa, respectively. The 30 g Athabasca bitumen mixture existed as a two phase vapour - liquid system throughout the entire experiment. Runs # 2 and #3 demonstrated complex phase transitions from vapour - liquid- "solid" to vapour - liquid to vapour - liquid - "solid". The appearance of the "solid" phase at the higher temperature began at the bottom of the view cell as a fine line of "solid" and then gradually grew to a set amount and stabilized. The "solid" did not disappear during the cooling down process. This behaviour shows that once the "solid" is formed at high temperature it remains stable.

Runs # 4, 5 and 7 exhibited very complex phase transitions, i.e., phase transitions such as vapour - liquid - "solid" to vapour - liquid to vapour - liquid - liquid to vapour - liquid - liquid - "solid" to vapour - liquid - "solid". Pressure - temperature phase diagrams for Runs # 2,3 4 and 7 can be found in Figures 4.3.9 to 4.3.12. These diagrams were constructed as an extension of the effect of solid on fluid phase behaviour of an extended Type V phase behaviour classification (as reviewed in section 2.3). Phase transition data are shown on the P-T and P-x phase diagrams.

Run #	Mass of Athabasca Bitumen (g)	Mass of Dodecane (g)	Initial Hydrogen Pressure(MPa)	Final Pressure (MPa)	Moles of Athabasca Bitumen	Moles of Dodecane	Moles of Hydrogen	Pentane Insoluble (wt.%)
1	30	150	1.90 ± 0.03	2.00 ± 0.03	0.030	0.879	0.957	6.4
2	75	150	1.97 ± 0.03	N/A	0.076	0.879	0.954	12.8
3	100	150	2.00 ± 0.03	2.07 ± 0.03	0.102	0.879	0.965	15.4
4	150	150	2.07 ± 0.03	2.01 ± 0.03	0.153	0.879	0.970	19.2
5	187	187	2.86 ± 0.03	2.84 ± 0.03	0.190	1.099.	1.196	19.2
6	187	150	2.86 ± 0.03	2.72 ± 0.03	0.190	0.660	1.338	21.3
7	350	0	2.07 ± 0.03	1.59 ± 0.03	0.356	0.000	0.960	38.4

Table 4.3.1 Series of experiments with Athabasca bitumen + n-dodecane + hydrogen

	Phase transition	Temperature (K)	Pressure (MPa)
Run 1	exhibited LV during the entire experiment up to	698	6.27
Run 2	"S"LV to LV	459	2.87
	LV to "S"LV	623	4.65
Run 3	"S"LV to LV	419	2.79
	LV to "S"LV	677	5.45
Run 4	"S"LV to LV	419	2.79
	LV to LLV	648	5.25
	LLV to "S"LLV	698	6.17
	"S"LLV to "S"LV	703	6.29
	"S"LV to "S"LLV	676	6.24
	"S"LLV to "S"LV	516	3.93
Run 5*	"S"LV to LV	409	3.74
	LV to LLV	623	6.34
	LLV to LV	515	4.89
Run 6*	"S"LV to LV	442	4.00
	LV up to	653	6.76
Run 7	"S"LV to LV	604	4.07
	LV to LLV	705	5.52
	LLV to "S"LLV	698	6.03
	"S"LLV to "S"LV	674	6.07

* For runs # 5 and 6 a solid phase was noted the following day when system had returned to room temperature .

Table 4.3.2 Observed phase transitions for ABVB + n-dodecane + hydrogen mixtures

Figure 4.3.3 : Pressure-temperature trajectory
Run #1 - 30g ABVB + 150g n-dodecane + 1.9 MPa hydrogen

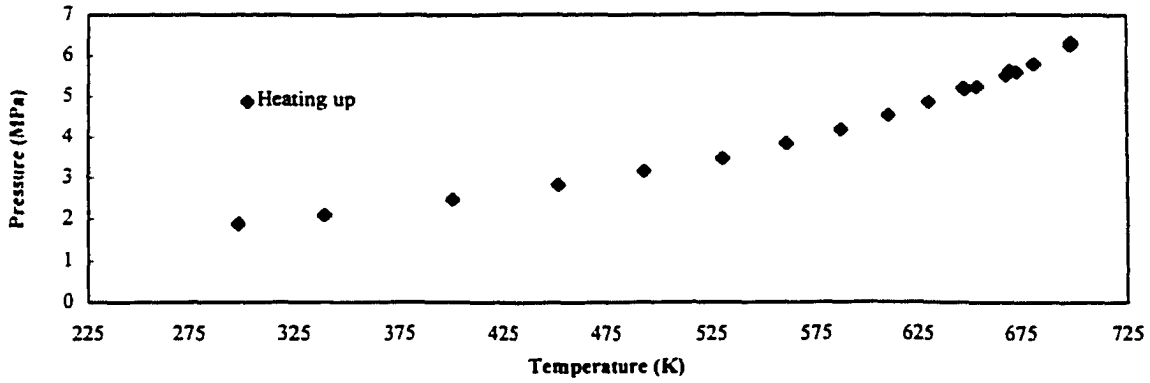

Figure 4.3.4 : Pressure-temperature trajectory
Run # 2 - 75g ABVB + 150g n-dodecane + 1.97 MPa hydrogen

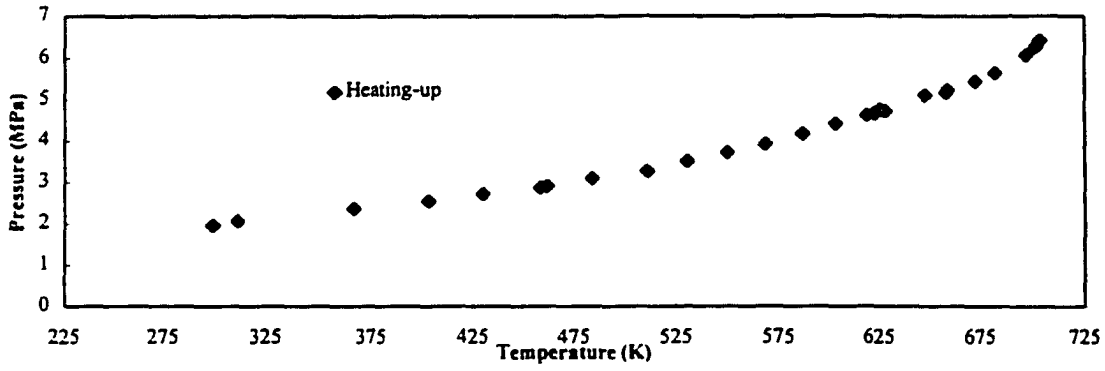

Figure 4.3.5 : Pressure-temperature trajectory
Run # 3 - 100g ABVB + 150g n-dodecane + 2.00 MPa hydrogen

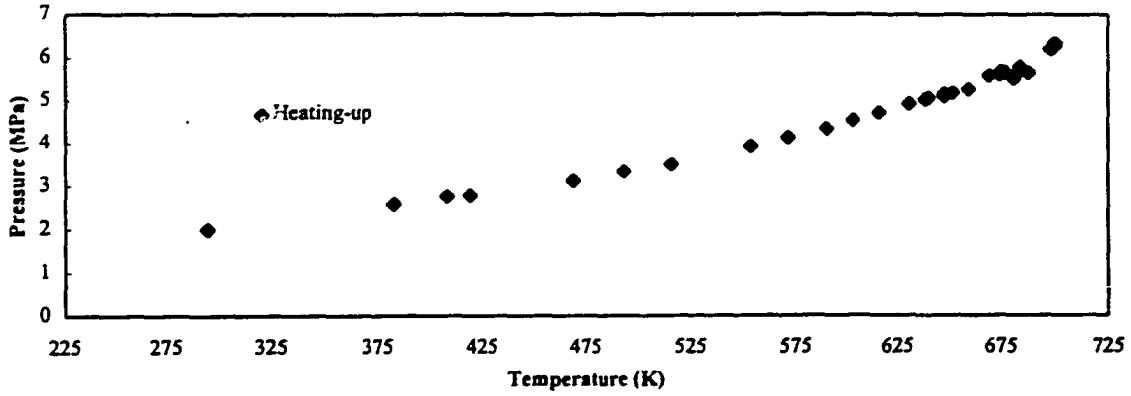

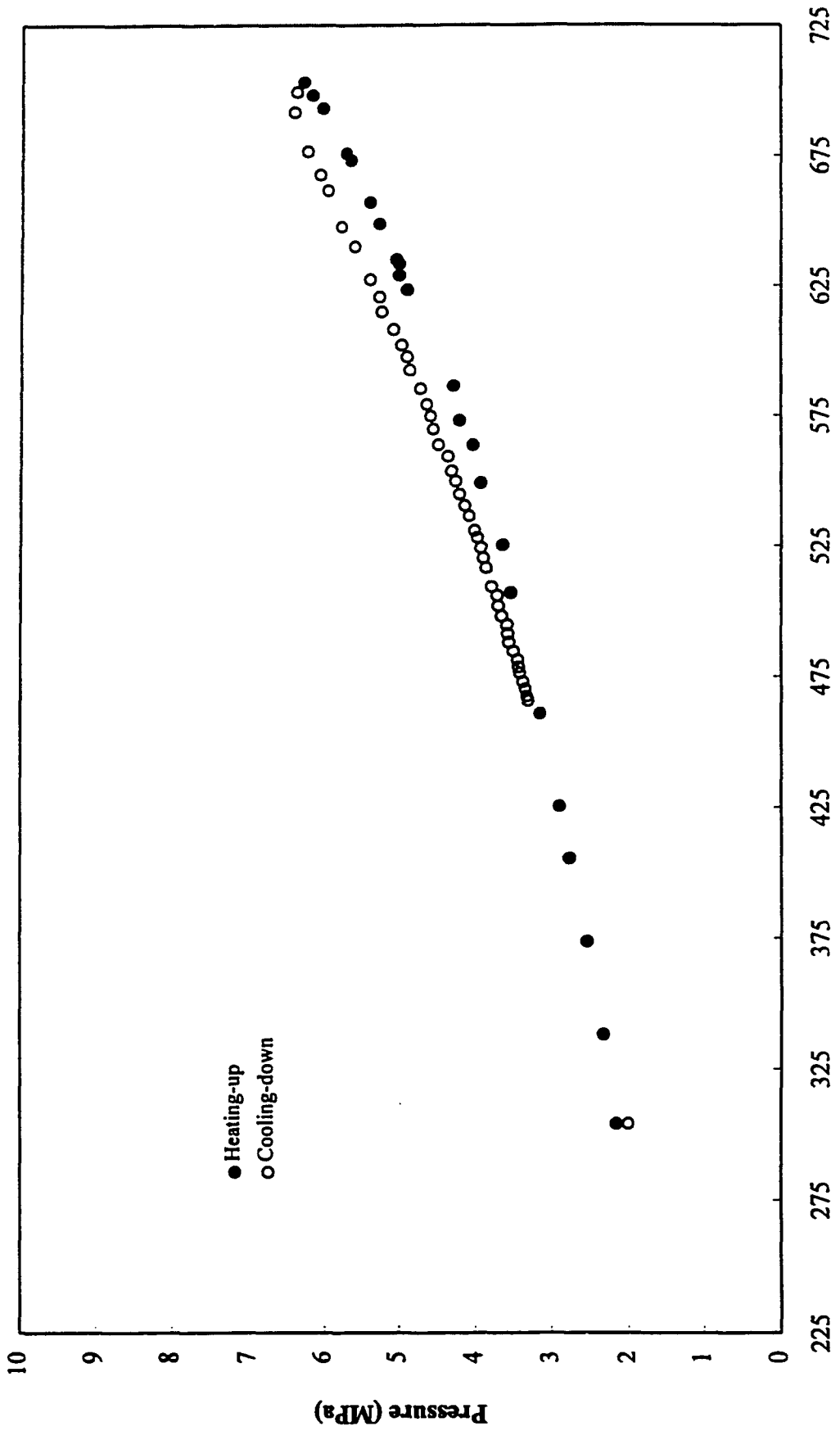

Figure 4.3.6 : Pressure - temperature trajectory - Run #4 - 150g ABVB + 150g n-dodecane + 2.07 MPa hydrogen

Figure 4.3.7 : Pressure-temperature trajectory - Run #5 -187g ABVB + 187g n-dodecane + 2.86 MPa hydrogen and Run #6 - 187g ABVB + 150g n-dodecane + 2.86 MPa hydrogen

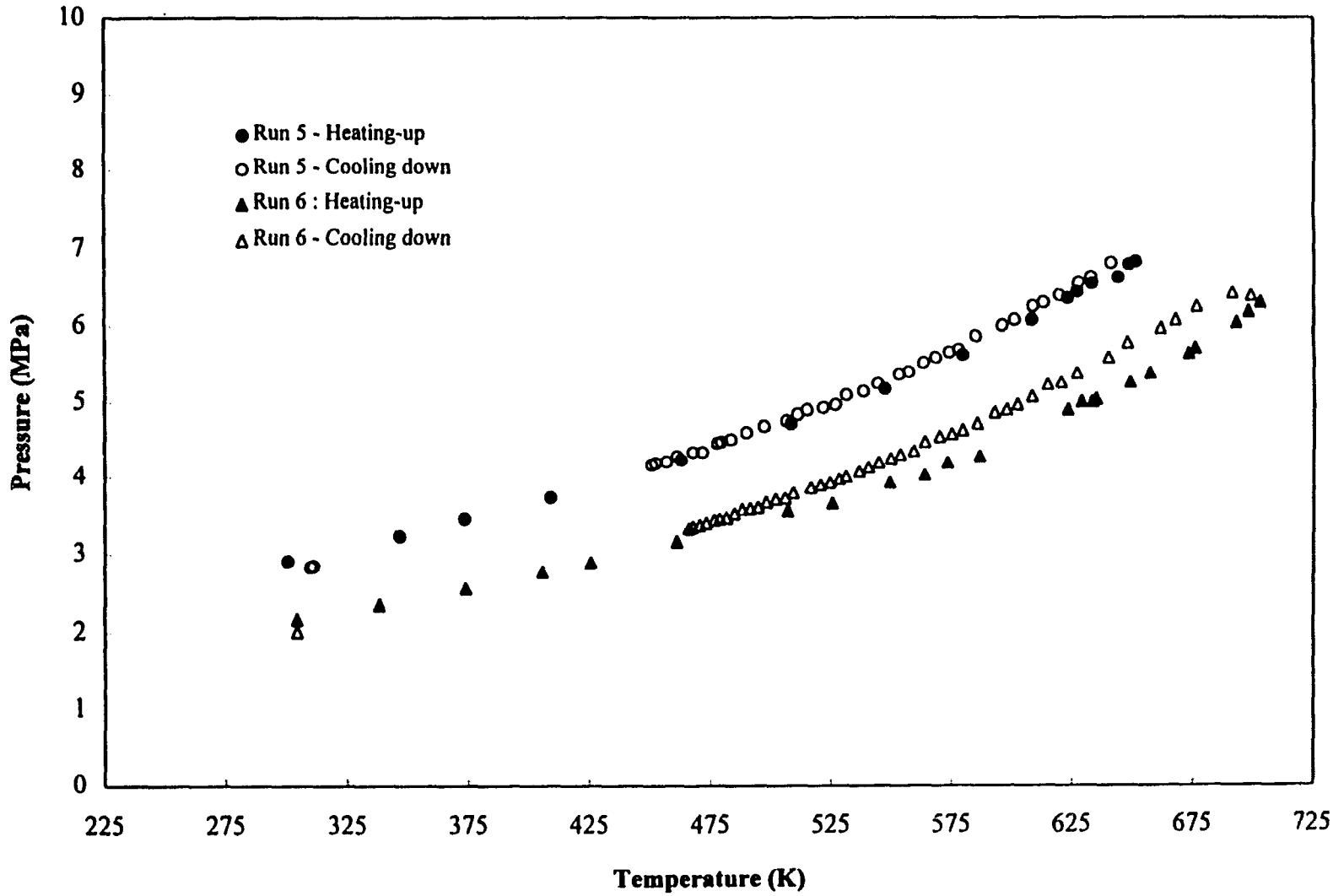

Figure 4.3.7 : Pressure-temperature trajectory - Run #5 -187g ABVB + 187g n-dodecane + 2.86 MPa hydrogen and Run #6 - 187g ABVB + 150g n-dodecane + 2.86 MPa hydrogen

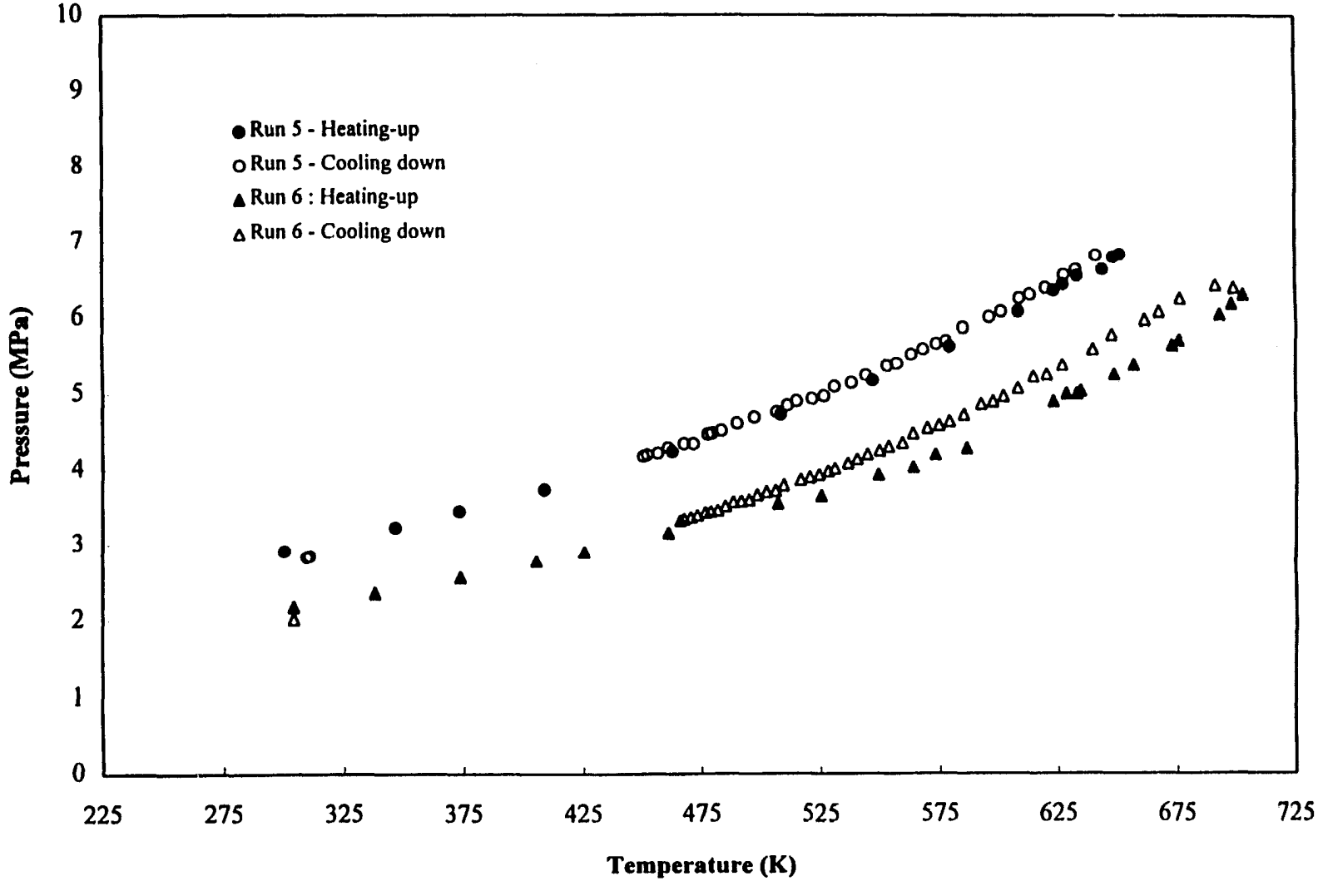

The appearance of the "solid" in these experiments was less uniform in comparison to the "solid" appearance in Runs # 2 and 3. The "solid" often appeared as a small "clump" of material swirling about in the liquid phase and in one instance it behaved like a "tumbleweed" and grew as it was being mixed about in the liquid. The "solid clump" would attach itself to the side or the bottom of the view cell and continue to grow. In most cases the amount of "solid" material formed appeared to be proportional to the amount of Athabasca bitumen in the mixture. From the pressure-temperature data from all experiments, preliminary pressure versus composition diagrams were constructed and an example at 674 K is shown in Figure 4.3.13. Digitized images of typical phase behaviour are presented in Figure 4.3.14 - 4.3.16.

Figure 4.3.9 : Pressure-temperature phase diagram for Run # 2 - 75g ABVB + 150g n-dodecane + 1.97 MPa hydrogen

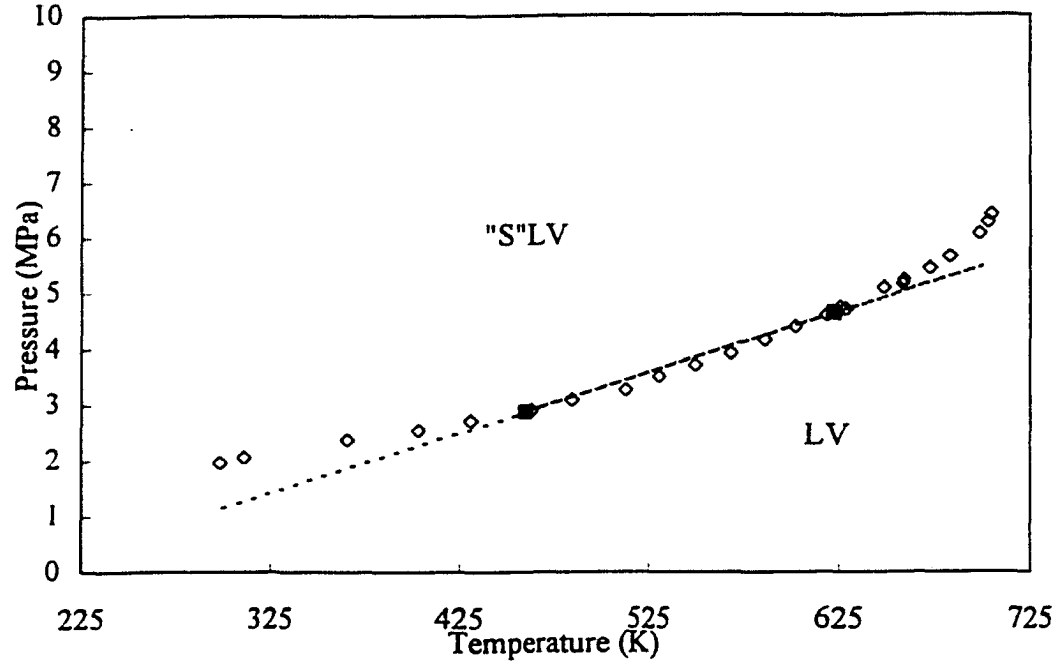

Figure 4.3.10 : Pressure-temperature phase diagram for Run #3 - 100g ABVB + 150g n-dodecane + 2.00 MPa hydrogen

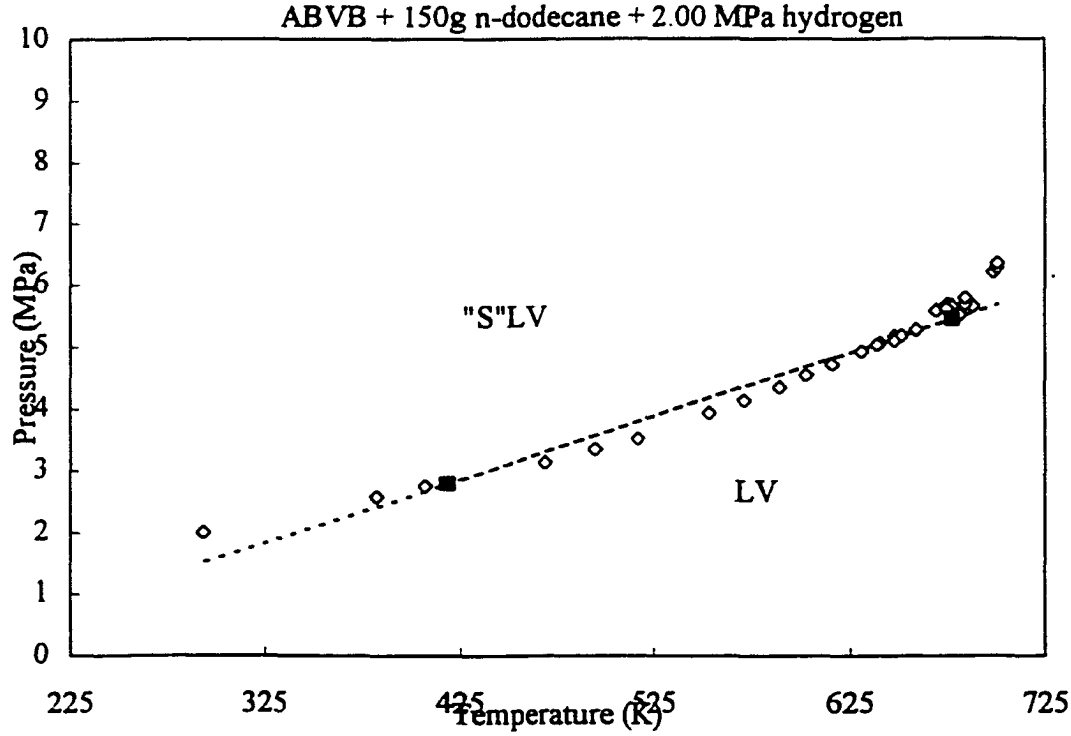

Figure 4.3.11 Pressure-temperature phase diagram for Run #4 150 g ABVB + 150g n-dodecane + 2.07 MPa hydrogen

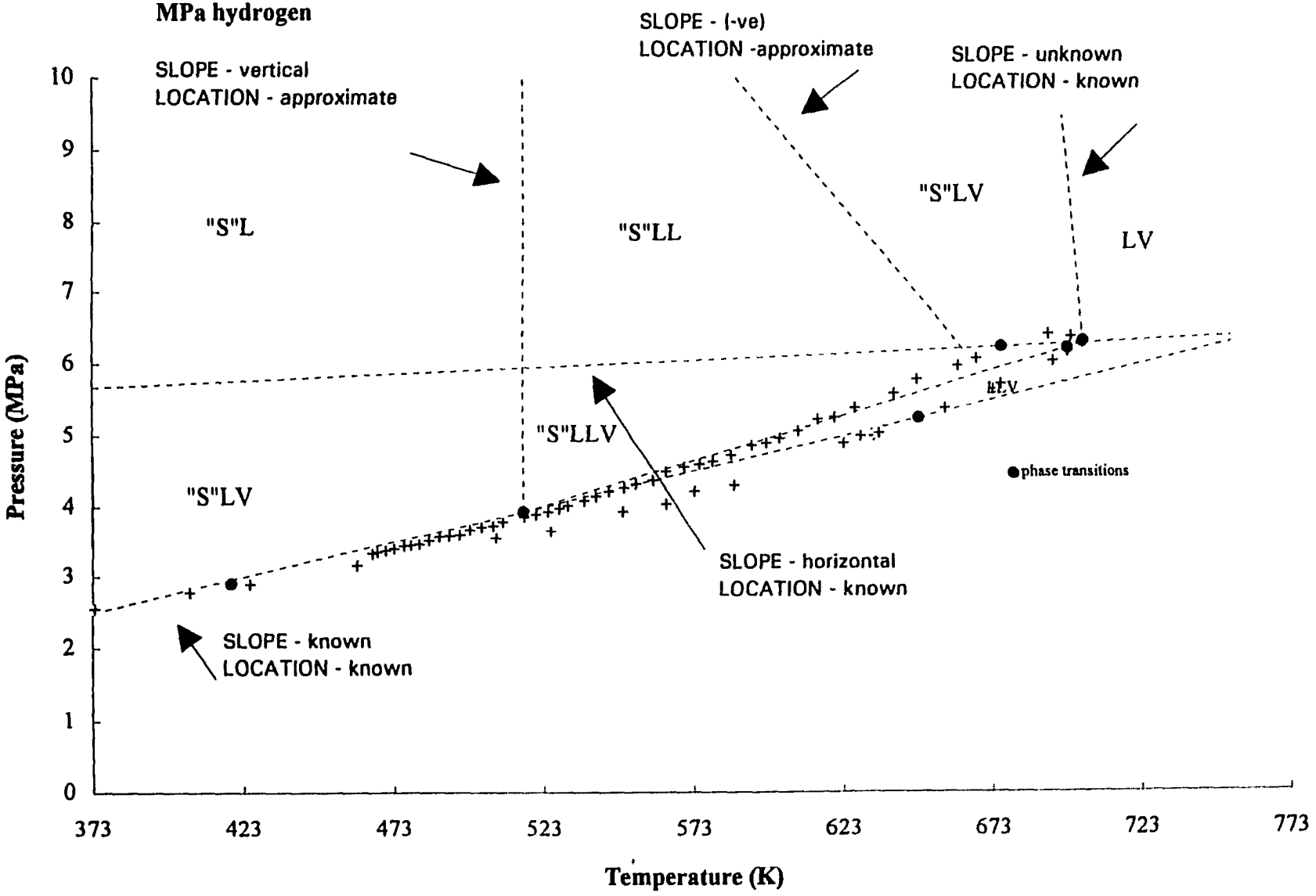

Figure 4.3.12 Pressure-temperature phase diagram for Run#7 350g ABVB + 2.07 MPa hydrogen

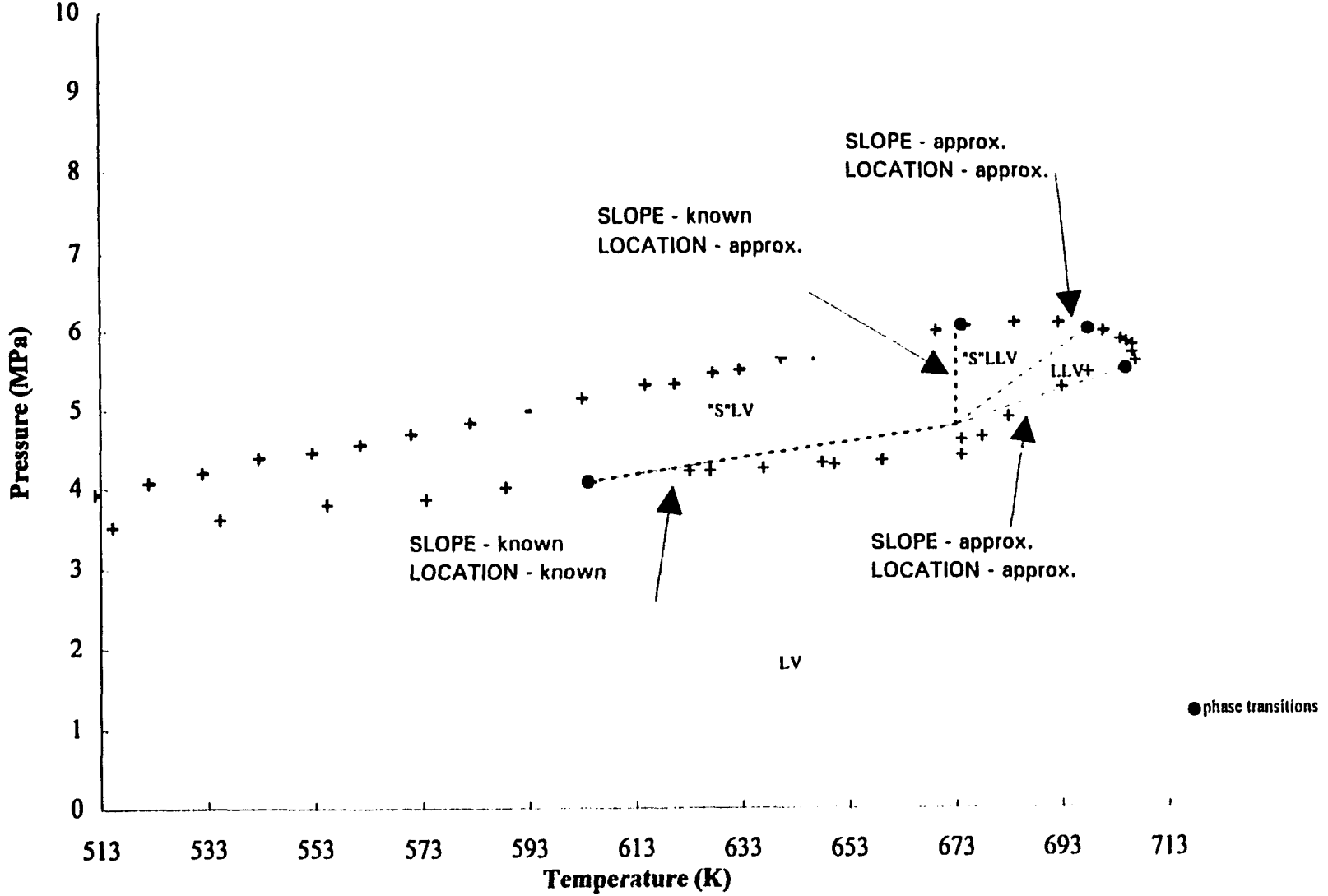

Figure 4.3.11 Phase diagram for ABVB + n-dodecane + hydrogen, P-x at T = 674 K

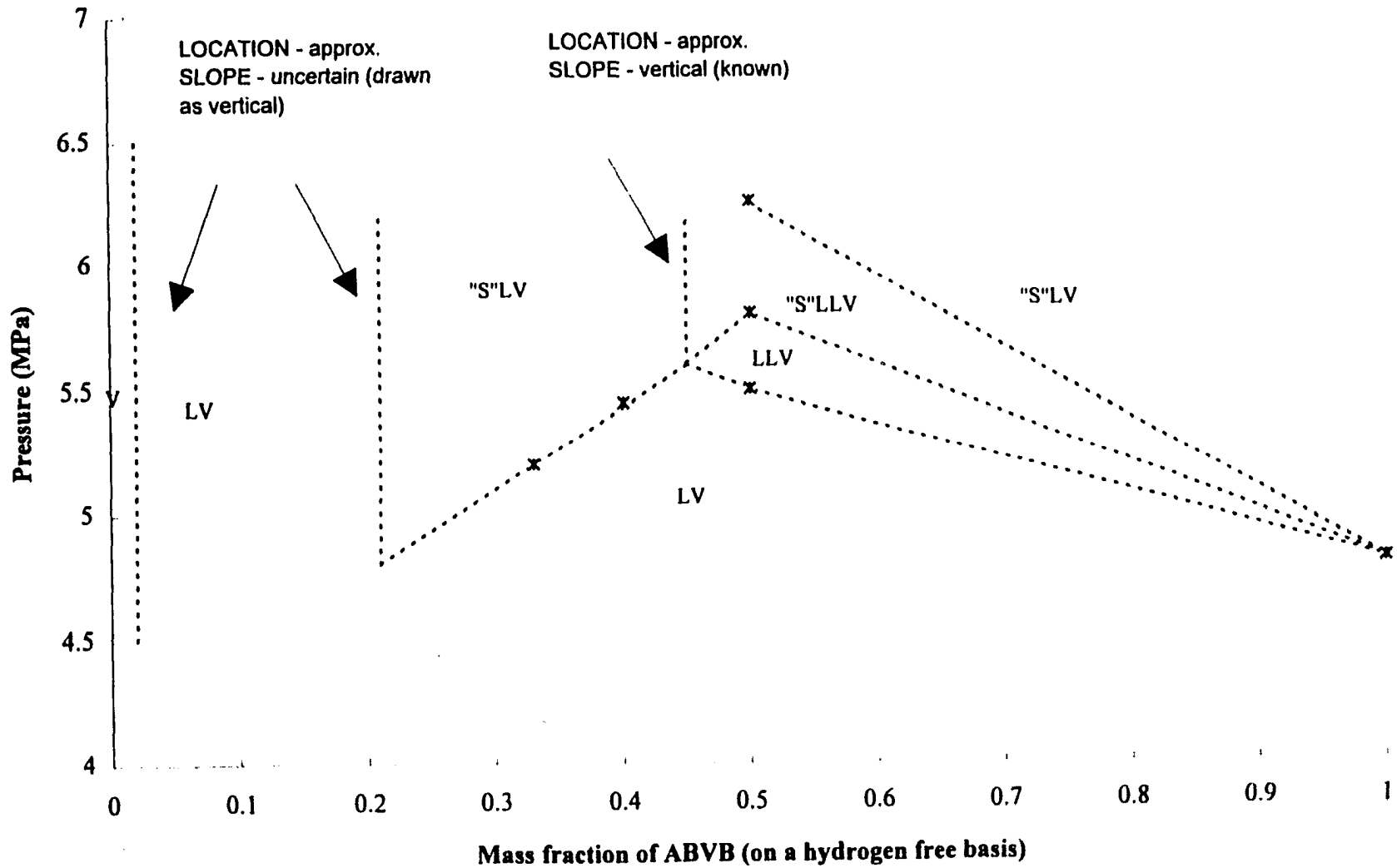

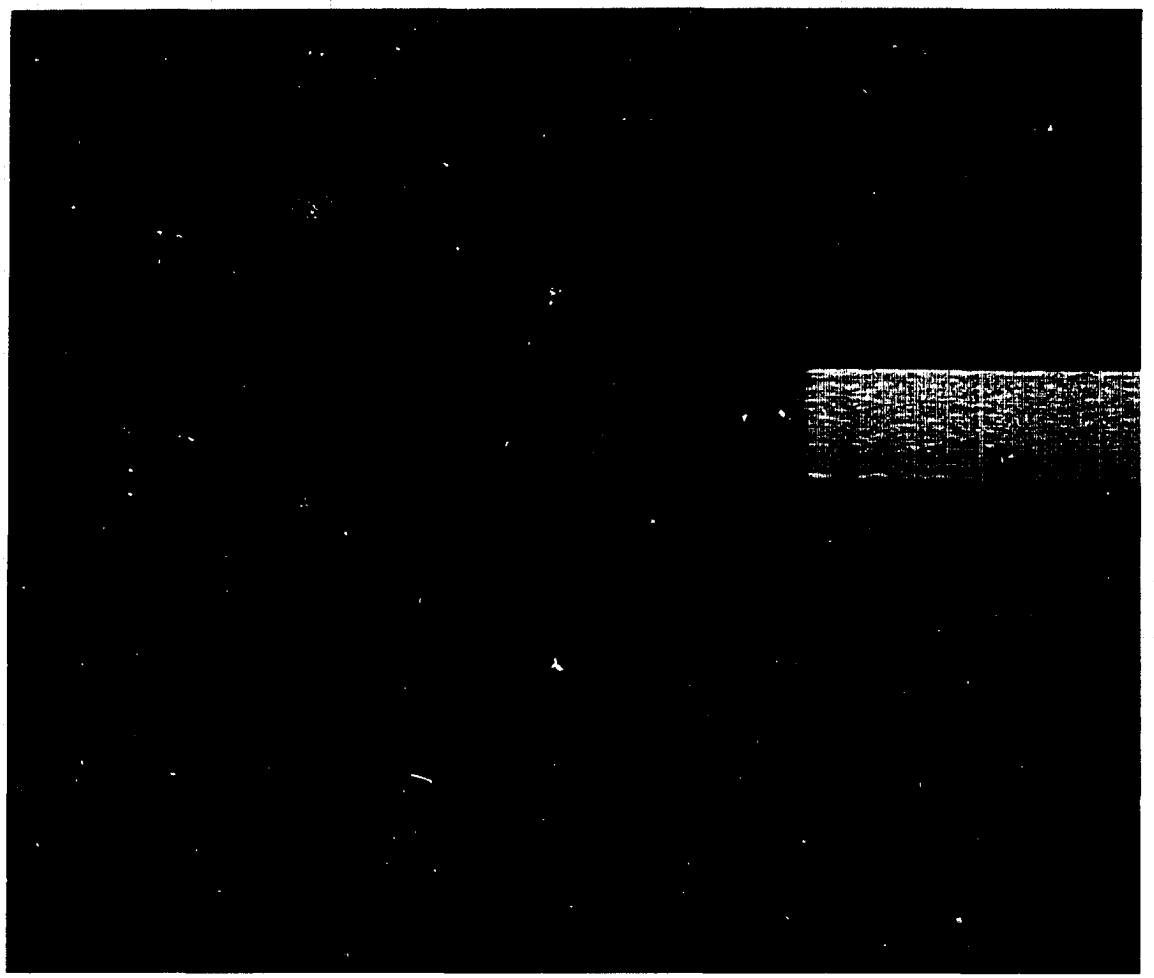

Figure 4.3.13 : Digitized image showing liquid - vapor phase behaviour

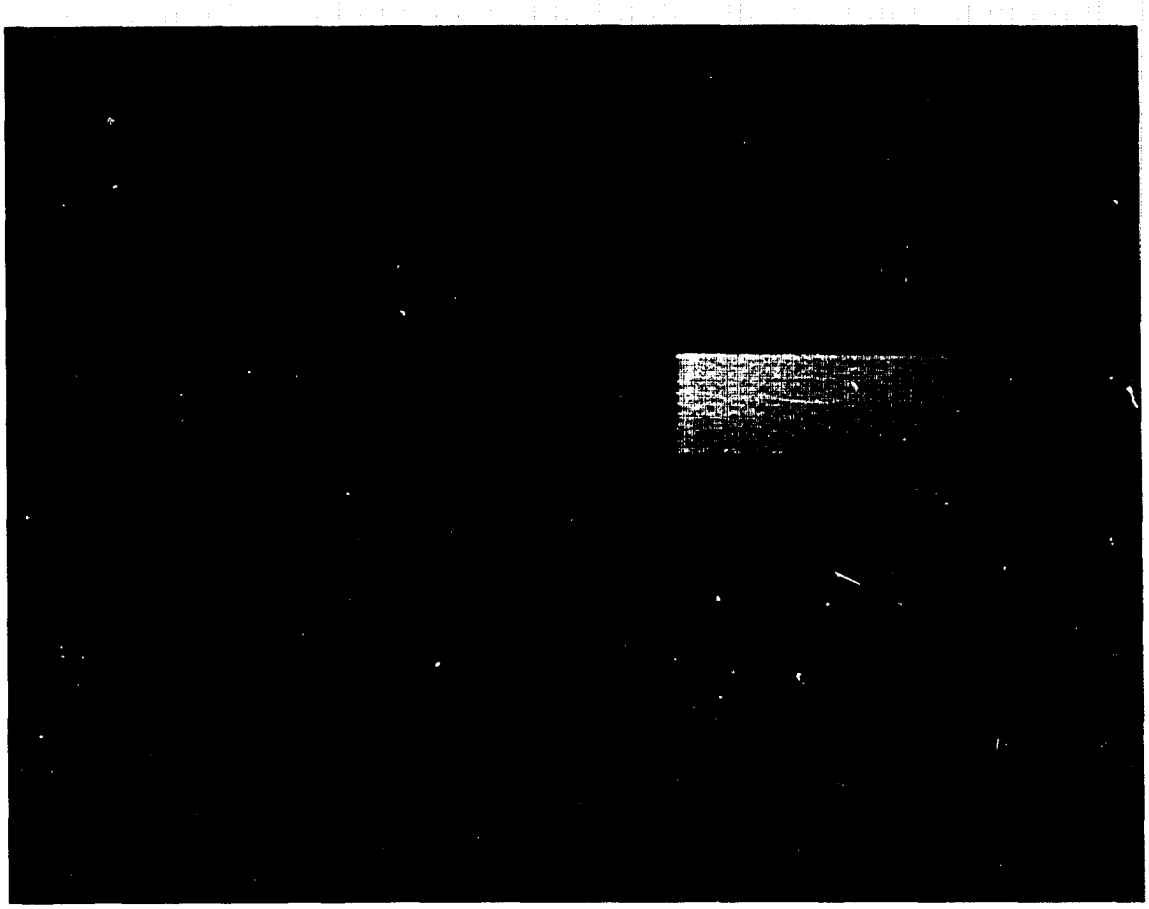

Figure 4.3.14 : Digitized image showing liquid-liquid-vapor phase behaviour

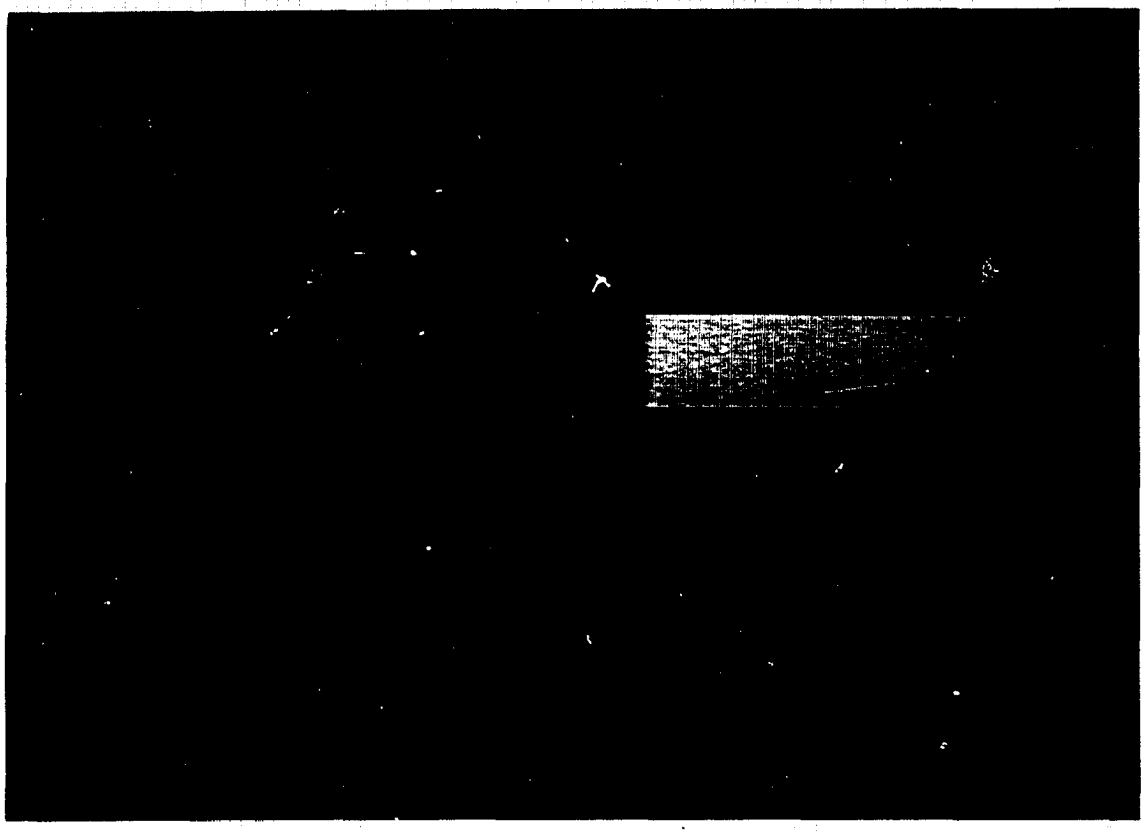

Figure 4.3.15 : Digitized image showing solid-liquid-vapor phase behaviour

4.4 Liquid Phase Density Measurements

The height (amount) and average intensity (i.e., level of grayness based on the intensity over an area) of various phases in the view cell were measured using the Jandel MOCHA digitizing software. Density correlations were then determined for opaque systems where the densities at ambient conditions were well known. Measurements were made at points during the experiment where the stirrer had been turned off and the mixture was allowed to settle. Densities of the experimental opaque fluid were determined by measuring the height of liquid as it expanded with increasing temperature. It was assumed that at temperatures below the "boiling point" , typically < 573 K, the total mass of material in the liquid phase was constant.

Table 4.4.1 displays the data used to determine a general density -intensity relationship and Figure 4.4.1 is a plot of the natural logarithm of intensity versus density. The plot displays significant scatter when data from all systems are plotted together. In general, the relationship between density and intensity is bounded by two lines :

lower bound	$\ln(\text{intensity}) = -1.509 \times \text{fluid density} (\times 10^3\ \text{kg/m}^3) + 6.103$
upper bound	$\ln(\text{intensity}) = -1.442 \times \text{fluid density} (\times 10^3\ \text{kg/m}^3) + 6.183$

Table 4.4.1 Data points used to compute a general intensity - density correlation

Run	Temperature (K)	Measured Density (x 10^3 kg/m^3)	Average Intensity
350g ABVB	344	1.009	101
	415	0.985	105
	469	0.942	108
	526	0.920	112
	589	0.885	117
	605	0.888	117
	623	0.866	119
	574	0.899	115
	648	0.855	129
	674	0.850	127
CHN001	298	0.973	111
CHN002-1	298	0.948	117
	648	0.799	140
CHN002-2	294	0.947	115
	326	0.927	116
	390	0.892	121
	494	0.843	130
	534	0.827	133
	566	0.815	135
	592	0.808	136
	615	0.802	136
	623	0.799	138
CHN003	297	0.926	127
	527	0.833	146
	623	0.833	147
	635	0.830	147
CHN00*	295	0.888	126
	331	0.87	130
	396	0.857	133
	454	0.819	139
	501	0.807	140
Gudao	297	0.999	112
	392	0.993	116
	446	0.963	117
	499	0.943	121
	544	0.920	123
	604	0.898	127
	623	0.888	127
	637	0.882	124
	654	0.872	128
	673	0.872	126
n-dodecane	294	0.749	146

Sample densities can be estimated to within ± 50 kg/m^3, with the general correlation. If correlations are developed for individual fluids, based on ambient densities, there is less scatter (e.g. : the 95% confidence level is ± 20 kg/m^3 . These plots are shown in Figures 4.4.1- 4.4.4 and the correlations are as follows :

ABVB + n-dodecane + hydrogen

ln (intensity) = -1.4406 x density (x 10^3 kg/m^3)+6.054, R= 0.9630

CHN001,2 & * + hydrogen

ln (intensity) = -1.2714 x density (x 10^3 kg/m^3)+5.952, R = 0.9554

CHN003 + hydrogen

ln (intensity) = -1.5312 x density (x 10^3 kg/m^3)+6.2621, R = 0.9984

GVR + hydrogen

ln (intensity) = -0.8900 x density (x 10^3 kg/m^3)+5.6254, R = 0.9132

Using the relationships for intensity versus density established above, densities of liquid phases at elevated temperatures were estimated. The ratio of initial volume of material to the amount of material at a specific temperature was also determined. In cases where complex phase behaviour was observed the amount of each phase was determined. The volume was calculated based on the height of material in the view cell, in the cases where "solid" was present in "clumps" the volume of "solid" could be determined accurately. Tables 4.4.2 - 4.4.13 are the results of fluid density computations using the above correlations.

Figure 4.4.1 Plot of Ln(intensity) versus measured density for all samples

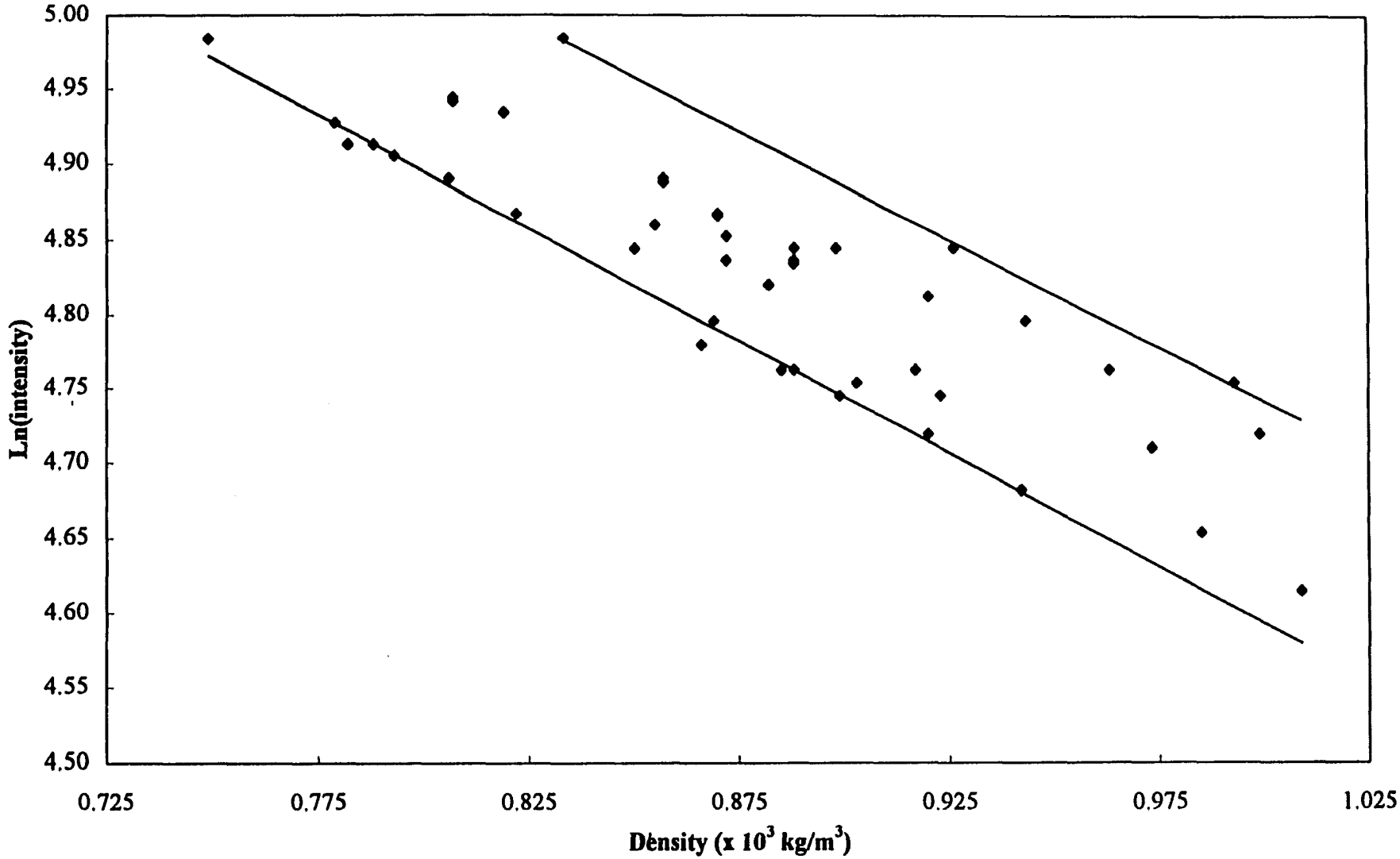

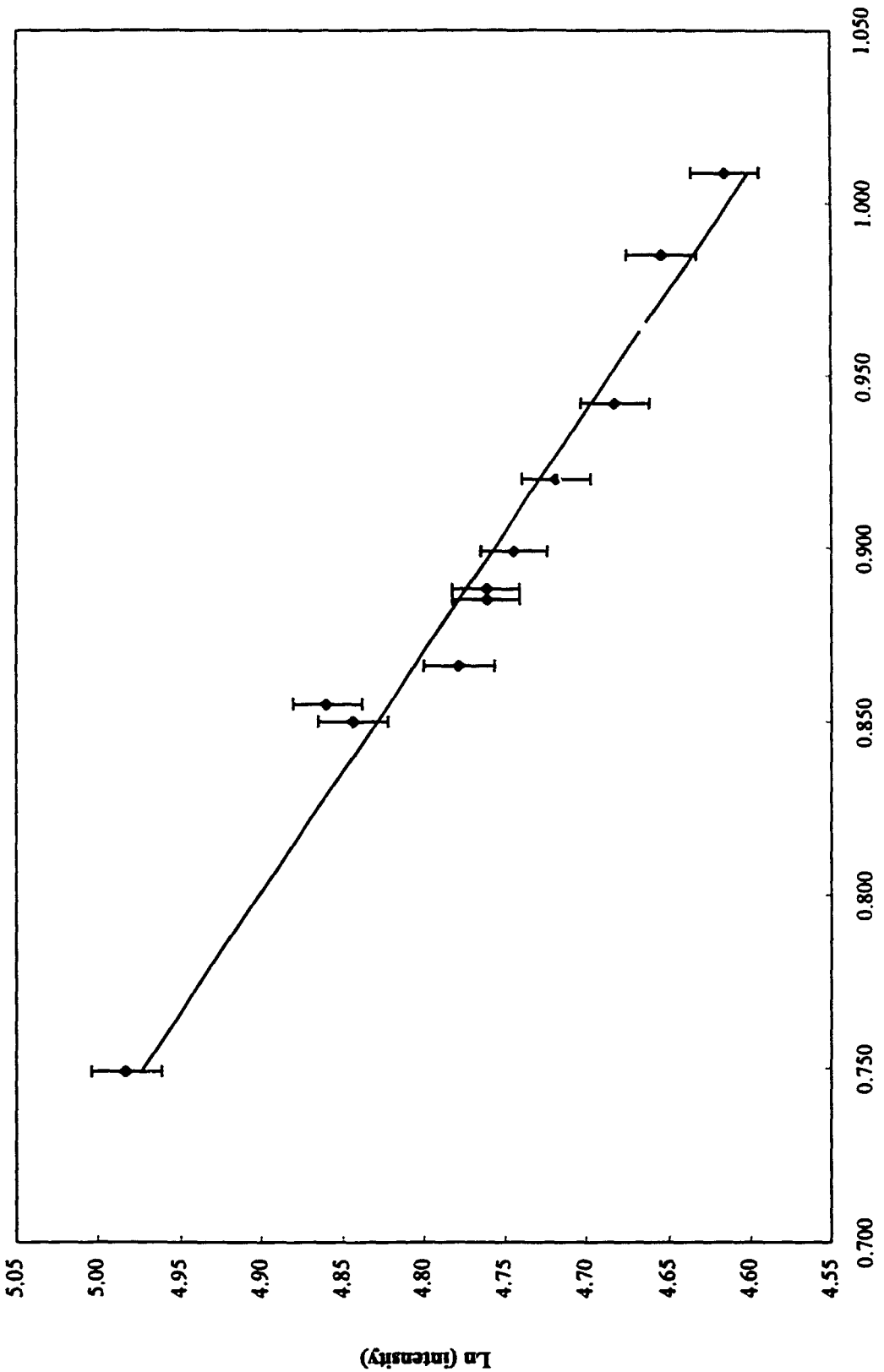

Figure 4.4.2 Plot of ln(intensity) vs. measured density for ABVB with hydrogen

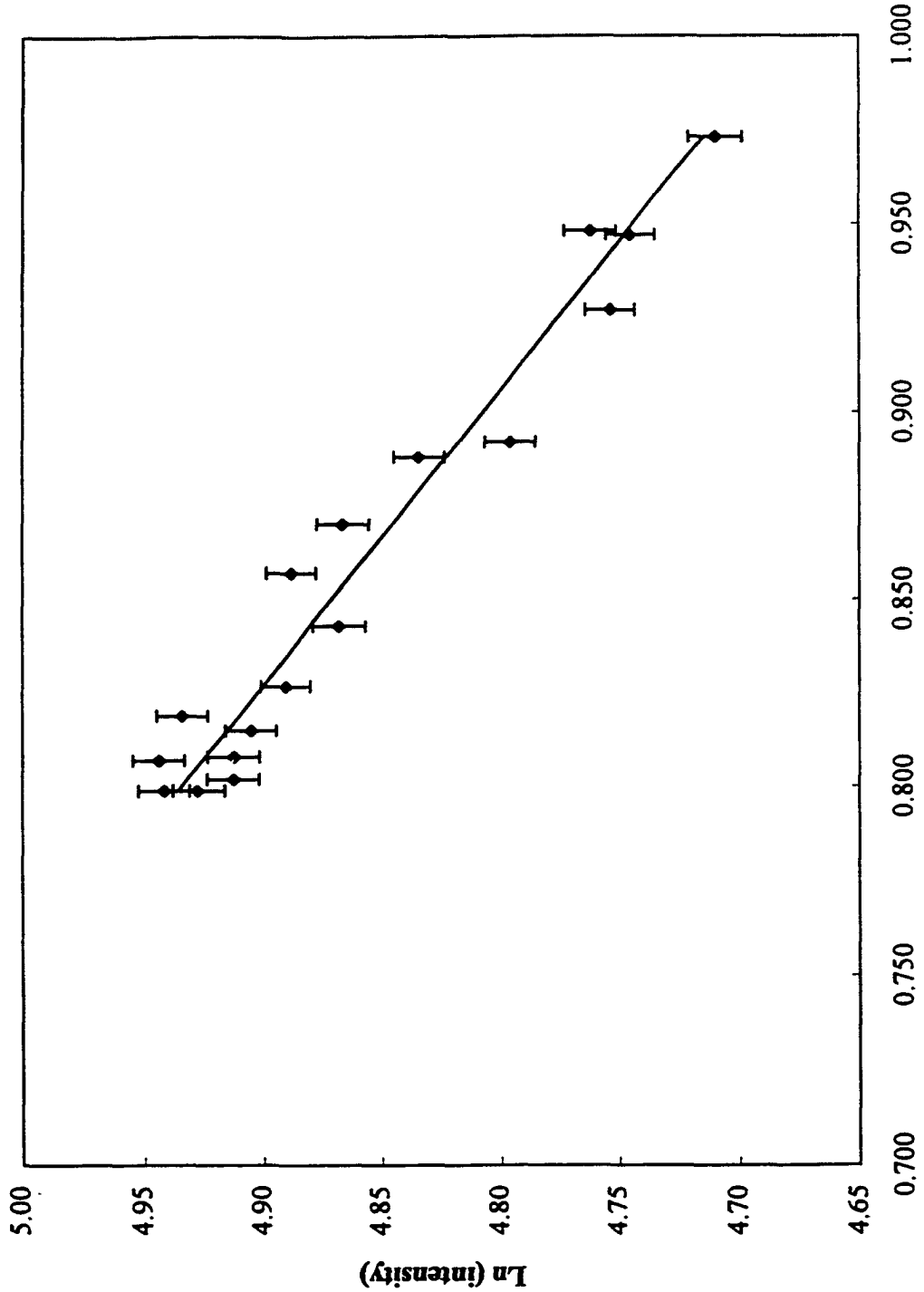

Figure 4.4.3 Plot of ln(intensity) vs. measured density for CHN001, CHN002 and CHN00ˣ with hydrogen

Figure 4.4.4 Plot of ln(intensity) vs. measured density for CHN003 with hydrogen

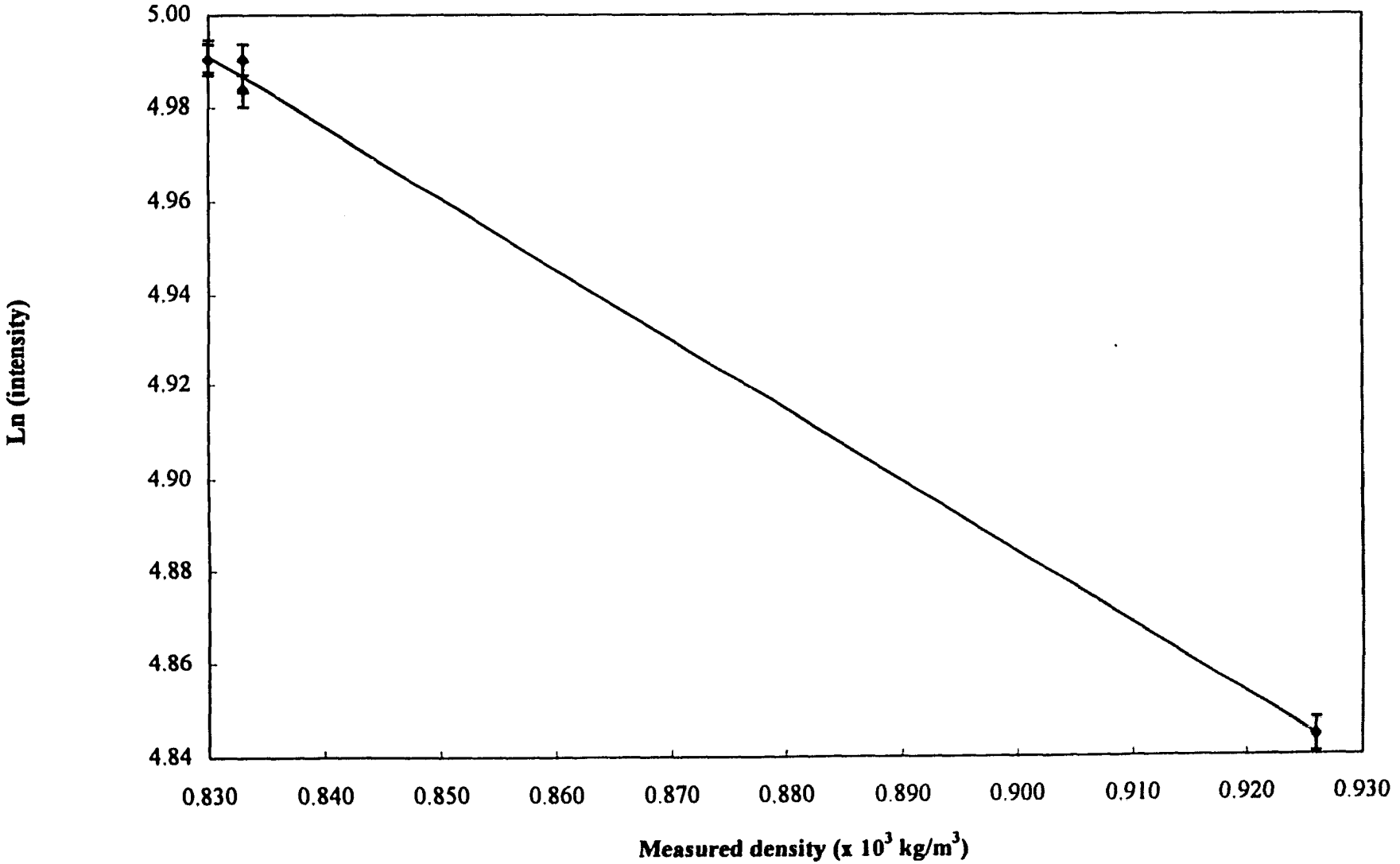

Figure 4.4.5 Plot of ln(intensity) vs. measured density for Gudao vacuum resid with hydrogen

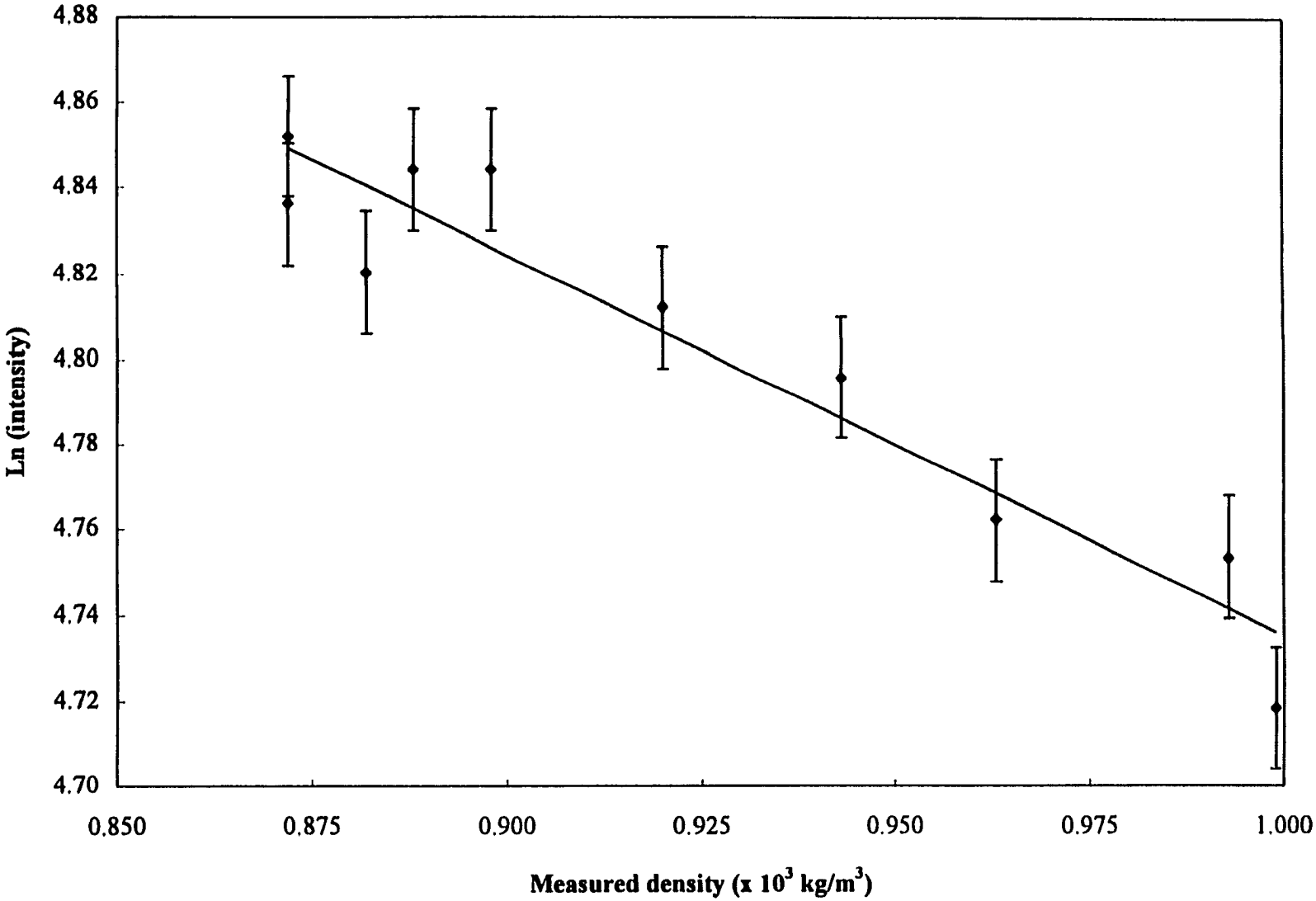

Table 4.4.2 -Density calculations : Run # 1 - 30g ABVB + 150 n-dodecane + 1.90 MPa hydrogen, liquid - vapour phase behaviour existed for the entire experiment

Temperature (K)	Pressure (MPa)	Average Intensity	Calculated density (x 10^3 kg/m^3)	(Volume of fluid present)/ (Initial volume of fluid)
298	1.896	137	0.785	1.000
339	2.103	145	0.747	1.032
400	2.482	149	0.729	1.086
494	3.172	157	0.691	1.160
530	3.482	161	0.675	1.166
561	3.861	163	0.666	1.139
587	4.206	163	0.666	1.064
611	4.551	159	0.683	0.930
630	4.861	157	0.691	0.775
647	4.875	146	0.743	0.615
648	5.171	147	0.738	0.588
698	6.274	122	0.868	0.144

Table 4.4.3 - Density calculations : Run # 2 - 75g ABVB + 150g n-dodecane + 1.97 MPa hydrogen

Temperature (K)	Pressure (MPa)	Phase	Average Intensity	Calculated Density (x 10^3 kg/m^3)	(Volume of fluid present)/ (Initial volume of fluid)	Volume (x 10^{-3} m3) of phase based on height {based on area}
298	1.965	S	92	1.060	1.000	
		L	152	0.715		
404	2.551	S	96	1.035	1.064	
		L	160	0.681		
430	2.723	L	145	0.749	1.102	
484	3.103	L	149	0.730	1.123	
619	4.619	L	150	0.725	0.979	
629	4.723	L	150	0.724	0.979	257
		S	n/a	n/a	n/a	9
659	5.171	L	144	0.750	0.843	
659	5.171	L	145	0.747	0.838	220
		S	n/a	n/a	n/a	8
673	5.447	L	142	0.764	0.749	194
		S	n/a	n/a	n/a	9
698	6.067	L	138	0.782	0.570	147
		S	n/a	n/a	n/a	8
702	6.274	S	95	1.045	0.574	16 {12}
		L	141	0.768		140{144}
704	6.412	S	94	1.050	0.570	21 {18}
		L	143	0.758		134 {137}

Table 4 4.4 - Density calculations : Run # 3 - 100 g ABVB+ 150 g n-dodecane + 1.999 MPa hydrogen

Temperature (K)	Pressure (MPa)	Phase	Average Intensity	Calculated Density (x 10^3 kg/m^3)	(Volume of fluid present)/ (Initial volume of fluid)	Volume (x 10^{-3} m3) of phase based on height {based on area}
294	1.999	S	81	1.155	1.000	
		L	132	0.812		
382	2.551	S	83	1.138	1.047	
		L	128	0.832		
469	3.137	L	124	0.856	1.115	
554	3.930	L	131	0.816	1.134	
616	4.723	L	131	0.818	1.016	
648	5.171	S	117	0.894	0.881	
		L	128	0.835		
670	5.585	S	112	0.927	0.779	
		L	128	0.835		
681	5.516	S	107	0.957	0.810	13{14}
		L	128	0.836		227{226}
688	5.654	S	110	0.939	0.806	20{21}
		L	131	0.817		219{218}
698	6.205	S	96	1.034	0.783	25{27}
		L	143	0.759		207{205}
317	1.586	S	79	1.168	0.992	31{28}
		L	120	0.876		263{266}

Table 4 4.5 - Density calculations : Run 4a - 150 g ABVB + 150 g n-dodecane + 2.068 MPa hydrogen

Temperature (K)	Pressure (MPa)	Phase	Average Intensity	Calculated Density (x 10^3 kg/m^3)	(Volume of fluid present)/ (Initial volume of fluid)	Volume (x 10^{-3} m3) of phase based on height {based on area}
294	2.068	S	81	1.151	1.000	
		L	130	0.822		
473	3.206	L	121	0.875	1.161	
573	4.068	L	128	0.836	1.177	
623	4.551	L	125	0.850	1.096	
648	4.482	L	123	0.861	1.032	
673	4.757	L	122	0.868	0.964	
698	5.929	S	95	1.039	0.631	29{19}
		L	124	0.854		188{198}
698	5.998	S	91	1.071	0.606	35{28}
		L	126	0.843		175{182}
331	1.586	S	76	1.194	1.048	48{41}
		L	114	0.917		313{321}

Table 4 4.6 - Density calculations : Run 4 - 150 g ABVB + 150 g n-dodecane + 2.068 MPa hydrogen

Temperature (K)	Pressure (MPa)	Phase	Average Intensity	Calculated Density (x 10^3 kg/m^3)	(Volume of fluid present)/ (Initial volume of fluid)	Volume (x 10^{-3} m3) of phase based on height {based on area}
305	2.172	S	93	1.058		
		L	148	0.733	1.000	
507	3.551	L	144	0.755	1.143	
549	3.930	L	143	0.755	1.154	
633	4.999	L	144	0.752	1.079	
623	4.895	L	147	0.738	1.079	
649	5.254	L2	124	0.855	1.025	57
		L1	143	0.759		293
673	5.640	L2	117	0.897	0.971	42
		L1	142	0.763		291
693	6.033	L2	118	0.888	0.896	41
		L1	145	0.748		267
703	6.288	L2+ S	108	0.952	0.842	n/a
		L1	142	0.761		n/a
536	4.082	S	95	1.038	1.140	n/a
		L	150	0.726		n/a
317	1.862	S	86	1.113	0.950	n/a
		L	118	0.891		n/a

Table 4.4.7 - Density calculations:Run # 5-187g ABVB+187g n-dodecane+2.86M Pa hydrogen

Temperature (K)	Pressure (MPa)	Phase	Average Intensity	Calculated Density (x 10^3 kg/m^3)	(Volume of fluid present)/ (Initial volume of fluid)	Volume (x 10^{-3} m3) of phase based on height
300	2.910	S	100	1.008	1.000	
		L	155	0.701		
346	3.227	S	100	1.006	0.973	
		L	157	0.693		
409	3.737	L	141	0.768	1.094	
462	4.240	L	148	0.736	1.136	
508	4.723	L	153	0.712	1.168	
547	5.171	L	151	0.717	1.195	
579	5.619	L	152	0.715	1.195	
608	6.067	L	153	0.712	1.186	
627	6.426	L2	128	0.834	1.171	71
		L1	152	0.713		513
644	6.619	L2	136	0.791	1.153	69
		L1	158	0.686		506
641	6.757	L2	124	0.857	1.118	69
		L1	149	0.727		488
627	6.550	L2	124	0.858	1.124	78
		L1	146	0.742		482
609	6.240	L2	126	0.846	1.145	74
		L1	143	0.758		497
526	4.964	L2	127	0.842	1.171	37
		L1	140	0.772		547
511	4.895	L2	126	0.847	1.165	
		L1	138	0.781		

Table 4.4.7 cont'd

Temperature (K)	Pressure (MPa)	Phase	Average Intensity	Calculated Density (x 10^3 kg/m^3)	(Volume of fluid present)/ (Initial volume of fluid)	Volume (x 10^{-3} m3) of phase based on height
497	4.688	L2	127	0.839	1.162	13
		L1	136	0.794		566
483	4.516	L2	138	0.783	1.156	12
		L1	138	0.781		565
471	4.344	L1	119	0.883	1.147	
		L2	135	0.795		
461	4.289	L	136	0.791	1.142	
450	4.192	L	135	0.798	1.136	
311	2.841	L	134	0.803	1.035	
307	2.792	L	128	0.834	1.024	
		S	n/a	n/a	n/a	5

Table 4.4.8 - Density calculations : Run # 6 - 187g ABVB + 112g n-dodecane + 2.861 MPa hydrogen

Temperature (K)	Pressure (MPa)	Phase	Average Intensity	Calculated Density (x 10^3 kg/m^3)	(Volume of fluid present)/ (Initial volume of fluid)
294	2.861	S	104	0.978	
		L	158	0.687	1.000
485	4.688	L	143	0.758	1.124
536	5.137	L	143	0.758	1.135
573	5.619	L	143	0.757	1.124
604	6.067	L	143	0.758	1.099
623	6.343	L	140	0.773	1.084
632	6.447	L	141	0.766	1.084
648	6.688	L	138	0.781	1.055
654	6.757	L	135	0.795	1.055
291	2.689	S	98	1.017	1.004
		L	125	0.852	

Table 4.4.9 - Density calculations : Run #7- 350g ABVB + 2.07 MPa hydrogen.

Temperature (K)	Pressure (MPa)	Phase	Average Intensity	Calculated Density (x 10^3 kg/m^3)	(Volume of fluid present)/ (Initial volume of fluid)	Volume (x 10^{-3} m3) of phase based on height
344	2.482	S+L	101	1.009	1.000	
415	2.896	S+L	105	0.985	1.025	
469	3.227	S+L	108	0.942	1.072	
526	3.530	S+L	112	0.920	1.097	
574	3.861	S+L	115	0.899	1.123	
589	3.999	S+L	117	0.885	1.141	
605	4.068	S+L	117	0.888	1.137	
623	4.206	L	119	0.866	1.166	
648	4.309	L	129	0.855	1.181	
674	4.413	L	127	0.850	1.188	
698	5.481	L2	116	0.904	1.072	109
		L1	136	0.795		263
706	5.792	L2	120	0.881	1.076	109
		L1	137	0.788		264
701	5.998	L2	106	0.965	1.014	95
		L1	134	0.802		257
657	5.861	S	100	1.005	0.982	n/a
		L	130	0.823		n/a
317	1.862	S	86	1.112	0.993	n/a
		L	118	0.890		n/a

Table 4.4.10 - Density calculations : 300ml CHN001 + 2.068 MPa hydrogen

Temperature (K)	Pressure (MPa)	Phase	Average Intensity.	Calculated Density (x 10^3 kg/m^3)	(Volume of fluid present)/ (Initial volume of fluid)	Volume (x 10^{-3} m3) of phase based on height
298	2.068	L	111	0.973	1.000	
623	3.875	L	133	0.834		
627	3.827	L2	115	0.952	1.146	48
		L1	134	0.828		296
629	3.813	L2	113	0.959	1.146	47
		L1	134	0.831		297
648	4.020	L2	108	0.998	1.154	37
		L1	135	0.825		309
673	4.551	L2	102	1.046	1.139	30
		L1	133	0.837		311
699	5.764	S	99	1.069	0.996	n/a
		L	134	0.828		n/a
704	6.688	S	100	1.063	0.994	n/a
		L	132	0.840		n/a
690	6.826	S	98	1.072	0.992	n/a
		L	132	0.841		n/a
299	2.068	S	91	1.133	0.921	n/a
		L	123	0.898		n/a

Table 4. 4.11 -Density calculations : 285ml CHN002 + 2.068 MPa hydrogen

Temperature (K)	Pressure (MPa)	Average Intensity	Calculated {Measured} Density (x 10^3 kg/m^3)	(Volume of fluid present)/ (Initial volume of fluid)
294	2.068	115	0.948{0.947}	1.000
326	2.261	116	0.936{0.927}	1.022
390	2.689	121	0.905{0.892}	1.062
494	3.413	130	0.846{0.843}	1.123
534	3.723	133	0.827{0.827}	1.145
566	3.985	135	0.817{0.815}	1.163
592	4.206	136	0.811{0.808}	1.172
615	4.413	136	0.809{0.802}	1.181
623	4.495	138	0.800{0.799}	1.185
646	4.778	134	0.819{0.802}	1.181
648	4.778	135	0.816{0.799}	1.185
657	4.930	138	0.800	1.176
664	5.206	134	0.823	1.150
670	5.157	136	0.811	1.163
695	6.205	138	0.797	1.035
704	6.688	136	0.809	0.960
701	6.757	135	0.815	0.956
683	6.688	133	0.829	0.947
669	6.550	132	0.833	0.956
663	6.536	132	0.833	0.974
658	6.378	132	0.832	0.982

Table 4.4.11 cont'd

Temperature (K)	Pressure (MPa)	Average Intensity	Calculated Density (x 10^3 kg/m^3)	(Volume of fluid present)/ (Initial volume of fluid)
652	6.309	132	0.836	0.987
644	6.309	132	0.834	0.996
637	6.102	136	0.808	1.000
630	6.019	129	0.849	1.013
605	5.654	128	0.859	1.031
599	5.585	127	0.862	1.040
592	5.495	129	0.854	1.040
623	5.929	129	0.849	1.013
617	5.826	128	0.861	1.022
610	5.757	129	0.852	1.022
586	5.412	126	0.869	1.040
581	5.343	128	0.860	1.044
575	5.274	126	0.870	1.044
570	5.206	126	0.873	1.048
565	5.137	126	0.873	1.048
560	5.068	127	0.866	1.048
555	4.999	125	0.876	1.048
544	4.964	125	0.880	1.048
540	4.826	124	0.882	1.053
531	4.723	125	0.877	1.053
515	4.551	123	0.889	1.057

Table 4.4.11 cont'd

Temperature (K)	Pressure (MPa)	Average Intensity	Calculated Density (x 10^3 kg/m^3)	(Volume of fluid present)/ (Initial volume of fluid)
503	4.413	122	0.897	1.053
483	4.158	124	0.886	1.048
465	3.951	120	0.912	1.048
449	3.785	120	0.909	1.044
434	3.620	121	0.906	1.040
401	3.241	120	0.912	1.031
416	3.392	120	0.913	1.035
387	3.089	120	0.914	1.022
376	2.930	118	0.924	1.022
299	2.172	121	0.904	0.987

Table 4.4.12 - Density calculations : 300 ml CHN003 + 2.068 MPa hydrogen

Temperature (K)	Pressure (MPa)	Average Intensity	Calculated {Measured} density (x 10^3 kg/m^3)	(Volume of fluid present)/ (Initial volume of fluid)
297	1.999	127	0.928{0.927}	1.000
527	3.723	146	0.835{0.839}	1.104
623	4.764	147	0.829{0.839}	1.104
635	4.840	146	0.833{0.836}	1.108
648	5.102	144	0.845	1.096
673	5.550	145	0.838	1.052
681	5.661	145	0.841	1.056
703	6.757	143	0.848	0.892
687	6.791	141	0.856	0.884
671	6.619	138	0.873	0.908
641	6.123	135	0.887	0.948
626	5.964	137	0.879	0.968
623	5.571	134	0.892	0.996
614	5.771	134	0.892	0.984
589	5.392	133	0.896	1.004
577	5.240	133	0.895	1.012
566	5.102	132	0.901	1.016
556	4.964	131	0.905	1.028
546	4.813	132	0.903	1.028
532	4.599	130	0.908	1.032

Table 4.4.13 cont'd

Temperature (K)	Pressure (MPa)	Average Intensity	Calculated {Measured} density(x 10^3 kg/m^3)	(Volume of fluid present)/ (Initial volume of fluid)
520	4.440	129	0.915	1.032
509	4.275	129	0.917	1.040
497	4.137	128	0.920	1.036
486	3.999	128	0.923	1.036
476	3.875	127	0.927	1.032
466	3.758	126	0.929	1.032
300	2.124	128	0.922	0.972

Table 4.4.13- Density calculations : 300ml CHN00* + 1.379 MPa hydrogen

Temperature (K)	Pressure (MPa)	Average Intensity.	Measured Density (x 10^3 kg/m^3)	Calculated Density (x 10^3 kg/m^3)	(Volume of fluid present)/ (Initial volume of fluid)
295	1.379	126	0.888	0.892	1.000
331	1.517	130	0.870	0.869	1.020
396	1.848	133	0.857	0.852	1.036
454	2.172	139	0.819	0.817	1.084
501	2.496	140	0.807	0.811	1.100

Table 4.4.14 - Density calculations : 150g GVR + 2.068 MPa hydrogen

Temperature (K)	Pressure (MPa)	Average Intensity	Measured density (x 10^3 kg/m^3)	Calculated density (x 10^3 kg/m^3)	(Volume of fluid present)/ (Initial volume of fluid)
297	2.068	112	0.999	1.016	1.000
392	2.586	116	0.993	0.975	1.007
446	2.930	117	0.962	0.973	1.040
499	3.172	121	0.943	0.930	1.060
544	3.516	123	0.920	0.911	1.087
604	3.861	127	0.898	0.877	1.113
623	3.930	127	0.888	0.873	1.127
637	4.068	124	0.882	0.904	1.133
654	4.164	128	0.872	0.866	1.147
673	4.344	126	0.872	0.891	1.147
693	5.978	125		0.897	0.813
693	5.792	124		0.907	0.827
694	5.847	123		0.915	0.820
695	5.792	124		0.902	0.840
697	5.757	125		0.895	0.847

4.5 "Solid"

4.5 1 The Appearance of "Solid" in the Phase Diagrams

The heavier material that separates and is not dispersed by mixing during the complex phase transitions has been referred to as a solid. Whether this material is in fact a solid remains an open question. There are several plausible answers to the question : what is the nature of the material. Possible answers include, a crystalline solid, a gel, a wax or very viscous liquid are just a few of the possibilities. One approach pursued was to compare the heats of fusion determined experimentally with values for various solids. A thermodynamic model was developed based on the assumption that the liquid mixture is in equilibrium with a mixed solid, that is, that the fugacity of component *i* in the liquid is equal to the fuagcity of component *i* in the solid phase. This model is presented in Appendix A. The composition of the liquid mixture is a function of temperature since hydrogen solubility in the mixture is temperature and pressure dependent. Hence the amount of hydrogen dissolved in the liquid was determined by the difference in the actual pressure and the calculated pressure using the ideal gas law ($Z \approx 1.00 \pm 0.0003$ under these conditions) and based on the volume of the view cell occupied by the gas. Initially a hydrogen solubility model [106,107], based on corresponding states theory, developed for heavy oil / bitumen mixtures and other ill-defined solvents, was used. The model is very sensitive to small changes in volume of gas present and because the ratio of liquid to vapour is less than 0.25 small changes in the volume of gas cannot be evaluated with the necessary precision.

The thermodynamic model assumes that the difference in the partial molar volumes of component *i* in the liquid and solid phases is very small and is within the order of magnitude of 0.001 m^3/mol. The model also assumes that the "solid" arises solely from the ABVB and the solid composition is not a function of temperature. Finally, enthalpies of transitions from "solid" to liquid were determined by evaluating $(\delta P/\delta T)_{S\rightarrow L}$ from the pressure - temperature trajectories and are reported in Table 4.5.1 along with enthalpies of fusion for other materials [106] reported in Table 5.4.2.

Table 4.5.1 : Enthalpy of fusion for "solid" existing at low temperatures

Mass of ABVB	T(K)	P(bar)	dP/dT* (bar/K)	S (moles of H_2/ bar kg solvent)	$\delta S/\delta T$(moles of H_2 K / bar kg solvent)	$\Delta H_{L\rightarrow S}$ (kJ/mol)	$\Delta H_{L\rightarrow S}$** (J/g)
75	459	28.75	0.110	0.0090	1.72E-05	46	9
100	419	27.92	0.086	0.0044	1.40E-05	35	7

* - an average value of 0.098 bar / K was used
** - based on a molecular weight of 5000 g/mol

Table 4.5.2 Enthalpy of fusion for miscellaneous substances[106]

Materials	Range of enthalpies of fusion (J/g)
Waxes (aliphatic)	135 - 610
Waxes (amorphous)	1.3 - 44
Organic solids (aliphatic)	58 - 247
Organic solids (aromatic)	8.7 - 31
Asphaltenes	2.0 - 6.3
Micelles	-63 - 79
Gels	-2.2 - 1.7

4.5.2 "Solid" and Fluid Analysis

"Solid" and liquid samples were removed from the view cell after some of the experiments were completed. The samples were analysed by CANMET-ERL and the results are shown in Figure 4.5.2.1 and 4.5.2.1 and Tables 4.5.2.1 and 4.5.2.2. The compositions of the liquid samples are reported as wt. % of petroleum fractions : IBP - 468 K naptha, 468 - 616 K middle distillate, 616 - 797 K gas oil and 797 + K residue. These compositions are compared with the initial composition of the mixture before the experiment and it should be noted that the n-dodecane (B.P. = 493 K) falls into the middle distillate fraction. The analysis was done on a gas-free basis and the "solid" present at the end of the experiment was not included since the "solid" would be 100 wt. % of the 797 + K boiling fraction.

Aromatic carbon content of the high temperature "solid" retrieved from experiments with the ABVB + n-dodecane + hydrogen runs was determined and these results are presented in Table 4.5.3 and Figure 4.5.3. "Solid" samples were also analysed for heavy metals. Mass balances for vanadium content were very good and since there is only one source of vanadium (from the ABVB) the heavy metals analyses suggest that the majority of the heavy metals appear in the "soiids". Other metals such as iron and nickel have multiple sources (such as contamination from the view cell walls and the gaskets) hence the analyses of these metals were less reliable.The results of the vanadium content in the "solid" samples are shown in Table 4.6.3 and Figure 4.6.3 and can be used as a reliable trace for the fate of the other heavy metals in the original hydrocarbon mixture.

Table 4.5.2.1 Chemical analysis (wt. %) of ABVB + n-dodecane + hydrogen mixtures - initial mixture (including "solids") and final liquid (on a gas free basis)

	#4 initial mixture	# 4 final liquid	#5 initial mixture	# 5 final liquid	# 6 initial mixture	# 6 final liquid	# 7 initial mixture	# 7 final liquid
Naptha	0	9	0	3	0	5	0	24
Mid. Distill.	50	54	38	34	50	60	0	22
Gas Oil	0	22	0	10	0	10	0	23
Residue	50	15	62	53	50	50	100	31

Table 4.5.2.2 Chemical analysis (wt. %) of partly processed crude mixture - initial mixture and final liquid (on a gas free basis)

	CHNOO*	CHNOO*	CHNOO1	CHNOO1	CHNOO2	CHNOO2	CHNOO3	CHNOO3
	initial	final	initial	final	initial	final	initial	final
Naptha	11	21	8	10	10	17	14	18
Mid. Distill.	30	45	20	36	33	45	38	48
Gas Oil	38	30	38	36	36	27	33	29
Residue	21	4	34	18	21	11	15	5

Table 4.5.2.3 Aromatic carbon content of ABVB + n-dodecane + hydrogen - initial mixture, final "solid" and final liquid

	Aromatic Carbon Content			
Run #	Mole fraction of ABVB (hydrogen free basis)	initial mixture (mass balance)	final "solid"	final liquid
2	0.080	11.8	58	0
4	0.148	17.7	38	13
7	1.000	35.4	54	34

Table 4.5.2.4 Vanadium content of ABVB + n-dodecane + hydrogen - initial mixture, final "solid" and final liquid

Run #	Vanadium Content (ppm)			
	Mole fraction of ABVB (hydrogen free basis)	initial mixture (mass balance)	final "solid"	final liquid
2	0.080	122	1073	44
4	0.148	183	2624	26
7	1.000	366	1044	76

Figure 4.5.2.1 Chemical analysis of initial mixture(including "solids") and final liquid for model bitumen mixtures

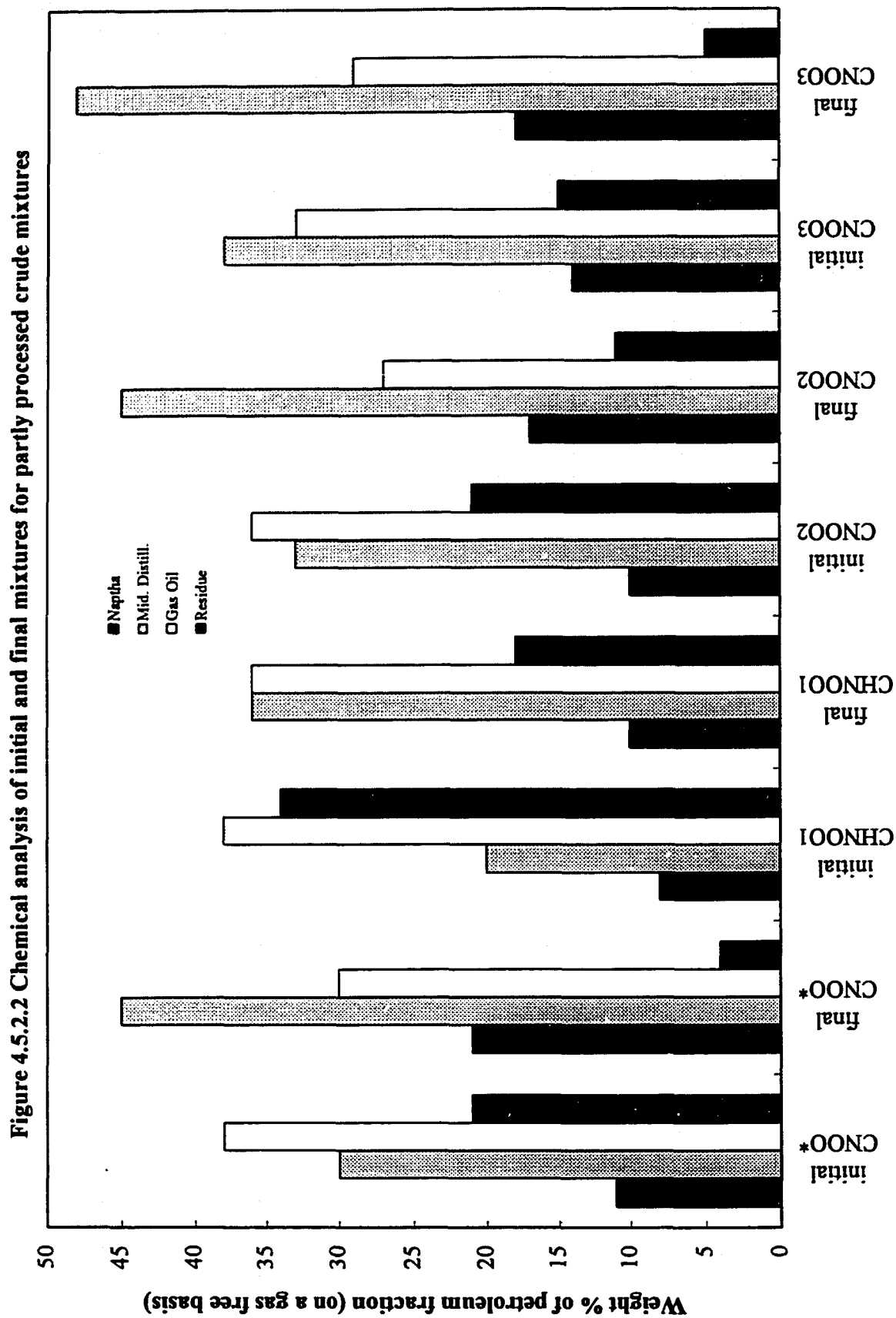

Figure 4.5.2.2 Chemical analysis of initial and final mixtures for partly processed crude mixtures

Figure 4.5.2.3 Aromatic carbon content of ABVB + n-dodecane + hydrogen mixtures - initial mixture (including "solid", final "solid" and final liquid

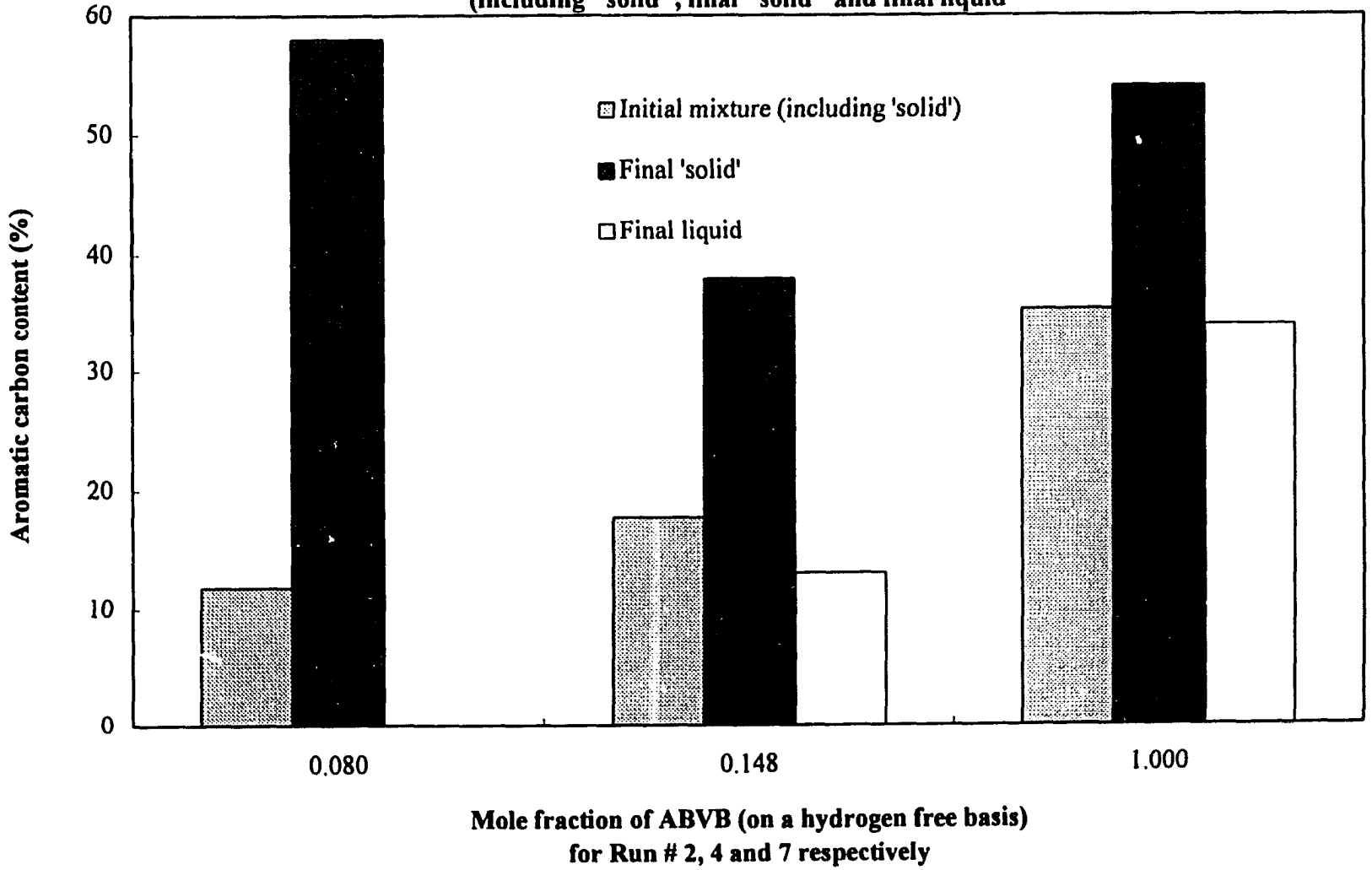

Figure 4.5.2.4 Vanadium content of ABVB + n-dodecane + hydrogen mixtures - initial mixture (including "solid"), final "solid" and final liquid

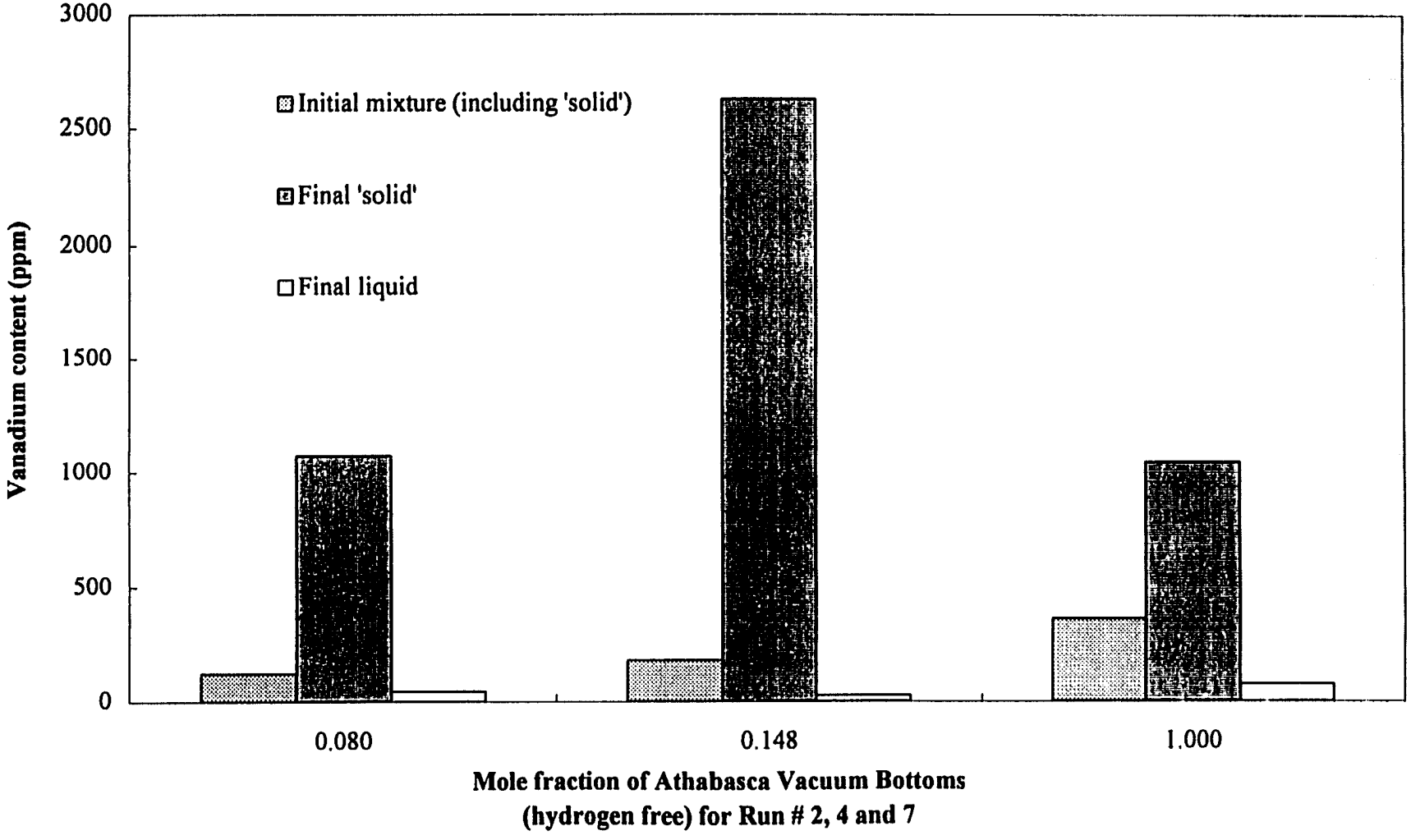

4.5.3 "Solids" Produced at Low and High Temperatures

A mixture comprising equal parts of ABVB and n-dodecane was stirred and allowed to equilibrate for several days under ambient conditions. The sample was then filtered under vacuum and the residue was air-dried and then oven-dried (323 K). This "solid" sample and a "solid" sample obtained from Run # 4 (150g ABVB + 150g n-dodecane + 2.07 MPa hydrogen) produced at 693 K, referred to as the low and high temperature "solids" respectively, were analysed. The low temperature "solid" had a H/C ratio of 1.3 and the high temperature "solid" had a H/C ratio of approximately 0.85. Aromatic carbon content analysis of the "solid" samples was also performed and was 57 wt. % and 47 wt.% for the low and high temperature "solids" respectively. The low temperature "solid" was completely soluble in toluene while the high temperature "solid" has a less than 5 wt.% fraction insoluble in toluene (ratio of sample to toluene was 1: 40 in both cases). This test suggests that the high temperature "solid" contained approximately 5 wt. % coke. However, only a small sample of high temperature "solid" was available for the solubility test hence the result is approximate.

4.5.4 Phase behaviour and Heavy oil upgrading

The pressure - temperature phase diagram for Run # 4 (model whole bitumen - 50 wt.% n-dodecane + 50 wt.% ABVB) is superimposed on the operating conditions for heavy oil / bitumen upgrading processes in Figure 4.5.4.1. The reader should note this diagram is intended for qualitative and comparative purposes only. The reader should also note that the phase boundaries are approximate e.g. the boundaries between liquid - liquid - "solid" and vapour - liquid - "solid", and vapour - liquid - "solid" and vapour - liquid regions are not fixed.

Figure 4.5.4.1 Heavy oil upgrading processes with typical phase behaviour exhibited by a model bitumen

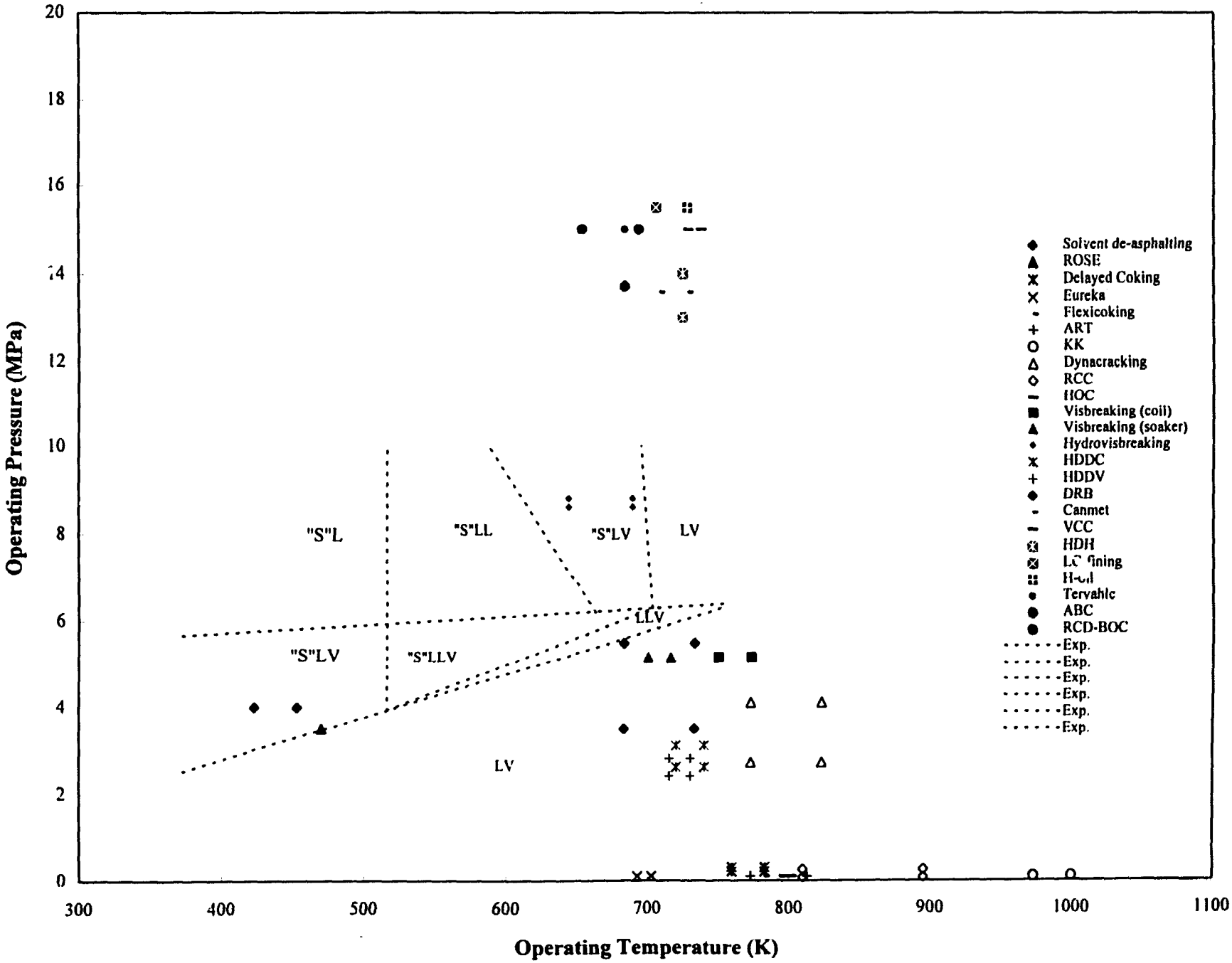

5.0 Discussion

5.1 X-ray Imaging

The X-ray imaging technique developed as part of this Ph.D thesis program has been used to make the first direct observations of complex phase behaviour of opaque organic fluids at elevated temperatures and pressures. This technique can distinguish relatively small density differences between liquid hydrocarbon phases in the order of magnitude of 0.04 g/cm^3. The x-ray imaging system has been used to investigate the phase behaviour of a series of Athabasca bitumen vacuum bottoms + n-dodecane + hydrogen and partly processed crudes + hydrogen systems. The different phases are distinguished easily and clearly. The intensity or shade of gray is such that :

Vapour < Liquid 1 < Liquid 2 < "solid"

With the current x-ray imaging system it is not possible to distinguish a discrete phase in a continuous one when the density differences is small. The resolution is not high enough but increasing the resolution may address this issue. At present the CCD camera has the lowest resolution in the imaging loop, followed by the video recorder and the monitor. Hence resolution would be improved with a better camera. Another major obstacle with the current set-up is the limitation imposed by the design pressure of the view cell. Typically design pressures are dictated by sealing mechanisms and stress analysis, in this sandwich type pressure vessel, the maximum allowable working pressures are dictated by the seal achieved with the gasketing material. Apparatus modification is among the current duties of S. Seyfaie, a post doctoral fellow.

5.2 Complex Phase Behaviour

The presence of complex phase behaviour in heavy oil + hydrogen systems is shown to be a common phenomenon. While the phase diagrams produced are crude they provide the first concrete evidence of the complex nature of phase behaviour that arises with heavy oil/bitumen mixtures under processing conditions. These findings will have a significant impact on the processing, design and operation of heavy oil upgrading processes. For example, reaction kinetic and hydrodynamic models must now consider the existence of not just the typical two phases (liquid and vapour) but must incorporate the possible appearance of three and four organic phases. One such consideration is the significant mass transfer resistance between liquids as opposed to gas liquid mass transfer resistance which is negligible by comparison. Varying gas solubilities in the different liquid phases imposes limits on hydrogen concentration and consequently affects kinetic models. Issues such as gas and liquid hold-up, especially in the fixed bed reactors, would be further complicated by the appearance of a second liquid phase or a "solid" phase. The probability of complex phase behaviour must also be considered in downstream processing where depressurization at elevated temperatures is a common practice. During a pressure let-down one could foresee phase transitions from liquid - vapour, to liquid - liquid - vapour and even "solid" - liquid - liquid - vapour where lines and vessels could become "plugged". There are many examples of such processing problems in industry and Syncrude and Amoco (who share common LC-fining processing technology) have consulted with this laboratory to address such issues.

The results of this research project also provide an initial starting point for further, more detailed, investigations of the phase behaviour of heavy oil systems (Ph.D. thesis (not yet published), J. Abedi) and provide some data to begin the task of modelling the phase behaviour of such systems (Ph.D thesis (not yet published), C. Cartlidge).

The onset of complex phase behaviour in the heavy oil systems appears to be dependent on the amount of "heavier material" in the mixture. In the experiments with partly processed crudes CHN002 ,CHN003 and CHN00*, which contain less than 21 wt. % of fraction 797 K + resid, complex phase behaviour was not encountered. Alternatively, the experiment with CHN001 which contained approximately 33 wt. % 797 K + resid exhibited complex phase transitions even at temperatures as low as 623 K well below the temperatures where hydrogenation or coking reactions become significant. Similarly with the ABVB + n-dodecane + hydrogen system once the amount of pentane insoluble material went from 6.4 wt.% to 12.8 wt.%, the occurrence of phase transitions from vapour - liquid to vapour - liquid - "solid" was apparent. As the amount of pentane insoluble material increased further, to greater than 20 wt.%, the phase behaviour became even more complex. This behaviour is entirely consistent if one considers the critical properties of n-dodecane. The critical temperature of n-dodecane is 658 K which corresponds to the temperature range where the onset of most of the complex phase behaviour by the heavy oil mixtures was exhibited. This type of behaviour is entirely consistent with the occurrence of multiphase behaviour in binary mixtures of dissimilar molecules near the critical point of the more volatile component where the behaviour is

further complicated by the appearance of a solid. Consequently the phase diagrams obtained for Run # 4 and # 7 were constructed with careful consideration and extrapolation of the effect of a solid on a binary system demonstrating type V behaviour according to the Van Konynenburg and Scott, 1980 classification scheme[88, 89]. These results are also consistent with the results of the impact of a solid on a model reservoir fluid exhibiting liquid - liquid - vapour phase behaviour[94]. The interference of the solid phase becomes more pronounced, as expected with the addition of the less volatile component i.e. as more ABVB is added. The phase diagrams were also drawn to be consistent with the necessary sequencing of the surrounding phases as explained in section 2.3.

5.3 Reversibility and non-equilibrium issues

The question as to whether the observed phase behaviour is a thermodynamically driven phenomenon or simply the result of chemical reaction must be addressed. While this researcher agrees that chemical reactions takes place at elevated temperatures the results cannot be fully and solely explained by reaction kinetics[102]. The most rigorous test for thermodynamic phase transitions is reversibility. During the course of an experiment one would expect that the paths be reversible. For example, once a mixture exhibiting "solid" at high temperatures begins to cool down the "solid" that appears at a high temperature should redissolve and finally reappear at ambient conditions. This expected course of events was not observed except in two of the experiments, runs # 5 and # 6, where

transitions from "solid" - liquid - vapour to liquid - vapour back to "solid" - liquid - vapour (at room temperature), and "solid" - liquid - vapour to liquid - vapour to liquid - liquid - vapour to liquid - vapour and back to "solid" - liquid - vapour (at room temperature) were observed, respectively. Only partial reversibility is observed in the case of the solids. Furthermore, following techniques outlined in this thesis, J. Abed is able to reproduce such transitions [113]. For the runs where phase transitions from liquid-vapour to liquid-liquid-vapour were observed, reversibility arose uniformly. Once the phase transition from liquid-vapour to liquid-liquid-vapour was observed the reverse phase transition could be obtained by turning off the heater and allowing the temperature and pressure to decrease.

The following justifications are discussed to reinforce the argument for a thermodynamic approach. While it is agreed that some reactions are taking place, it is accepted that dehydrogenation and hydrogenation reactions do not begin to occur at high rates below 673 K. In the cases where the experiments were carried to temperatures above 673 K it is most likely that dehydrogenation reactions had begun to occur in the "solid" phase and would explain the presence of some coke. The formation of coke is irreversible and would explain the presence of the "solid" phase during the descent to ambient temperatures also once coke forms it tends to deposit and attach to view cell walls. In runs # 5 and 6 where the temperatures did not exceed 653 K the disappearance and reappearance of the "solid" was observed.

If we assume that the "solid" is essentially asphaltene, then a factor that must be considered is the very nature of the asphaltene molecule. At ambient conditions the asphaltene molecule is existing in a metastable state i.e. it is surrounded by resin molecules in a layered sheet-like manner. As the temperature is increased the resin molecules are stripped from around the asphaltene molecule leaving a more stable, less soluble material which remains in a separate phase as the temperature is decreased .

By comparing the chemical analysis of the initial mixture with the final liquid present at the end of an experiment a shift in the amounts of the various petroleum fractions is observed which is consistent with desolvation. Chemical reaction also plays a significant but not necessarily an overriding role at temperatures greater than 675 K (e.g. Run # 7) where a pressure decrease was observed. The largest change in composition is seen with Run # 7.

Another way to assess the impact of reaction on the result is to compare the initial and final pressures obtained for the experiments. A decrease in pressure can reflect a net hydrogen consumption or it can reflect a change in the hydrogen solubility of the mixture. An increase in the pressure can reflect production of light gases or also a change in hydrogen solubility of the mixture. In runs #6 and #7 there was significant decrease of approximately 4.8 % and 23 % or 0.065 moles and 0.22 moles, respectively. . For runs # 1-5 this pressure difference is not significant and suggests that the extent of reaction is

not significant. In a typical experiment the system is subjected to temperatures > 673 K for approximately 2 hours (not applicable to runs # 5 and 6 which was not heated above 653 K. Another factor that must be considered is that at the very beginning of each experiment the systems are not at equilibrium. Once the temperature goes above 373 K, the point at which the ABVB begins to soften, and the point at which stirrer is switched on, the system quickly reaches equilibrium. Hence for the experiments with higher concentrations of ABVB some decrease in pressure is expected as more hydrogen is dissolved at the end of than at the beginning of an experiment. This difference accounts for approximately 0.02 MPa. Mixtures with higher ABVB concentrations would also have final compositions with higher hydrogen solubilities as the resins are "stripped" from the asphaltene molecules. Resins have higher hydrogen solubilities than asphaltenes. For the experiments considered here hydrogen consumption is less than 0.1 wt. % of the feed. Thus the impact of reaction is also anticipated to be modest, as long as one considers stripping of asphaltenes to be a physical process.

5.4 The Nature of the "Solid"

From the analysis of the high and low temperature "solid" samples it would appear that the compositions are dissimilar i.e. the high temperature "solid" has a lower hydrogen to carbon ratio and a 5 wt. % coke content. However, it is proposed that the dissimilarity is more a function of the nature of the asphaltenic materials present. Asphaltenes are defined simply by a solubility class i.e. the n-alkane insoluble fraction of a petroleum[95].

Typically the n-alkane is either n-pentane, n-hexane or n-heptane with the solubility test determined in a 40 : 1 ratio of solvent to petroleum. Furthermore asphaltenes have been characterized as being toluene or benzene soluble. Asphaltenes are one of the most studied fractions of petroleum since they are the cause of major problems due to their propensity to flocculate and precipitate during recovery and refining. Unfortunately there is no general agreement upon the definition in industry and the subjectivity of the definition encompasses a wide range of chemicals with different molecular weights, chemical structures and properties. However, it is generally agreed that asphaltenes comprise of high molecular weight molecules which tend to be polynucleararomatic in nature. The average molecular weight of asphaltenes is between 2,000 - 300, 000 g/mol depending on the method of determination. Asphaltenes from the Alberta Oil Sands have molecular weights in the range of 5000 - 8000 g/mol[96]. Asphaltenes are dark brown to black friable solids with no definite melting point (typically in the range of 373 to 423 K). They are generally thought of as very complex aromatic molecules surrounded and linked by aliphatic chains and heteroatoms [96, 97]. Asphaltenes have hydrogen to carbon ratios from 0.65 to 1.65. One view of asphaltenes is that of a traditional colloid [98,100]. Another view is one of the basic asphaltene molecule existing in a "sheet" like manner surrounded by layers of resins[99] (n-heptane and toluene soluble but ethylacetate insoluble fraction). It is believed that the tendency for resin to associate with asphaltenes influences the solubility of asphaltenes in the crude oil mixtures.

From the aforementioned classification of asphaltenes and the analytical results it is believed that the high and low temperature "solid" materials are in fact asphaltenic in nature. They both have hydrogen to carbon ratios that fall in the classification range and aromatic carbon content in the right range. It is proposed that as the temperature and pressure increase the amount of asphaltenic material in the liquid mixture increases allowing for complete dissolution and a transition from "solid" - liquid - vapour to liquid - vapour. Once the temperature and pressure are further increased and the system begins to approach the critical temperature of n-dodecane then the dissimilarity in the heavy asphaltenic material and light n-dodecane drives the system to complex phase behaviour. It is clear that the onset of complex phase behaviour is dependent on the amount of asphaltenic material in the mixture or conversely the amount of n-dodecane or solvent present in the mixture. The influence of the concentration and nature of the solvent in the mixture is also consistent with the phase behaviour observed with run # 7 (350g ABVB + 2.07 MPa hydrogen). As the amount of the middle distillate fraction, i.e., the n-dodecane, was decreased and the amount of heavier material was increased the onset of phase behaviour had shifted up in temperature and down in pressure. This type of behaviour is also very consistent with previous findings[89].

The analysis of the "solid" samples further corroborates the idea that the "solid" sample is made up almost entirely of asphaltenic material since it is well known that asphaltenes have a high heteroatoms and a high heavy metal content. The thermodynamic analysis determined that enthalpies of fusion at the low temperatures were in the range of

7 to 9 J/g. The enthalpies of fusion for polyaromatic materials such as benzene, fluorene and dibenzofuran are 127 J/g, 118 J/g and 108 J/g respectively [104]. Enthalpies of fusion for some petroleum waxes have been reported to be as low as 5.4 J/g [103] and those for asphaltenes are around 6.3 J/g [105]. These findings thus reinforce the hypothesis that the "solid" material is in fact asphaltenes.

5.5 Other Uses for the X-ray Imaging System

The x-ray imaging system is a powerful tool, it has permitted studies of complex phase behaviour to be performed and also it has provided an excellent method for determining densities of heavy oils at high temperatures and pressures. For mixtures that are based on the same heavy oil / bitumen source the data are readily regressed. However if all the data from the various heavy oil / bitumen samples are pooled then the degree of scatter in the results increases and the "goodness" of fit is reduced. This lack of fit when the data are pooled probably reflects a change in the mass absorption coefficient and the assumption that it is constant in the analysis would no longer be valid. It should also be noted that the heavy metal contents of the various samples are different and this variability would also affect the mass absorption coefficient. The degree of scatter may also reflect the fluctuations in the voltage of the x-ray source, i.e., the number of x-rays hitting the target. Although the x-ray tube is a constant source tube it is not immune to fluctuations in line voltage.

5.6 Complex Phase Behaviour and Heavy Oil Upgrading

The plot of heavy oil upgrading technologies superimposed on the phase diagram for a model bitumen demonstrates that the phase behaviour observed is consistent with current industrial technologies. It should be noted that the zone where the multiphase behaviour is observed is devoid any of known processing schemes and perhaps reflects a region where processing difficulties have been encountered. This type of plot is useful not only for assessing processing strategies but also for downstream processes (e.g., depressurizing). In several heavy oil upgrading schemes low pressure separators are used to fractionate product streams of which a portion is often used as a recycle. Clearly if low pressure separators are operating in the region where three- or four-phase behaviour arises then product (or recycle) streams would not behave as expected in subsequent process steps. In the fixed bed processes a recycle stream which contained a "solid" phase or heavy liquid phase could see the accumulation of the heavy material eventually leading to plugging. This type of scenario for the unexpected presence of liquid-liquid-gas and solid-liquid-liquid-gas phases during processing in heavy oil systems is just one example (in a wide range of possibilities) of the effect of complex phase behaviour.

The experiments reported in this thesis were carried out under operating conditions and with reactant compositions which closely mimic those of donor solvent processes. These processes were designed to operate at lower severities, by employing hydrogen donor solvents, while maintaining high conversions. With the donor solvent processes the

availability of labile hydrogen is high and as a result one would expect high conversions with less coke formation but these processes (e.g., DRB process) tend to have lower than expected conversions. The results reported in this thesis suggest that similar complex phase behaviour, accompanied by high mass transfer resistances and lower kinetic rates, may account for the lower than expected conversions in the donor solvent processes. The operating parameters chosen for the higher severity processes, like H-Oil, VCC, LC-fining etc., reflect an avoidance of the complex phase behaviour zone. While the solvent de-asphalting processes like the ROSE process exploit the three phase (solid-liquid-vapour) region.

6.0 Conclusions

1. X-ray imaging can be used to identify the number and nature of bulk phases arising in opaque organic fluids. Density differences, between two hydrocarbon liquids, in the order of 0.04 g/cm^3 can be distinguished even at elevated temperatures and pressures.

2. The x-ray imaging system can also be utilized to determine the densities of fluid phases arising in opaque hydrocarbons at elevated temperatures and pressures.

3. Heavy oil and bitumen mixtures exhibit complex phase behaviour. Partly processed crudes + hydrogen and Athabasca bitumen vacuum bottoms + n-dodecane + hydrogen have demonstrated complex phase transitions such as "solid" - liquid - vapour to liquid - vapour and "solid" - liquid - vapour to liquid - vapour to liquid - liquid - vapour to "solid" liquid - liquid - vapour to "solid" - liquid - vapour. Mixtures with more than 30 wt.% 797 + K resid are most susceptible to multiphase behaviour

4. Complex phase behaviour observed with the heavy oil / bitumen mixtures are consistent with the expansion of Type V phase behaviour for binary fluids (according to the Van Konynenburg and Scott (1980) classification scheme[88, 89]) to more complex systems with the interference of a "solid".

5. "Solids" obtained at high temperatures and pressures from phase equilibria studies with heavy oil and bitumen mixtures are asphaltenes based on the enthalpies of fusion and chemical analysis. "Solids" present at the low and high temperatures are similar in nature.

6. Phase behaviour of model heavy oil / bitumen mixtures is consistent with existing industrial practice in that the zones which show complex phase behaviour are avoided by operating at pressures above or below those at which multiphase behaviour occur. Many processing problems can be traced to impingement on the multiphase region. Some processes such as solvent de-asphalting processes exploit the multiphase region.

7.0 References

1. Energy Survey, The Economist, June 18, 1994
2. OGJ Special, "China's New Oil Import Status Underpins World's Most Dynamic Petroleum Scene", Oil & Gas J., May 9, 1994, p. 33-35
3. OGJ Special, "China's Refiners Face Massive Overhaul Expansion To Meet Demand Growth", Oil & Gas J., May 9, 1994, p. 36-42
4. R. A. Corbett, "Canada's Heavy Oil, Bitumen Upgrading Activity is Growing", OGJ Special, Oil & Gas J., June 26, 1989, p.33-41
5. A. G. Bridge, G. D. Gould and J. F. Berkman, "Residua Processes Proven", Oil & Gas J., Jan. 19, p. 85-96
6. D. G. Green and H. Broderick:, "Residuum Hydroprocessing in the mid 1980's", Chem. Eng. Prog., Dec 1981, p 33-39
7. J. Chrones and R. R. Germain, "Bitumen and Heavy Oil Upgrading in Canada", Fuel Sci. Tech. Int., vol. 7, no. 5-6, 1989, p. 783-821
8. L. Dukhedin-Lalla, S. Yushun, P. Rahimi and J.M. Shaw, "Phase Splitting of Complex Hydrocarbon Mixtures", Fluid Phase Equilibria, vol. 53, 1989, p.415-422
9. L. Dukhedin-Lalla, "Phase Behaviour of Complex Hydrocaron Mixtures", M.A.Sc. Thesis, University of Toronto, 1990

10. J. L. Shelton and L. Yarborough, "Multiple Phase Behaviour in Porous Media During CO_2 or Rich-Gas Flooding", SPIE-AIME Conf. Tulsa Okla March 22-24, 1976, paper # SPE 5827

11. E.A. Turek, R.E. Metcalfe and R.E. Fishback, "Phase Behaviour of Several CO_2 / West Texas Reservoir Oil Systems", SPERE, May 1988, p.505-516

12. P. Fotland, H. Andfindsen and F. H. Fadnes, "Detection of Asphaltene Precipitation and Amounts Precipitated by Measurement of Electrical Conductivity", Fluid Phase Equilibria, vol. 82, 1993, p.157-164

13. Vince, M.A. and Lahey, R.T.Jr., NUREG / CR - 1692 R1, R2, R4, Prepared. for Division of Reactor Safety Research Office of Nuclear Regulation Research U.S. Nuclear Regulation Commission Washington D.C.

14. K. Ohkawa and R. T. Lahey, Jr., "The Development of a Gamma -ray Scattering Densiometer for the Nonintrusive Measurement of Local Void Fraction", Nuc. Tech., vol. 67, Dec. 1984, p. 437 - 451

15. D. Cronauer, Amoco Naperville Illinois, Private Communication, 1991

16. J. G. Ondeyka, J. P. Henry and F. H. Verhoff, " Indirect Measurements of Sedimentation Rates at High Temperatures and Pressures by X-ray Photography", Ind. Eng. Chem. Fund., vol. 17, no.3, 1978, p. 217-221

17. J. G. Speight, " The Chemistry and Technology of Petroleum", 2nd. ed. Marcel Dekker Inc., New York, 1991, 1980 1st. ed.

18. 1984 Refining Process Handbook, Hydrocarbon Process. , vol. 63, no. 9, Sept 1984, p. 67-146

19. A. Billon, J.P. Peries, E. Fehr and E. Lorenz, "SDA - Key to Upgrading Heavy Crudes", Oil & Gas J., vol. 75, no. 4, Jan 24, 1977, p. 43-48

20. S.R. Nelson and R.G. Roodman, "ROSE : The Energy Efficient Bottom of the Barrel Alternative ", Chem. Eng. Prog., vol. 81, May 1985, p. 63-68

21. J.A. Gearhart and L. Garwin, "Resid Extraction Process offers Flexibility", Oil & Gas J., vol. 74, no. 24, June 14, 1976, p. 63-70

22. R. De Biase and J.D. Elliott, "Delayed Coking: latest trends", Hydrocarbon Process., vol.5, 1982, p.99-104

23. T. Aiba and K. Kajii, "Residue Thermal Cracking by the Eureka Process", Chem. Eng. Prog., vol. 77, no. 2, 1981, p. 37-44

24. R. Takahashi and K. Washimi, "Residue Thermal Cracking bt the Eureka Process", Hydrocarbon Proc., vol. 55, no. 11, Nov 1976, p. 93-96

25. D.E. Allan, W.J. Metrailer and R.C. King, "Advances in Fluid and Flexicoking Technology", Chem. Eng. Prog., vol. 77, no. 12, Dec. 1981, p. 40-44

26. D.E. Allan, D.E. Blaser and M.M. Lambert, "Dual Gasification Coking Process Offers Option for Synthetic Gas Production from Heavy Feed", Oil & Gas J., vol. 80, no. 20, May 1982, p. 93-102

27. "Upgrading Processes can be used Upstream or Downstream", Oil & Gas J., vol. 87, no. 4, Jan. 23, 1989, p. 55-61

28. D.B. Bartholic, "Selective Vaporization Process and Dynamic Control Thereof", USA Patent 4311580, Jan. 19, 1982

29. N. Fujita, Y. Kumagai, Y. Shoji, H. Kubo and T. Maruyama, "Olefins from Heavy Oils", Chem. Eng. Prog., vol.79, no. 1, 1983, p.76-84

30. M.S. Rakow and M. Claderson, "The Dynacracking Process - An Update", Chem. Eng. Prog., vol. 77, no. 2, 1981, p. 31-36

31. C. L. Hemler, D. A. Lomas, D. G. Tajbl, "FCCU Reflects Technolgical Response to Resid Cracking", Oil & Gas J., vol. 82, no.22, May. 23, 1984, p. 79-88

32. G. Meyers, "Carbo-Metallic Oil Conversion", USA Patent 4341624, July 27, 1982.

33. T.E. Johnson, A.G. Silver and G.E. Kain, "New Oil Era Prompts Unique Resid Refinery", Oil & Gas J., vol. 80, no.12, March 22, 1982 p. 92-116

34. L.C. Yen, R.E. Wrench and C.M. Kuo, " FCCU Regenerator Temperature Effects Evaualted", Oil & Gas J., vol. 87, no.22, Sept. 16, 1985, p. 87-92

35. J.W. Wills, R.E. Wrench and L.C. Yen, "Improved Flexibility of Resid Cracking", Chem. Eng. Prog., vol. 81, no. 7, 1985, p. 33-40

36. R. R. Dean, J. L. Manleon and W. S. Letzsch, "New Resid Cracker 1. - Resid puts FCC Process in New Perspective", Oil & Gas J., Oct. 4 1982, p. 75-79

37. R. R. Dean, J. L. Manleon and W. S. Letzsch, "New Resid Cracker 2- Total Introduces New CC Process", Oil & Gas J., Oct. 11, 1982, p. 168-176

38. J.H Gary and G.E. Handwek, Petroleum Refining, 2nd ed. Marcel Dekker Inc., New York, 1984

39. M. Akbar and H. Geelen, "Visbreaking uses Soaker Drums", Hydrocarbon Processing, vol. 60, no. 5, 1981, p. 81-85

40. N.Y. Chen and D.S.Shihabi, "Hydrovisbreaking Process", USA Patent 4441770, Oct. 25, 1983

41. A. Langer, J. Stewart, C. Thompson, H.T. White and R.M. Hill, " Thermal Hydrogenation of Crude Residua", Ind. Eng. Chem., vol 53, no. 1, 1961, p. 27-30

42. A. Langer, J. Stewart, C.E. Thompson, H.T. White and R.M. Hill, "Hydrogen Donor Diluent Visbreaking of Residua", Ind. Eng. Proc. Des. Dev., vol 1, 1962, p.309

43. C.S. Carlson, A.W. Langer, J. Stewart and R.M. Hill, "Transfer of Hydrogen from Tetralin to Cracked Residua", Ind. Eng. Chem., vol. 50 , no. 7, 1958, 1067-1070

44. I.P. Fisher, H.J. Woods and F. Souhrada, "Process for Upgrading Heavy Hydrocarbonaceous Oils", USA Patent 4294686, Oct. 13, 1981

45. I.P. Fisher, F. Souhrada and H.J. Woods, "New Non-Catalytic Heavy-Oil Process Developed in Canada", Oil & Gas J., vol. 80, no. 47 Nov. 22, 1982, p. 111-116

46. P.L. Simpson, R.J. Parker and G.A. Beaulieu, "Some Chemical Aspects of Donor Solvent Upgrading of Heavy Oil ", AIChE, Series - no. 282, vol. 87, p. 24-34

47. R.T. Bailey, "AOSTRA's Upgrading Demonstration Program", Energy Progress, vol.8, no.2, June 19988, p 100- 102

48. A.E. Silva, H.K. Rohrig and A.R. Dufresne, "Canmet's Process going into Montreal Refinery", Oil & Gas J., vol. 82, no. 13, March 1984, p. 81-88

49. J.F. King, C. Fairbridge and M.F. Wilson, "Hydroprocessing of Distillates Derived from Oil Sands and Coal : A Summary of Canmet Findings", Fuel Sci. & Tech. Int., vol. 6, no. 5, 1988, p. 489-508

50. K. Fernie, G. Muir and B. Pruden, "The Canmet Hydrocracking Process", Proc. Int. Symp. on Heavy Oil and residue Upgrading Utilization, Editor in Chief, H. Choynen and H. Chi, China Building Ind. Press. Acad. Publ., 1992.

51. L.W. Chambers, R.J. Waugh, A.E. Silva and J.M. Denis, " The Canmet Residuum Hydrocracking Process : An Update", Future Heavy Crdue Oils Tar Sands, Int. Conf., 2nd Meeting Date 1982, Chapter 127, p.1206-1210, Edited by R.F. Meyer and J.C. Wynn and J.C. Olson , Mc-Graw-Hill, New York, N..Y. 1984

52. K. Kretschmar, L. Merz, J. Guitian, J. Krasuk and F. Marruffo, " Process for the Hydrogenation of Heavy and Residual Oils", USA Patent 4851107, Jul. 25, 1989.

53. K. Niemann and F. Wenzel, "The VEBA-COMBI-CRACKING- Technology : An Update", Fuel Proc. Tech, vol. 35, 1993, p. 1-20

54. G. De Drago, J. Guitian, J. Krasuk, J. Larrauri, R. Marzin, F. Silva and B. Solari,

" The Development of HDH Process : A Refiners Tool for Rresidual Upgrading ", Symposium on Resid Upgrading, Div. Petr. Chem. Inc., Amer. Chem. Soc., Washington, Aug. 26-31, 1990, p. 584-591

55. G. Rahbe, R. Marzin, I. Cavicchioli and J. Krasuk, " Recycle of Unconverted Residual to Hydrocracker after Removal of Unstable Polynuclear Hydrocarbons", USA Patent 4655903, Apr. 7, 1987

56. Y. Jacquin, M. Davidson and J.F. Le Page, "Process For Hydrotreating Heavy Hydrocarbons in Liquid Phase in the Presence of a Dispersed Catalysts", US Patent 4285804, Aug. 25, 1981

57. J.F. Le Page et al., ACS Prepr. Div. Pet Chem., vol. 32, no. 2, 1987, p. 470

58 H. Unger, M.C. Sze and R.P. Driesen, "Hydrogenation of High Boiling Hydrocarbons", US Patents 4411768, Oct. 25, 1983

59. J. Casper and R. Kramer, " Recovery of Hydrogen", USA Patents 4457834, Jul. 3, 1984

60. W.J. Beaton, V. McDaniel, W. McWhirter, R. Petersen & R. Van Driesen, "Resid Hydrocracker Expands Crude Processing Flexibility", Oil & Gas J., July 7, 1986, p.47

61. R.P. Van Driesen, J, Gaspers, A.R. Campbell and G. Lunin, " LC-Fining Upgrades Heavy Crudes ", Hydrocarbon Proc., May 1979, p. 107-111

62. R.E. Boening, N.K. McDaniel, R. Petersen and R. Van Driesen, " Recent Data on resid Hydrocracker ", Hydrocarbon Proc., Sept.1987, p. 359-362

63. W. Beaton, N. McDaniel, W. McWhirter, R. Petersen, R. van Driesen, " Operating Experience with Amoco's LC-Fining Resid Cracker ", Ener. Proc., vol. 45, 1987, p. 20-25

64. R.P. Van Driesen and L.L. Fornoff, " Upgrade Resids with LC-Fining ", Hydrocarbon Proc., Sept. 1985, p. 91-95

65. R.M. Eccles, " H-Oil Processing of Tar Sand Bitumen For Maximum Oil Yield and Cash Flow ", Future Heavy Crdue Oils Tar Sands, Int. Conf., 1st Meeting Date 1979, Chapter 70, p. 625-631, Edited by R.F. Meyer and C.T. Steele, Mc-Grwa-Hill, New York, N..Y. 1981.

66. R.M. Eccles, " Recent Technical Advances in H-Oil Upgrading of Heavy Crudes " Future Heavy Crdue Oils Tar Sands, Int. Conf., 2nd Meeting Date 1982, Chapter 121, p. 1166-1170, Edited by R.F. Meyer, J.C. Wynn and J.C. Olson , Mc-Graw-Hill, New York, N.Y., 1984

67. R.M. Eccles, A.M. Gray and W.B.Livingston, " New Resid Conversion Scheme set for Louisiana Refinery ", Oil & Gas J., April 12, 1982, p. 123-129

68. B.A. Seymour, R.H. Wolk and M.C. Chervenak, " High Conversion of Level Hydrogenation of Residuum ", US Patent 3412010, Nov. 19, 1968

69. L. Zanzotto, A.J. Faber, D.P. Foley, R.B. Jeffries and R.D. Watson, " Novel Asphaltenic Composition ", US Patents 4904305, Feb. 27, 1990

70. J. Sudoh, Y. Shiroto, Y. Fukul and C. Takeuchi, " Upgrading of Heavy Oils by Asphaltenic Bottom Cracking" Ind. Eng. Chem. Proc. Des. Dev., vol. 23, 1984, p. 641-648

71. C. Takeuchi, Y. Fukul, M. Nakamura, Y. Shiroto, "Asphaltene Cracking in Catalytic Hydrotreating of Heavy Oils. 1. Processing of Heavy Oils by Catalytic Hydroprocessing and Solvent Deasphalting Ind. Eng. Chem. Proc. Des. Dev., vol. 22, 1983, p. 236-241

72. C. Takeuchi, Y. Fukul, M. Nakamura, Y. Shiroto, "Asphaltene Cracking in Catalytic Hydrotreating of Heavy Oils. 2. Study of Changes in Asphaltene Structure during Catalytic Hydroprocessing", Ind. Eng. Chem. Proc. Des. Dev., vol. 22, 1983, p. 242-248

73. C. Takeuchi, Y. Fukul, M. Nakamura, Y. Shiroto, "Asphaltene Cracking in Catalytic Hydrotreating of Heavy Oils. 3 Characterization of Products from Catalytic Hydroprocessing of Khafji Vacuum Residue", Ind. Eng. Chem. Proc. Des. Dev., vol. 22, 83, p. 248-257

74. J. Sikonia, " New Data for RCD Unibon"Hydrocarbon Proc., June 1980, p. 73-78

75. L. Walliser, "Black Oil Conversion at Natref", Oil & Gas J., vol. 78, no.12, March 24, 1980, pg. 118-127

76. "X-ray Technology", vol. 24, Encyclopaedia of Chemical Tehnology - Kirk - Othmer - 3rd ed. John Wiley & Sons, Wiley Interscience Publishers, 1984, p. 678 - 708

77. A. St. John and H. R. Isenburg, " Industrial Radiology - X-rays and Gamma rays", John Wiley & Sons Inc., New York, 2nd ed., 1943

78. J. C. Rockley, "An Introduction to Industrial Radiology", Butterworth & Co. Ltd., London, England, 1964

79. I. P. Csorba, "Image Tubes", Howard W. Sams & Co. Inc., Indiana, U.S.A., 1985

80. I. P. Csorba, Editor, B. J. Thompson, General Editor, "Selected Papers on Image Tubes", SPIE Milestone Series, vol. MS 20, SPIE Optical Engineering Press, 1990

81. C. A. Taylor, "Images : A Unified View of Diffraction and Image Formation with all Kinds of Radiation", Wykeham Publications, London, 1978

82. J. Durandet, Y. L. Gladel and F. Graziani, "Etude de la Separation des Hydrocarbures par extraction Liquide - Liquide avec L'alcool benzyliquez", Revue De L'Institut Francais du Petrole, no. 6, June 1955, p. 585-591

83. L.L. Larson, M.K. Silva, M.A. Taylor and F.M. Orr Jr., "Temperature Dependence of L_1 / L_2 / V Behaviour in CO_2 / Hydrocarbon Systems", SPE Reservoir Engineering, February 1989, p.104 - 114

84. G. Schneider, Z. Alwani, W. Heim, E. Horvath and E. Franck, "Phasengleichgewichte und kritische Erscheinungen in binaren Mischsytemen bis 1500 bar", "Chemie. Ind. Techn., vol. 39, Jan. 1967, p 649 - 656

85. D.J. Fall, J.M. Fall and K.D. Luks, "Liquid-Liquid-Vapor Immiscibility Limits in Carbon Dioxide + n-Paraffin Mixtures", J. Chem. Eng. Data., vol. 30, no.1, 1985,

p 82-88

86. J.D. Hottovy, K.D. Luks and J.P. Kohn, "Three Phase Liquid-Liquid-Vapor Equilibria Behaviour of Certain Binary CO_2 - n-Paraffin Systems", J. Chem. Eng. Data, vol. 26, 1981, p. 258-262

87. *CMGPROP v.94.00*, Computer Modelling Group, Calgary, Alberta, Canada, 1994

88. P.H. Van Konynenburg and R.L. Scott, "Critical Lines and Phase Equilibria in Binary Van Der Waals Mixtures", Phil. Trans. of the Royal Society (London), 1980, 298, p. 495-540

89. J. Gregorowicz, Th. W. de Loos, J. De Swaan Arons, " Liquid-liquid-vapour phase equilibria in the system ethane + propane + eicosane : retrograde behaviour of the heavy liquid phase", Fluid Phase Equilibria, vol. 84, 1993, p. 225-250

90. J.M. Shaw, Th. W. De Loos and J. De Swaan Arons, "Prediction of Unusual Retrograde Condensation in Model Reservoir Fluids", Fluid Phase Equilibria, vol. 84, 1993, p. 251-266

91. Th. W. De. Loos, "Understanding Phase Diagrams", Supercritical Fluids. E. Kiran and J. M. H. Levelt Sengers (editors), Kluwer Academic Publishers, Netherlands. 1994

92. C.J. Peters, "Multiphase Equilibria in Near Critical Solvents", Supercritical Fluids, E. Kiran and J. M. H. Levelt Sengers (editors), Kluwer Academic Publishers, Netherlands. 1994

93. D. Stamoulis, "Patterns of Fluid Phase Behaviour in Binary & Quasi Binary Mixtures", Ph.D. Thesis, T. U. Delft, Netherlands, 1994.

94. J. M. Shaw, Th. W. De Loos and J. De Swaan, " An Explanation for Solid-Liquid-Liquid-Vapour Phase Behaviour in Reservoir Fluids", submitted for publication, 1995

95. "Standard Test Method for Insolubless in Used Lubricating Oils, "MethodD-893-80, Annual Book of ASTM Standards, PArt 23 : Petroleum Products and Lubricants (1980) no. 1, p. 401 -407

96. O. P. Strausz, "Some Recent Advances in the Chemistry of Oil Sand Bitumen", Future Heavy Crdue Oils Tar Sands, Int. Conf., 1st Meeting Date 1979, Chapter 24, p. 187-194, Edited by R.F. Meyer and C.T. Steele, Mc-Grwa-Hill, New York, N..Y. 1981.

97. E. Furimsky and P.J. Champagne, "Characterization of Athabasca Bitumen Fractions Derived by Gel Permeation Chromatography", Fuel Proc. Tech., no. 6, 1982, p. 269-275

98. V. Calemna, P. Iwanski, M. Nali, R. Scotti and L. Montanari, "Structural Characterization of Asphaltenes of Different Origins", Energy & Fuels, vol. 9, no. 2, 1995, p. 225 - 230

99. D. A. Storm, R. J. Barresi, S. J. DeCanio, "Colloidal Nature of Vacuum Residue", Fuel, 1991, vol. 70, p. 779

100. B. A. Watson and M. A. Barteau, "Imaging of Petroleum Asphaltenes Using Scanning Tunneling Microscopy", Ind. Eng. Chem. Res., vol.33, no. 10, 1994, p. 2358-2363

101. A. Hirschberg, L. N. J. deJong, B. A. Schipper and J. G. Meijer, "Influence of Temperature and Pressure on Asphaltene Flocculation", SPEJ, June 1984, p. 283-293.

102. M. Gray, University of Alberta, Dept. Chem. Eng., Private Communication, 1993

103. T. H. Chung, "Thermodynamic Modelling for Organic Solid Precipitation", SPE Annual Technical Conference and Exhibition, 1993. p. 869 - 878

104. U. Domanska, F. R. Groves Jr. and E. McLaughlin, "Solid-Liquid Phase Equilibria and Ternary Mixtures of Benzene and Polynuclear Aromatic Compounds", J. Chem. Eng. Data., vol. 38, no. 1, 1993, p. 88 - 94

105. C. Barnes, "Characterization of Unknown Solids in Heeavy Oil Upgrading Using Enthalpies of Fusion", University of Toronto, B.A.Sc. Thesis, 1995

106. J. Shaw, "A Correlation for Hydrogen Solubility in Alicyclic and Aromatic Solvents", Can. J. Chem. Eng., vol. 65, April 1987, pg. 292 - 298

107. H. Sharifi and J.M. Shaw, "Prediction of Hydrogen Solubility in Complex Hydrocarbon Solvents", in preparation

Cartlidge, C., Dukhedin-Lalla, L., and Shaw, J.M., " Preliminary Phase Diagrams for

108. Athabasca Vacuum Bottoms + n-dodecane + hydrogen ", poster presented at the Seventh International Conference on Fluid Properties and Phase Equilibria for Chemical Process Design and accepted for publication in Fluid Phase Equilibria, June 1995 and accepted for publication in Fluid Phase Equilibria to be published in Jan. 1996.

109. Cartlidge, C., Dukhedin-Lalla, L. , Rahimi, P. and Shaw, J.M., " Preliminary Phase Diagrams for Heavy Oil Mixtures ", Fuel Science and Technology International, paper presented at AIChE meeting in Austin, Texas, March 1995 and accepted for publication in Fuel Sci. Tech.

110. Dukhedin-Lalla, L. and Shaw, J.M., " Phase Equilibria For Opaque Organic Fluids at Elevated Temperatures and Pressures ", Paper presented at 44th Canadian Chemical Engineering Conference, 465-466, Calgary, October, 1994

111. Dukhedin-Lalla, L. and Shaw, J.M., " The Study of Complex Phase Behaviour of Opaque Fluids using X-ray Imaging ", Poster presented at the 43rd Canadian Chemical Engineering Conference, Ottawa, October 1993

112. Dukhedin-Lalla, L., Seyfaie, S. and Shaw, J.M., " Prediction of Liquid-liquid Equilibria for Complex Organic Mixtures ", Presented at the 16th AOSTRA Technical Review Meeting, Banff, October, 1991

113. Abedi, J., Ph D. Thesis, University of Toronto, in progress (1996)

8.0 Appendix A -
Thermodynamic model - enthalpy of fusion for "solid"

$$f_{i,mix}^{S} = f_{i,mix}^{L} \quad (1)$$

$$f_{i,mix}^{L} = x_i \gamma_i^{L} f_{pure,i}^{L} \quad (2) \text{ and } \quad f_{i,mix}^{S} = z_i \gamma_i^{S} f_{pure,i}^{S} \quad (3)$$

$$\left(\delta \ln \gamma_i^{L} / \delta P\right)_{T,x_i} = \left(\bar{v}_i^{L} - v_i^{L}\right)/RT \quad (4)$$

$$\left(\delta \ln \gamma_i^{S} / \delta P\right)_{T,z_i} = \left(\bar{v}_i^{S} - v_i^{S}\right)/RT \quad (5)$$

$$\gamma_i^{S,P} = \exp\left\{\int_{P_o}^{P}\left(\frac{\bar{v}_i^{S} - v_i^{S}}{RT}\right)dP\right\} (6) \text{ and } \gamma_i^{L,P} = \exp\left\{\int_{P_o}^{P}\left(\frac{\bar{v}_i^{L} - v_i^{L}}{RT}\right)dP\right\} \quad (7)$$

$$RT \ln\left(\frac{f_{pure,i}^{S}}{P}\right) = \left[\int_{P_o}^{P_{sat}}\left(v_i^{G} - \frac{RT}{P}\right)dP + \int_{P_{sat}}^{P_{SL}}\left(v_i^{L} - \frac{RT}{P}\right)dP + \int_{P_{SL}}^{P}\left(v_i^{S} - \frac{RT}{P}\right)dP\right] \quad (8)$$

$$f_{pure,i}^{S} = \left[\int_{P_o}^{P_{sat}} v_i^{G}dP + \int_{P_{sat}}^{P_{SL}} v_i^{L}dP + \int_{P_{SL}}^{P} v_i^{S}dP\right] \quad (9)$$

substituting equation (6) and (9) into equation (3) gives

$$f_{i,mix}^{S} = z_i \exp\left[\frac{1}{RT}\left\{\int_{P_o}^{P_{sat}} v_i^{G}dP + \int_{P_{sat}}^{P_{SL}} v_i^{L}dP + \int_{P_{SL}}^{P} v_i^{S}dP + \int_{P_o}^{P}\left(\bar{v}_i^{S} - v_i^{S}\right)dP\right\}\right] \quad (10)$$

$$RT \ln\left(\frac{f_{pure,i}^{L}}{P}\right) = \left[\int_{P_o}^{P_{sat}}\left(v_i^{G} - \frac{RT}{P}\right)dP + \int_{P_{sat}}^{P}\left(v_i^{L} - \frac{RT}{P}\right)dP\right] \quad (11)$$

$$f_{pure,i}^{L} = \left[\int_{P_o}^{P_{sat}} v_i^{G}dP + \int_{P_{sat}}^{P} v_i^{L}dP\right] \quad (12)$$

substituting equations (7) and (12) into equation (2) gives

$$f_{i,mix}^{L} = x_i \exp\left[\frac{1}{RT}\left\{\int_{P_o}^{P_{sat}} v_i^{G}dP + \int_{P_{sat}}^{P} v_i^{L}dP + \int_{P_o}^{P}\left(\bar{v}_i^{L} - v_i^{L}\right)dP\right\}\right] \quad (13)$$

substituting equation (10) and (13) into equation (1) gives

$$\frac{x_i}{z_i} = \exp\left[\frac{1}{RT}\left(\int_{P_o}^{P_{SL}}\left(v_i^L - v_i^S\right)dP + \int_{P_o}^{P}\left(\bar{v}_i^S - \bar{v}_i^L\right)dP\right)\right] \quad (14)$$

taking natural logarithms on both sides and differentiating with with respect to temperature

$$\frac{\delta \ln\left(x_i/z_i\right)}{\delta T} = \frac{\left(v_i^L - v_i^S\right)}{RT}\frac{\delta P_{SL}}{\delta T} + \frac{(P_{SL} - P_o)}{RT}\frac{\delta}{\delta T}\left(v_i^L - v_i^S\right)$$
$$- \frac{P_{SL} - P_o}{RT^2}\left(v_i^L - v_i^S\right) + \frac{\bar{v}_i^L - \bar{v}_i^S}{RT}\frac{\delta P}{\delta T}$$
$$+ \frac{P - P_o}{RT}\frac{\delta}{\delta T}\left(\bar{v}_i^L - \bar{v}_i^S\right) - \frac{(P - P_o)}{RT^2}\left(\bar{v}_i^L - \bar{v}_i^S\right) \quad (15)$$

$$\frac{\delta P_{SL}}{\delta T} = \frac{\Delta H_{S\to L}}{T\left(v_i^L - v_i^S\right)} \quad \text{then} \quad P_{SL}(@\ T_0)P_o + \left(\frac{\delta P_{SL}}{\delta T}\right)(T - T_0)$$

i.e. $$P_{SL} \approx P_o + \frac{\Delta H_{S\to L}}{T\left(v_i^L - v_i^S\right)}(T - T_0)(17)$$

for a pure component $\frac{\delta P_{SL}}{\delta T}$ = constant

and $$\frac{\delta\left(v_i^L - v_i^S\right)}{\delta T} = \frac{-\left(v_i^L - v_i^S\right)}{T} \quad (18)$$

$$\frac{\delta \ln\left(x_i/z_i\right)}{\delta T} = \frac{-(m_i + \sum_{j\neq i} m_j)}{\left[S.P.(m_i + \sum_{j\neq i} m_j) + n_i + \sum_{j\neq i} n_j\right]}\left\{S\frac{\delta P}{\delta T} + P\frac{\delta S}{\delta T}\right\} \quad (23)$$

equating equations (21) and (23)

$$\left(2\frac{T_0}{T} - 1\right)\frac{\Delta H_{S\to L}}{RT^2} + \frac{\bar{v}_i^L - \bar{v}_i^S}{RT}\frac{\delta P}{\delta T} - 2\frac{P - P_o}{RT^2}\left(\bar{v}_i^L - \bar{v}_i^S\right) =$$

$$\frac{-(m_i + \sum_{j\neq i} m_j)}{\left[S.P.(m_i + \sum_{j\neq i} m_j) + n_i + \sum_{j\neq i} n_j\right]}\left\{S\frac{\delta P}{\delta T} + P\frac{\delta S}{\delta T}\right\} \quad (24)$$

let $P_o = 1$ then

$$\frac{\delta P}{\delta T} = \frac{\left\langle \left(2\frac{T_0}{T} - 1\right)\frac{\Delta H_{S\to L}}{RT^2} + 2\frac{\bar{v}_i^L - \bar{v}_i^S}{RT^2} + \left\{-2\frac{\bar{v}_i^L - \bar{v}_i^S}{RT^2} + \frac{-(m_i + \sum_{j\neq i} m_j)}{\left[S.P.(m_i + \sum_{j\neq i} m_j) + n_i + \sum_{j\neq i} n_j\right]}\frac{\delta S}{\delta T}\right\}P \right\rangle}{\left\{-\frac{\bar{v}_i^L - \bar{v}_i^S}{RT} + \frac{-(m_i + \sum_{j\neq i} m_j)}{\left[S.P.(m_i + \sum_{j\neq i} m_j) + n_i + \sum_{j\neq i} n_j\right]}\right\}} \quad (25)$$

$$\frac{\delta \ln\left(x_i/z_i\right)}{\delta T} = \left(2\frac{T_0}{T} - 1\right)\frac{\Delta H_{S\to L}}{RT^2} + \frac{\bar{v}_i^{\,L} - \bar{v}_i^{\,S}}{RT}\frac{\delta P}{\delta T} +$$

$$\frac{P - P_o}{RT}\frac{\delta}{\delta T}\left(\bar{v}_i^{\,L} - \bar{v}_i^{\,S}\right) - \frac{P - P_o}{RT^2}\left(\bar{v}_i^{\,L} - \bar{v}_i^{\,S}\right) \quad (19)$$

and similarly $\dfrac{\delta\left(\bar{v}_i^{\,L} - \bar{v}_i^{\,S}\right)}{\delta T}$ can also be approximated as $\dfrac{-\left(\bar{v}_i^{\,L} - \bar{v}_i^{\,S}\right)}{T}$ (20)

$$\frac{\delta \ln\left(x_i/z_i\right)}{\delta T} = \left(2\frac{T_0}{T} - 1\right)\frac{\Delta H_{S\to L}}{RT^2} +$$

$$\frac{\bar{v}_i^{\,L} - \bar{v}_i^{\,S}}{RT}\frac{\delta P}{\delta T} - 2\frac{P - P_o}{RT^2}\left(\bar{v}_i^{\,L} - \bar{v}_i^{\,S}\right) \quad (21)$$

Evaluating x_i and z_i

assuming that z_i is fixed and is approximately equal to one ($z_i \approx 1$) and representing the mole fractionof component i in the liquid phase as a function of hydrogen solubility then

$$x_i = \frac{n_i}{\left[S.P.(m_i + \sum_{j\neq i} m_j) + n_i + \sum_{j\neq i} n_j\right]} \quad (22)$$

$f_{i,mix}^{S}$ – fugacity of component i in a mixed solid

$f_{i,mix}^{L}$ – fugacity of component i in a mixed solid

$f_{i,pure}^{S}$ – fugacity of pure component i as a solid

$f_{i,pure}^{S}$ – fugacity of pure component i as a liquid

ΔH_{SL} – enthalpy of fusion (transition from solid to liquid)

m_i – mass of component i in the liquid

n_i – moles of component i in the liquid

P – pressure

P_o – reference pressure

P_{sar} – saturation pressure

P_{SL} – pressure at solid to liquid transition

S – solubility of hydrogen in liquid phase (moles of hydrogen / ($P \times$ mass of solvent))

T – temperature

T_o – temperature at the reference pressure

x_i – mole fraction of component i in the liquid phase

z_i – mole fraction of component i in the solid phase

$\bar{v}_i^S$ – partial molar volume of component i in a mixed solid

$\bar{v}_i^L$ – partial molar volume of component i in a liquid mixture

v_i^S – molar volume of pure component i as a solid

v_i^L – molar volume of pure component i as a liquid

v_i^G – molar volume of pure component i as a gas

END

17-09-96

FIN